KfK 3347
Mai 1982

# The Capture Cross Sections of the Neon Isotopes and the s-Process Neutron Balance

J. Almeida
Institut für Angewandte Kernphysik

Kernforschungszentrum Karlsruhe

KERNFORSCHUNGSZENTRUM KARLSRUHE

Institut für Angewandte Kernphysik

KfK 3347

# THE CAPTURE CROSS SECTIONS OF THE NEON ISOTOPES AND THE s-PROCESS NEUTRON BALANCE

J. Almeida

Kernforschungszentrum Karlsruhe GmbH, Karlsruhe

---

Von der naturwissenschaftlichen Gesamtfakultät der Universität Heidelberg genehmigte Dissertation

Kernforschungszentrum Karlsruhe GmbH
ISSN 0303-4003

ABSTRACT

The neutron capture cross sections of the three stable neon isotopes have been measured by the time-of-flight method in the energy range from 5 to 200 keV, using hydrogen free fast liquid scintillator detectors and the Maier-Leibnitz pulse height weighting technique. The sensitivity of the experimental set-up has been increased by about 50% through improvements in the high pressure samples, neutron collimation, and shielding. The data analysis has been refined, especially with respect to the crucial problem of background elimination. This allowed the 30 keV Maxwell averaged cross sections to be determined with an accuracy of better than 1 mb. The total cross sections, which are needed for the background correction in the capture measurements, were also measured between 5 and 800 keV.

The neutron source of the s-process is believed to be the $^{22}Ne(\alpha,n)$ reaction, taking place in the He burning shell of a pulsating red giant. Such a periodic neutron irradiation leads to an exponential distribution of neutron fluences for the seed nuclei, which can be deduced from the observed solar system abundances. Using this empirically determined distribution of neutron fluences and the abundances of the elements present in the He shell, the number of neutrons captured by each nuclear species during the s-process has been calculated.
As a result it was found that neutron absorption by the light elements, from $^{20}Ne$ to $^{56}Fe$, is dominated not by $^{22}Ne$ but by $^{25}Mg$. The condition that as many neutrons should be produced as are absorbed has led to the conclusion that at least 80% of the $^{22}Ne$ must undergo the $(\alpha,n)$ reaction, which implies that less than 20% can undergo the $(\alpha,\gamma)$ reaction.Therefore the $(\alpha,n)$ reaction rate must be at least 4 times faster than the $(\alpha,\gamma)$ rate.An inspection of these reaction rates as a function of temperature shows that this condition can be satisfied only for $T > 3.2\ 10^8$ K, or $kT > 28$ keV.

This lower limit for the average s-process temperature is in good agreement with other estimates of this quantity,and is also compatible with the time dependent temperature and neutron density obtained from a realistic stellar model.

Die Neutroneneinfangquerschnitte der Neonisotope und die Neutronenbilanz im s-Prozeß


ZUSAMMENFASSUNG

Die Neutroneneinfangquerschnitte der drei stabilen Neonisotope $^{20,21,22}Ne$ wurden mit der Flugzeitmethode im Energiebereich von 5-200 keV gemessen. Dazu wurden wasserstofffreie schnelle Flüssigszintillatoren verwendet, auf die die Maier-Leibnitz-Methode zur Impulshöhenwichtung angewendet wurde. Die Empfindlichkeit des experimentellen Aufbaus wurde gegenüber einer bestehenden Version durch Optimierung der Hochdruckgasproben, der Neutronenkollimation und Abschirmung sowie der Datenanalyse um 50% verbessert. Dies ermöglichte die Messung der Maxwell-gemittelten Querschnitte für kT=30 keV mit einer Genauigkeit von < 1 mb. Die zur Untergrundkorrektur benötigten totalen Wirkungsquerschnitte dieser Isotope wurden ebenfalls gemessen, und zwar im Energiebereich 5-800 keV.

Als Neutronenquelle für den s-Prozeß wird die $^{22}Ne(\alpha,n)$-Reaktion in der He-brennenden Schale von pulsierenden Roten Riesen angenommen. Dies hat eine periodische Neutronenbestrahlung zur Folge, die zu einer exponentiell verteilten Neutronenfluenz für die Saatkerne führt, wie sie von den beobachteten Häufigkeiten im Sonnensystem für die reinen s-Prozeß-Kerne abgeleitet werden kann.

Mit dieser empirisch bestimmten Neutronenfluenzverteilung, sowie den Häufigkeiten und den Querschnitten der Elemente, die in der He-Schale vorliegen, wurde die Anzahl der von jedem Isotop im s-Prozeß absorbierten Neutronen berechnet. Dabei wurde gefunden, daß im Bereich der leichten Kerne von $^{20}Ne$ bis $^{56}Fe$ die Neutronenabsorption hauptsächlich durch $^{25}Mg$ bestimmt wird, und daß Neutroneneinfang an den Neonisotopen kaum ins Gewicht fällt. Die Bedingung, daß gleich viele Neutronen produziert und absorbiert werden, führte zu dem Ergebnis, daß mindestens 80% des $^{22}Ne$ in $(\alpha,n)$-Reaktionen verbraucht wurde. Dies bedeutet, daß der Anteil der $(\alpha,\gamma)$-Reaktion kleiner als 20% der gesamten Reaktionsrate gewesen sein muß. Dieses Ergebnis, daß die $(\alpha,n)$--Reaktion mindestens 4 mal schneller ablief als die $(\alpha,\gamma)$-Reaktion, ermöglichte wegen der Temperaturabhängigkeit der Reaktionsraten eine Aussage über die untere Grenze der effektiven Temperatur im s-Prozeß : $T > 3{,}2 \cdot 10^8$ K oder $kT > 28$ keV.

Diese Untergrenze für die mittlere s-Prozeß-Temperatur ist in guter Übereinstimmung mit anderen Abschätzungen und auch mit den Ergebnissen eines realistischen Sternmodells.

CONTENTS

# I. INTRODUCTION

The observed relative abundances of the heavy elements in the solar system and in population I matter ( star surfaces, planetary nebulae, interstellar matter ) are very similar. This suggests that the same nucleosynthesis mechanisms were at work throughout the galaxy. The description of these mechanisms was put forward in 1957 /1/ and may be shortly outlined as follows.

Nucleosynthesis of elements heavier than He takes place in stars. Charged particle reactions build heavier nuclei from lighter ones. The elements around Fe are the heaviest produced in this way, in explosive Si burning, at temperatures $>10^9$ K; production of still heavier nuclei is prevented by the growing coulomb barrier, and by the decreasing binding energy per nucleon. Instead, successive neutron captures on elements of the Fe abundance peak produce the heavier elements. Two different neutron capture processes are postulated: 1) In the s-process, the Fe peak seed nuclei are exposed on a long time scale to a weak neutron flux, such that the time interval between successive neutron captures ( $\Delta t \sim 10^1$-$10^3$ a ) is much larger than almost all of the concurrent β-decay half lives. The s-process produces elements up to Bi and part of this synthesis path on the nuclide chart is shown in Fig.1 . 2) In the r-process, the seed nuclei are exposed in a short time (~1-100s) to a very high neutron flux, such that $\Delta t \sim 10^{-6}$ -$10^{-9}$ s, much shorter than the β-decay half lives.Neutron rich isotopes are thus produced from each seed nucleus ( with up to 20 extra neutrons ), which subsequently decay back to the β-stability line. This r-process is believed to take

place in supernova explosions.

The need for two capture processes is apparent from an inspection of the nuclide chart in Fig.1. $^{86}$Sr is a s-only nucleus because it is shielded by $^{86}$Kr from β-decay of neutron rich isobars formed in the r-process. On the other hand $^{82}$Se is a r-only nucleus which cannot be produced by the s-process because of the short half life of $^{81}$Se. The r-process is also needed to bridge the gap of unstable nuclei between Bi and the Th and U isotopes. Most isotopes however, can be made by both processes. Branching points in the s-process path, as at $^{85}$Kr, arise when the β-decay half life is comparable to the time interval between neutron captures, Δt.

## I.1. Thermal pulses in red giants and the s-process

The s-process, with which we are concerned in this work, has been extensively studied and is believed to be fairly well understood /2/; we return to its quantitative treatment in Section IV. By comparing the observed abundances of the s-process nuclides with their calculated values as a function of the conditions under which this process took place, one obtains estimates for the following parameters: neutron density ($10^8$-$10^9$/cm$^3$), time scale (>$10^4$a), temperature(3-6 $10^8$K), density( ~$10^3$g/cm$^3$).

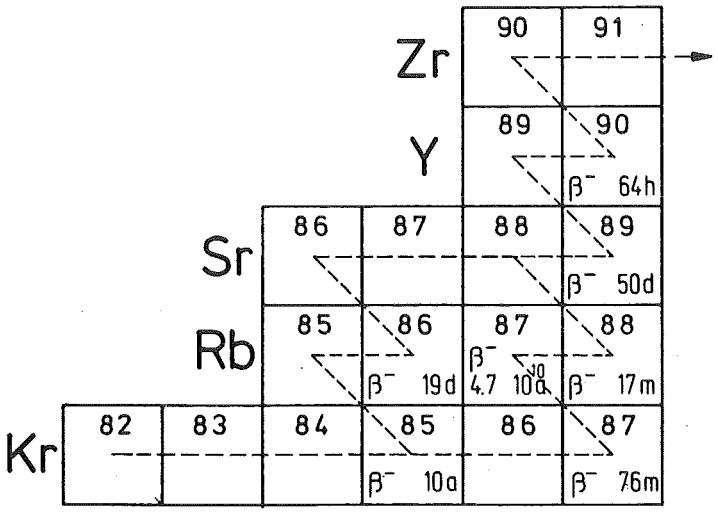


Fig. 1. The s-process path between Kr and Zr.

Apart from the neutron flux, the values of these quantities are compatible with the conditions of He burning regions in red giant stars. If this is indeed the site (or one of the sites) of the s-process two conditions must be satisfied: 1) A neutron source must be provided, through (α,n) reactions on one or several nuclear species, and 2) Some mechanism must exist to bring the s-processed matter, without further reactions, out to the star's surface, from where it can be returned to the interstellar medium.

The structure of red giants has been worked out in sufficient detail that an answer can be given to these questions; it turns out that both conditions may be fulfilled in realistic stellar models of red giants with several solar masses. Extensive stellar model calculations /3,4/ for a red giant of mass $7M_\odot$ result in the following simplified picture, where convection provides both a neutron source and a way of bringing s-processed material to the surface.

At the center of the star (Fig. 2) there is an electron degenerate core ( of mass $\sim 1M_\odot$ ) where the produts of He burning accumulate; He is burning in the high temperature inner part of a He shell of of mass $\sim 10^{-2}M_\odot$ ; H is burning in a convective envelope. The energy released by the He burning causes the local temperature gradient to increase until convection sets on. A convection cell appears that takes matter both into and out of the He burning region; the convection cell reaches a maximum extent and then, as the temperature gradient decreases due to the high efficiency of convective heat transport, it shrinks back until it almost disappears. A new convection cell will appear when the temperature gradient will have increased again to the critical value ( duration of the convective pulse ~20 a, interpulse interval ~2500a) and this cycle will repeat at least several hundred times during the red giant stage of the star. The He shell grows outwards, with each pulse encompassing new matter left behind by the H burning region.

We assume this is a second generation star,that is, it condensed out of material containig some matter already processed through all the stages of nuclear burning up to the supernova explosion; it therefore contains elements up to Fe, in particular C, N and O, with relative abundances approximately equal to those of the solar system. In H burning, matter is converted mostly into $^4$He and $^{14}$N, the latter being what is left by consuming the C, N and O in the CNO cycle. In this

reaction cycle, the C and O isotopes are transformed into $^{14}N$ through (p,n) and (p,$\gamma$) reactions /5/ ; the cross sections for these reactions on $^{14}N$ being extremely small, virtually all the C,N,O ends up as $^{14}N$. Therefore at each thermal pulse, the matter carried down by the convection cell contains $^{14}N$ and $^{56}Fe$ with relative abundance ( C+N+O ) / $^{56}Fe$ = 38.8 /6/ . In the hotter environment of the He shell the $^{14}N$ is transformed into $^{22}Ne$ by the rapid reaction chain $^{14}N(\alpha,\gamma)^{18}F(\beta^+)^{18}O(\alpha,\gamma)^{22}Ne$, a fraction of which releases neutrons through $^{22}Ne(\alpha,n)^{25}Mg$ ; these neutrons can then be captured by $^{56}Fe$ and its progeny, thus building up the heavier elements.

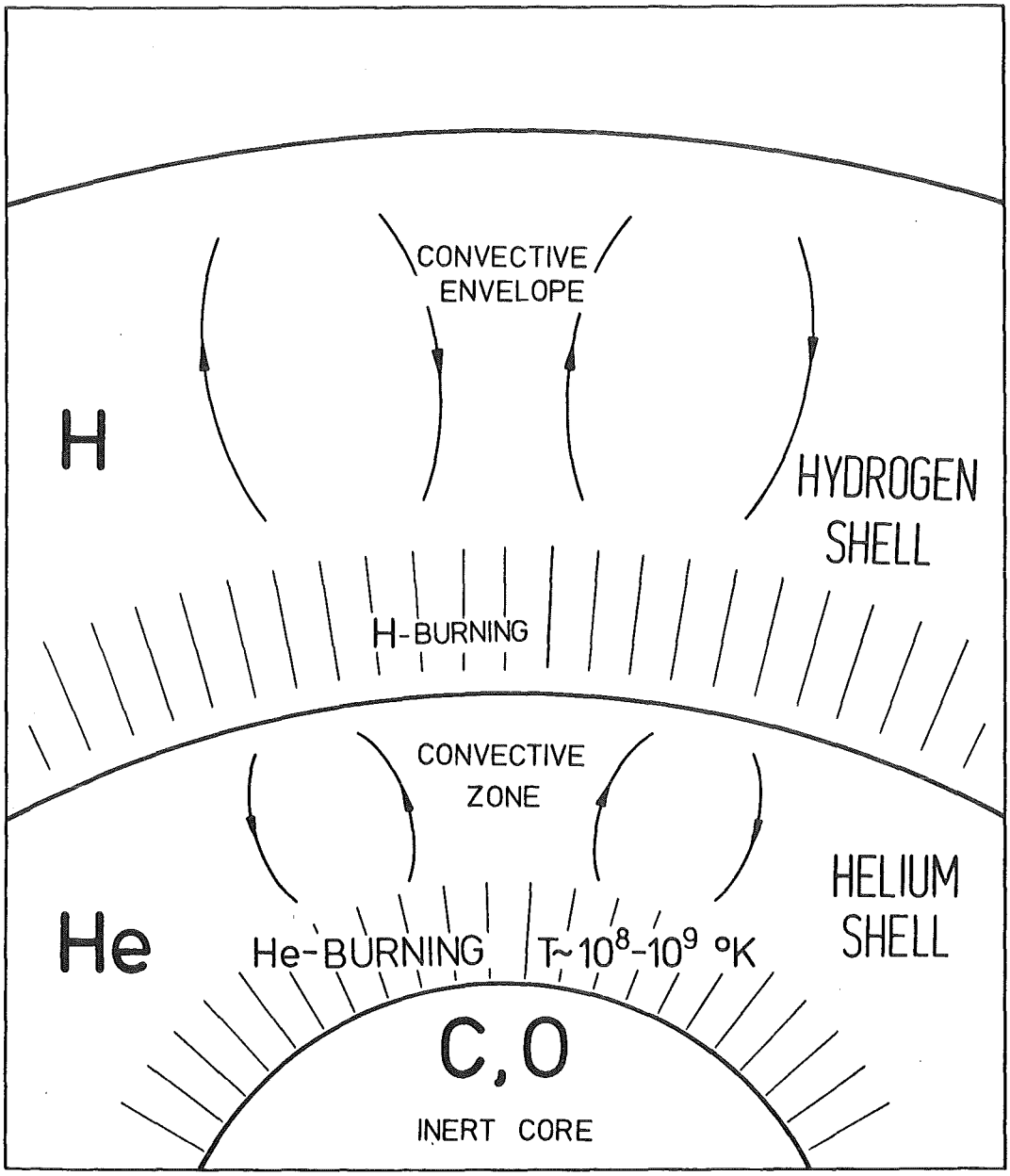


Fig. 2. Schematic structure of a 7 $M_\odot$ pulsating red giant.

## I.2. The Ne isotopes and the s-process neutron balance

From the point of view of the s-process the question is: does this mechanism provide enough neutrons to build the heaviest elements and, if yes, are the resulting relative abundances the same as in the solar system. Reaction network calculations /7/ show that, within this pulsed He burning model, $^{22}Ne$ is a strong enough neutron source, and that the observed solar abundance curve is approximately reproduced for isotopes with $85 < A < 200$. There are, however, inevitable uncertainties, due to the approximations needed to tackle such complex stellar models. An important one is the following:

The shape of the abundance curve of the elements synthesized in the s-process is a sensitive function of the number of neutrons, $n_c(Fe)$, captured in each pulse by the heavy elements (Fe and its progeny), which must compete with the light elements (Ne to Mn) for the available neutrons. This filtering action of the light elements is important, less than half of the produced neutrons being left for the heavy elements. Since in the He burning region $^{22}Ne$ and $^{25}Mg$ are by a large margin the most abundant of the light elements, their neutron capture cross sections at the relevant energy (kT~30keV) are an important factor in the calculation of $n_c(Fe)$; the next most abundant light species is $^{20}Ne$. The neutron capture cross sections, $\sigma_{n,\gamma}$, of these light nuclei in the keV range ar e very small, of the order of 1 mb, which makes them difficult to measure. Up to now, no experimental value of $\sigma_{n,\gamma}$ was available for the neon isotopes. In addition, the theoretical estimates of $\sigma_{n,\gamma}$ for such light nuclei are much less reliable than those for heavy ones, because the assumptions of the statistical model which is commonly used for theoretical calculations do not apply to very light nuclei. We have therefore set out to measure the total neutron cross sections and the neutron capture cross sections of the three stable neon isotopes, $^{20,21,22}Ne$, in the energy range from 5 keV to 400 keV.

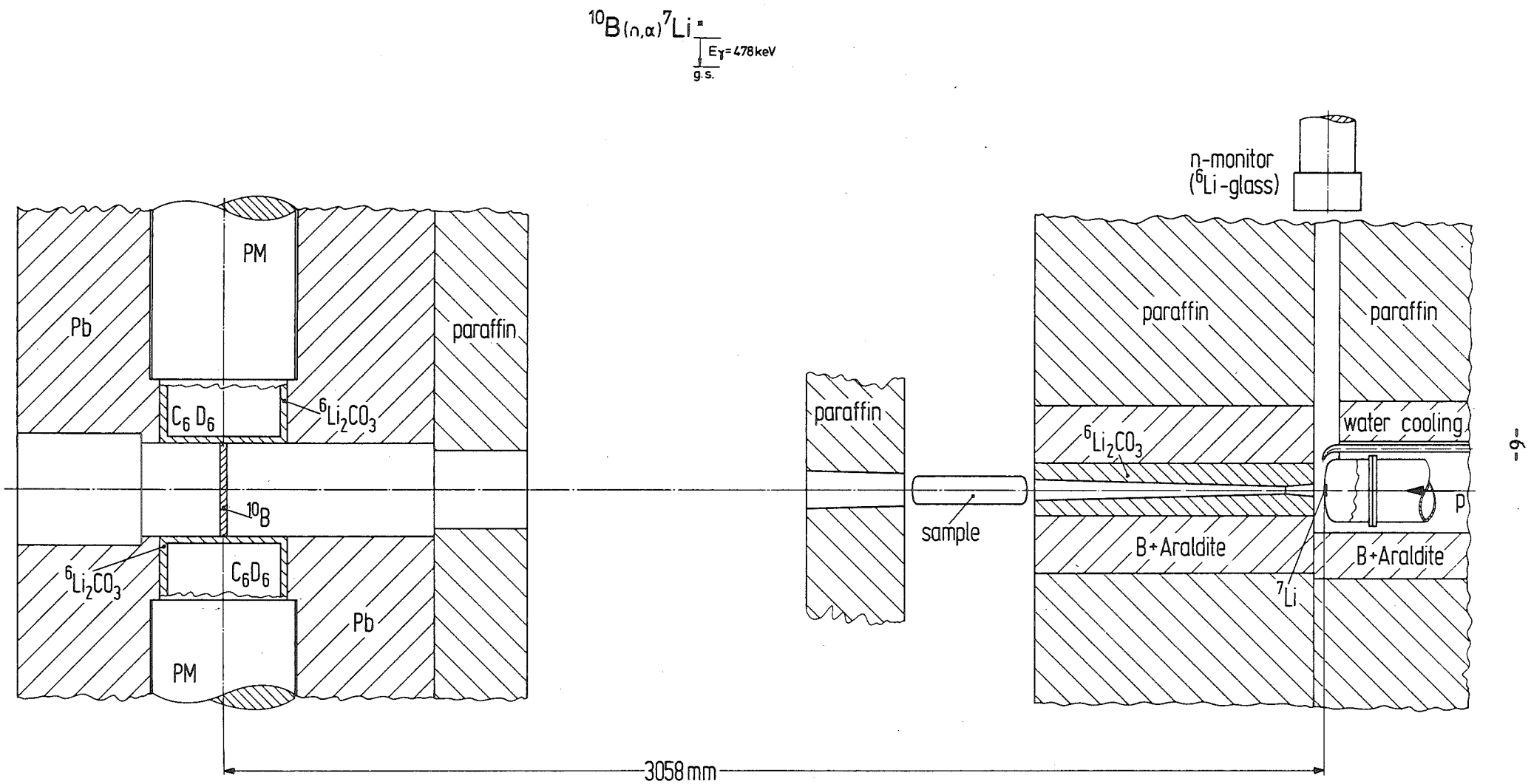


Fig. 3 Experimental set-up of the transmission measurements.

## II. TOTAL CROSS SECTION MEASUREMENT

The total cross section of the neon isotopes is needed for the analysis of our capture data (Section III). Since only natural neon had been previously measured /8/, we performed a transmission experiment on samples of natural neon and enriched samples of $^{22}Ne$ (95.4% ) and $^{21}Ne$ (99.8% ), the neutron energies being measured by time-of-light. Two series of runs were made, covering the energy ranges 5 -350 keV and 150 -800 keV.

### II.1. Experimental set up and data acquisition

The experimental set up is shown in Fig.3 . The pulsed proton beam from the accelerator hits a $^{7}Li$ target, producing neutrons with a wide range of energies through the $^{7}Li(p,n)$ reaction; the protons that don't react are stopped in the tantalum backing of the target. The neutron beam passes through a $^{6}Li_2CO_3$ collimator and the sample. The transmitted neutrons are detected at 3m flight path by a 10×10cm $^{10}B$ slab, 5 mm thick, through the $^{10}B(n,\alpha)^{7}Li$ reaction. The $^{7}Li$ deexcites to the ground state by a 478 keV $\gamma$-ray; these $\gamma$-rays are detected by two $C_6D_6$ liquid scintillator detectors (cylindrical, with 6cm diameter, 4cm height, thin aluminium walls ) coupled to fast photomultipliers ( VALVO XP2041 ). The combined time resolution of these two detectors was better than 600 ps. The neutron detection efficiency of this arrangement is about 3% ; a $^{6}Li$-glass neutron detector would be simpler and would have a better efficiency but the time resolution would be poorer than what we achieved: 0.4 ns/m. The timing signal from the accelerator is a pulse induced by the passage of the proton pulse through a pick-up electrode placed a few cm in front

of the Li-target (time resolution ~ 0.5 ns).

A $^{6}$Li-glass detector beside the $^{7}$Li-target was used to monitor the neutron flux. The measured time integrated flux for the different samples was used to normalize the time-of-flight spectra to the same total neutron flux.

The neon gas was contained in stainless steel cylinders ( with 0.5mm thick walls, 100 mm length, 28 mm diameter ) mounted on an automatic sample changer with 5 sample positions : 3 containers with the neon isotopes,an empty container, and a position with no container. The 5 transmission spectra were cyclically measured, each of these short runs lasting about 10 minutes. The collimated neutron beam at the sample position had a smaller diameter than the container, to prevent it from touching the 10 cm long walls. The neon gas inside the containers was under a pressure of up to 150 atmospheres.

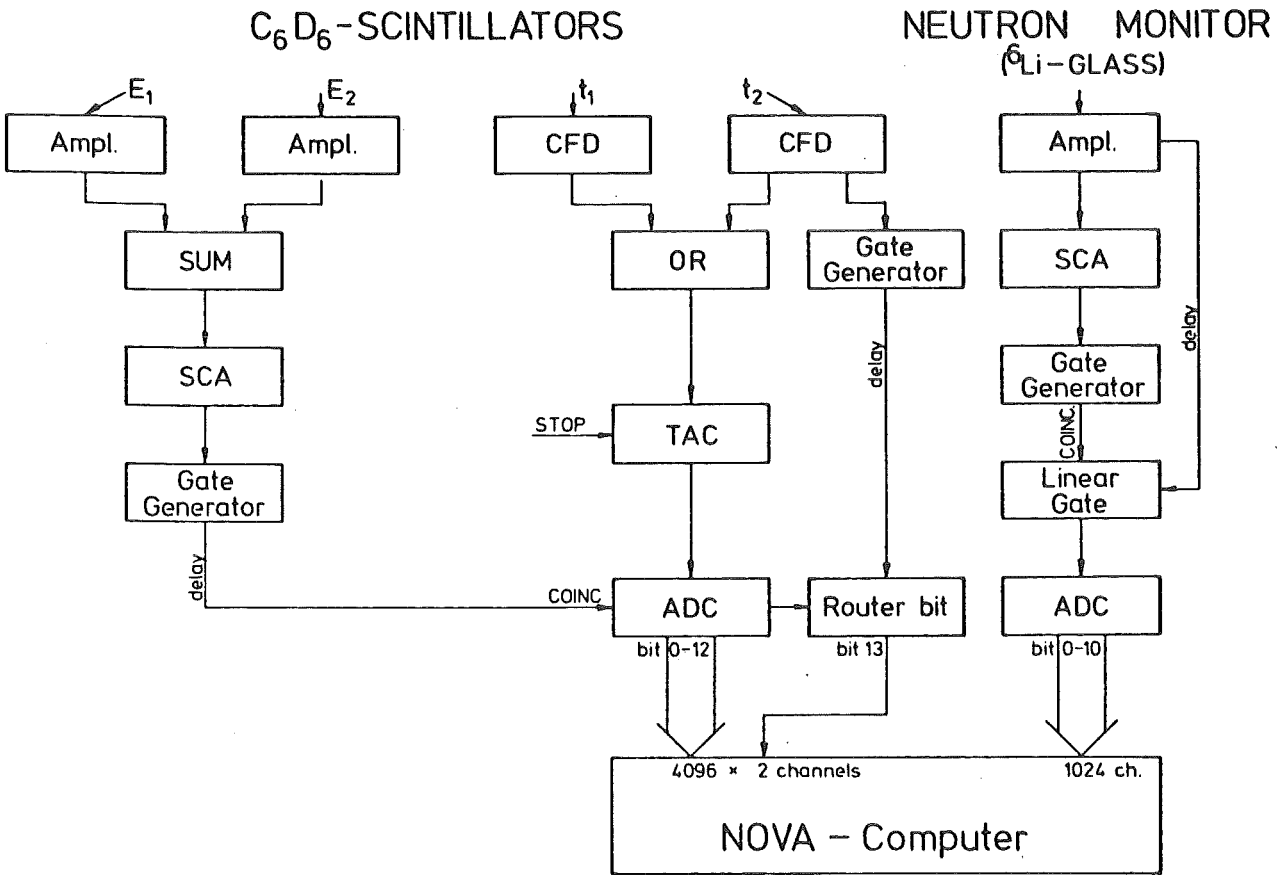


Fig. 4. Data acquisition electronics for neutron total cross section measurements.

The electronics and a TOF (time-of-flight) spectrum are shown in Figs. 4 and 5, respectively. The TOF spectrum of each detector was recorded separately. The anode signals from the photomultipliers trigger the constant fraction discriminators, which start the time-to-amplitude (TAC) converter; the stop signals come from the accelerator, at its repetition frequency. In this way the TAC dead time was kept to a minimum, being triggered only when an event was detected, with a frequeny of a few hundred Hz instead of the accelerator's 250 kHz. With this arrangement, the TAC output gives the time interval between an event and the arrival at the Li-target of the next proton pulse. The time zero point in the TOF spectrum is given by the position of the $\gamma$-peak, which is due to $\gamma$-rays produced when the proton pulse hits the target. The $\gamma$-peak width of 1.2ns gives an upper limit of the time resolution. The neutron TOF is then counted from right to left as shown in Fig. 5a, the zero TOF channel being given by the $\gamma$-peak position with a small shift to account for the flight time of the $\gamma$-rays. The small time dependent background starting just after the $\gamma$-peak is due to neutron captures, at a very short flight path, by the material surrounding the Li-target. The narrow spikes appearing at regular intervals (corresponding to the frequency of the bunching system) are secondary $\gamma$-peaks, due to bunching of the very weak residual proton current in the accelerator between pulses.

In order to reduce the background, the pulse height signals (taken from the 10th dynode of the photomultipliers ) went through a single channel analyzer with a window corresponding to a 90-480 keV $\gamma$-ray energy range.

The pulse height spectrum of the Li-glass neutron monitor was stored in a 1024 channel spectrum (Fig. 5b).

The spectrum from each detector was independently measured,by identifying the detector in which each event originated through a router bit. For each of the short 10 minute runs, the two spectra were compared in order to detect any anomaly in the operation of one of the detectors.

The data were acquired in a Data General NOVA-2 computer, and the accumulating spectra displayed on a CRT screen. The spectra from each of the 10 minute runs were sequentially written on magnetic tape. The summing of these short runs and all the data analysis, were carried out with an IBM 370/168 computer.

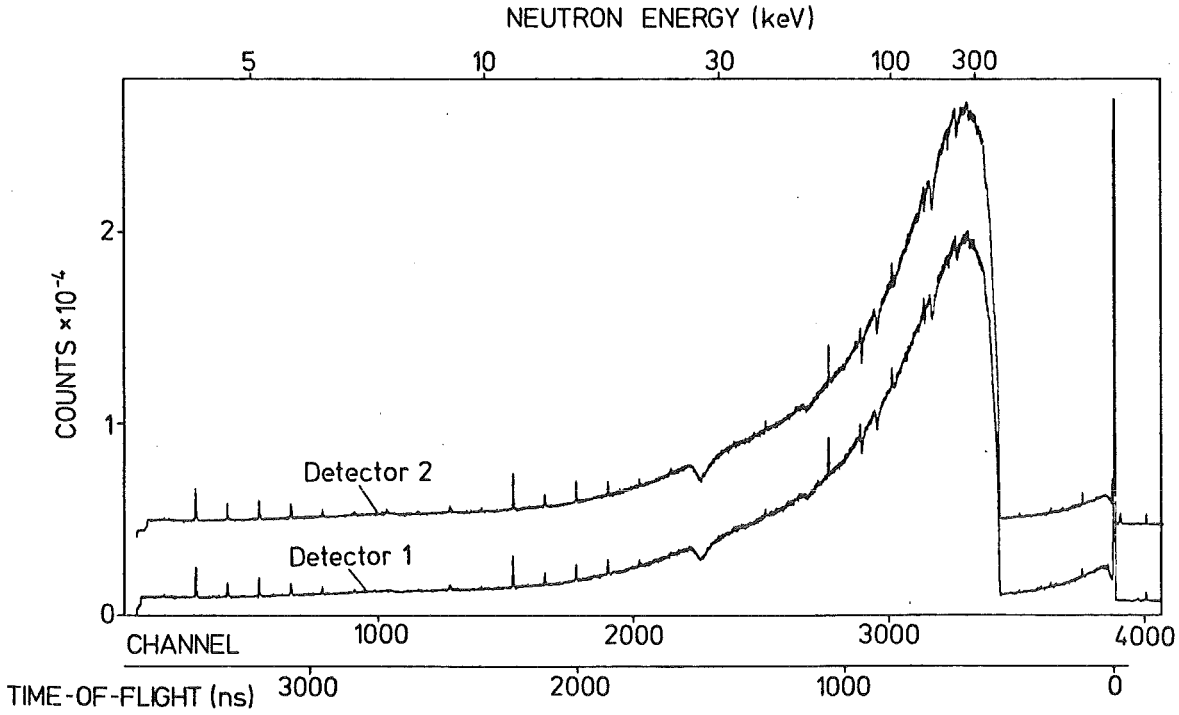


a)

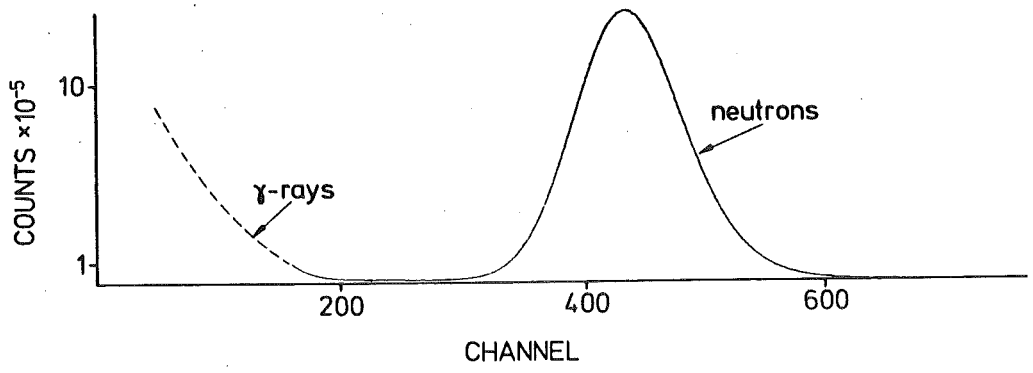


b)

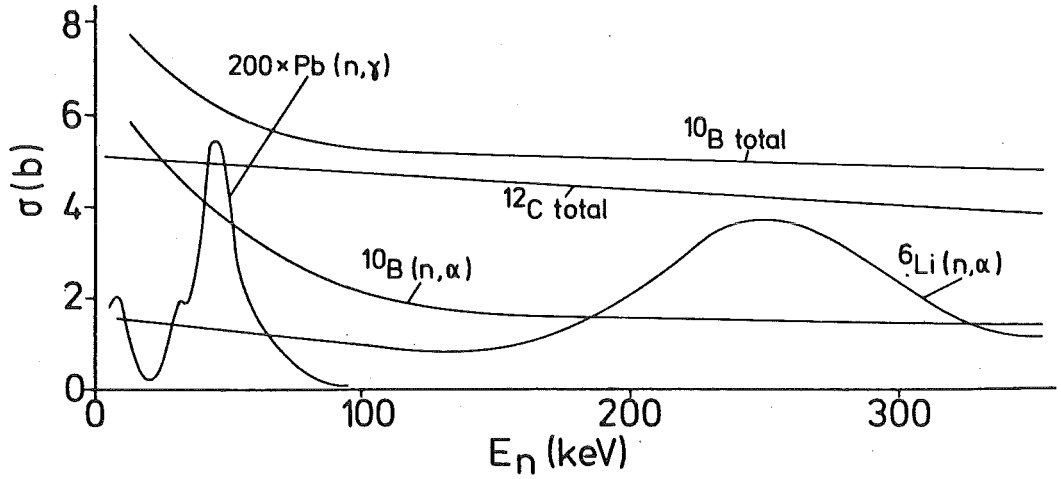


c)

Fig. 5 a) TOF spectra of the empty container (the curve for detector 2 is shifted).

b) Pulse height spectrum of the neutron monitor.

c) Cross sections of some shielding materials.

## II.2. Data Anaysis and Results

The transmission of a sample, at any neutron energy, is

$$T = \frac{z-u}{z_o-u_o} \qquad (1)$$

where z is the total count rate and u is the background, $z_o$ and $u_o$ corresponding to the position with no sample.

The background can be determined in the region to the right of the $\gamma$-peak (Fig.5a), provided that it is time independent.This is the purpose of the paraffin blocks placed after the sample and before the lead shielding (Fig.3): they prevent the fast neutrons from reaching the lead shielding, where they would produce a time dependent backgroud through Pb(n,$\gamma$). By measuring the TOF spectrum with the $^{10}B$ slab removed from the beam path, it was verified that the spectrum was flat.

Another time dependent component of the background is due to capture of of neutrons scattered by the $^{10}B$. This small component was found to amount to less than 1 % of the signal ( the relevant cross sections are shown in Fig. 5c), and was also experimentally checked by a separate run with a lower maximum neutron energy, $E_{max}$ = 35 keV. The TOF spectra for $E_{max}$ = 350 keV and $E_{max}$ = 35 keV , after subtraction of the time independent background, are sketched in Fig.6. The broken curves represent, greatly exaggerated, this background due to scattered neutrons. After being scattered by the $^{10}B$ slab, these neutrons must still travel a minimum

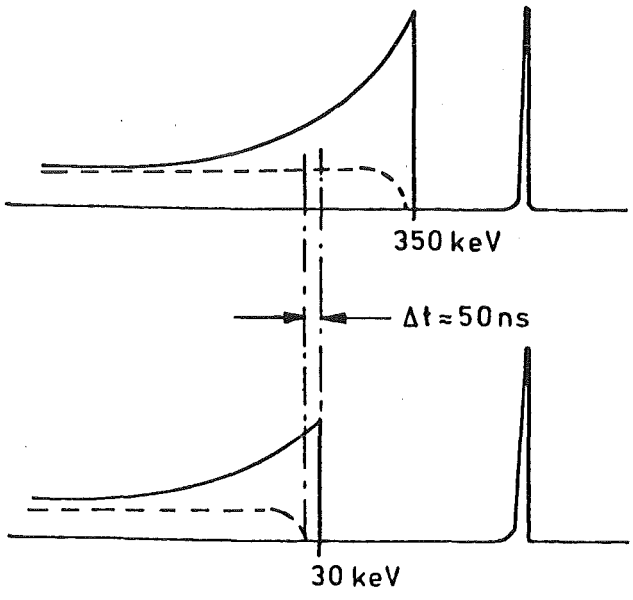


Fig. 6.
Schematic TOF spectra illustrating the direct measurement of a possible background due to sample scattered neutrons.

distance of about 10 cm before being captured (mainly in the lead shielding) and are therefore detected later than those captured in the $^{10}B$. Because of this time delay ( about 50 ns for 30 keV neutrons ) the TOF spectra, after the arrival of the fastest neutrons, have some TOF channels free of background. In the interval, $\Delta t$, shown in Fig.6 the $E_{max}$ = 350 keV spectrum has some background, whereas the $E_{max}$= 30 keV spectrum has none. For all neon isotopes, the cross section in this small energy range was calculated for both runs and found to be equal within the experimental error, thereby confirming that this background was negligible.

The transmission of a neon sample is

$$T_{sample} = T_{empty} \times T_{Ne} \qquad (2)$$

$T_{Ne}$ being the transmission of the neon gas alone, and $T_{empty}$ that of the empty container. The neon cross section is, since $T_{Ne} = \exp(-\sigma n)$,

$$\sigma = \frac{-\ln T_{Ne}}{n} \qquad (3)$$

If in eq.(1) we take $u = u_o$ , a condition met to better than 5% by our data, we find for the statistical uncertainty of T

$$\frac{\Delta T}{T} = \left[\frac{1+T^{-1}+2v(1+T^{-2})}{z_o-u_o}\right]^{1/2} \quad , \quad v \equiv \frac{u_o}{z_o-u_o} \qquad (4)$$

Taking eq.(2) into account, for the neon cross section uncertainty we get

$$\frac{\Delta\sigma}{\sigma} = \frac{[f(T_{sample})+f(T_{Ne})]^{1/2}}{-\sqrt{z_o-u_o}\ \ln T_{Ne}} \qquad (5)$$

where $f(T) = 1 + T^{-1} + 2v(1 + T^{-2})$

Two series of runs were performed: one covering the neutron energy range 5 - 350 keV, with the accelerator operating at 250 kHz repetition rate, and using 4096 TOF channels; the other covering the range 130 - 800 keV, at 1 MHz with 1024 TOF channels.

The total cross sections are shown in Fig. 7. The results from the two runs are in excellent agreement in the overlapping energy interval. The curves labeled $^{20}Ne$ correspond in fact to natural neon, which contains

9 % of $^{22}$Ne (whence the small bumps at the energies of $^{22}$Ne resonances). For $^{21}$Ne at neutron energies above 250 keV, conflicting cross section values were obtained for many runs, and no plausible explanation was found for this behaviour. In addition, the error bars for $^{21}$Ne are much larger than for the other isotopes, because only 1 l of this expensive isotope was available.

The systematic error is much smaller than the statistical uncertainty, which alone is included in the error bars plotted in Fig. 7.

For neutron energies >30keV, we estimate the systematic error on these cross sections to less than 0.5%, resulting mainly from the error on n in eq.(3), determined by the difference in weight between filled and evacuated sample containers. Since the transmission was higher than 95% for all isotopes,the effect of multiple scattering is totally negligible.

For neutron energies < 30keV, where the signal, z-u, decreases sharply, the error introduced by neglecting the time dependent background from scattered neutrons increases rapidly. In the worst case, this background would be as large at $E_n$=5 keV as at $E_n$=30 keV, where it represents at most 1% of the signal; in this case, the systematic error would still be <5% .

For the isolated resonances in $^{20}$Ne and $^{22}$Ne having a width large compared to the experimental resolution,which is less than two TOF channels, the spin of the compound nucleus can be immediately obtained. The Breit-Wigner dispersion formula gives for the peak height of the total cross section the value $\sigma_{max} = 4\pi \lambda\!\!\!^{-}_0 (2J+1)/2(2I+1)$, where I,J are the spins of the target nucleus and compound state respectively, and $\lambda\!\!\!^{-}_0$ is the reduced neutron wave length. The measured peak cross sections clearly show that J=1/2 ( the calculated $\sigma_{max}$ values for J=1/2 are indicated on the cross section plots in Fig. 7). For J=3/2 the calculated $\sigma_{max}$ would be twice as large. The numerical results are given in Appendix 1.

With respect to the analysis of the capture cross sections, it is important to note that none of the neon isotopes has strong scattering resonances in the relevant energy region below 150 keV. This and the small magnitude of the total cross sections means that the effect of sample scattered neutrons on the capture cross section measurement will be small and can be simulated by a graphite scatterer.

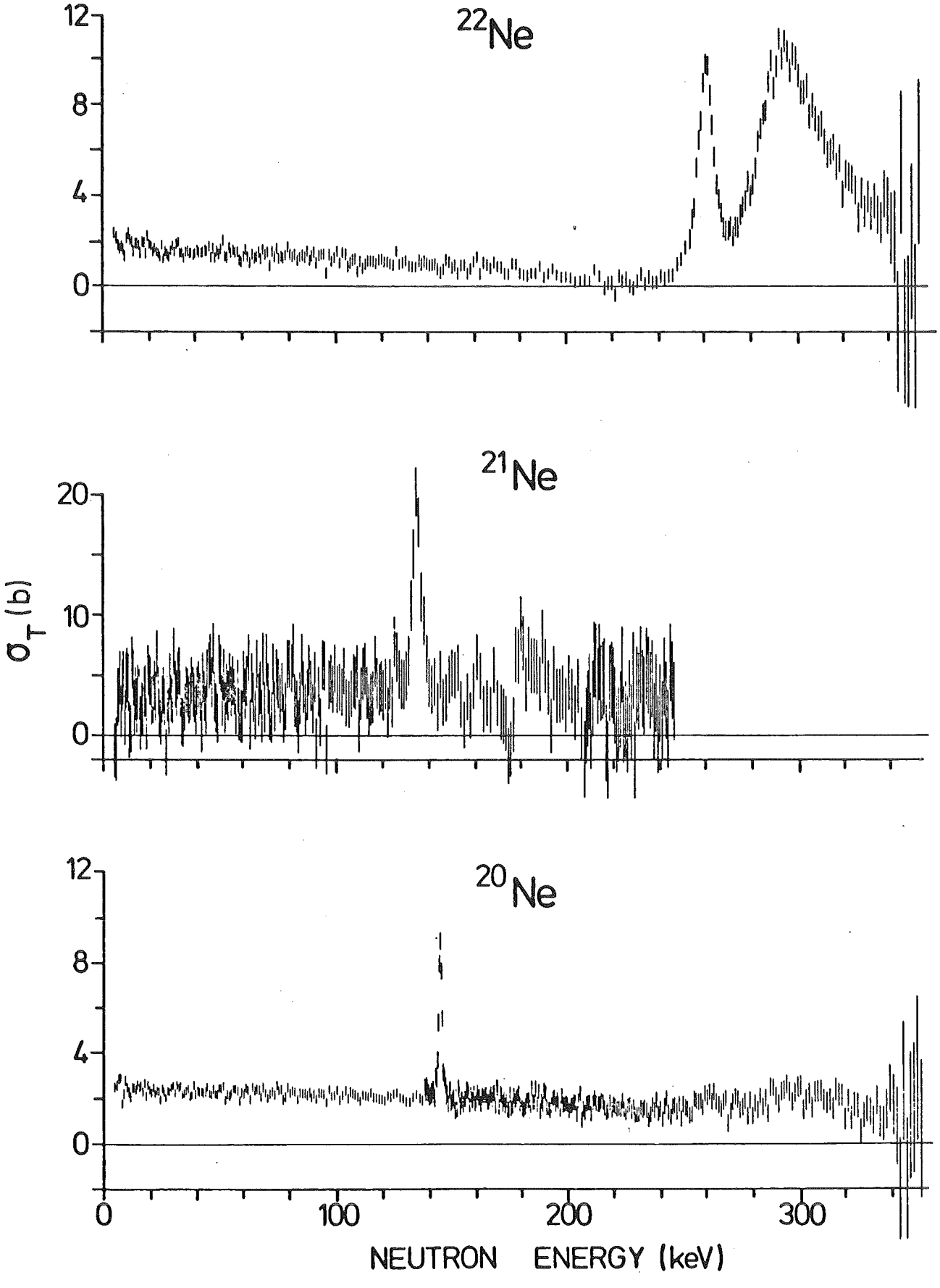


Fig. 7a. Measured total cross sections for $E_n$ < 350 keV.

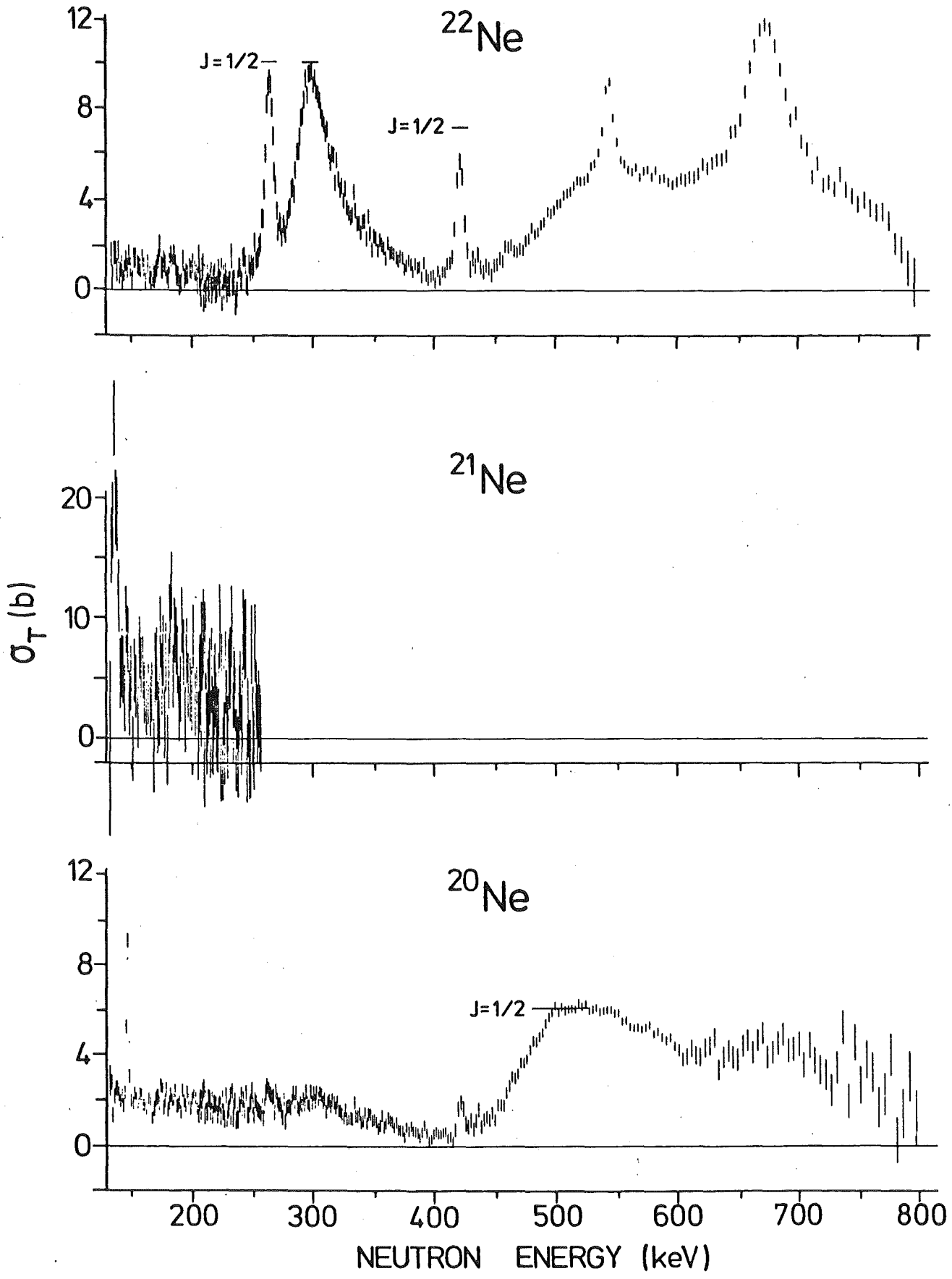


Fig. 7b. Measured total cross sections between 150 and 800 keV.

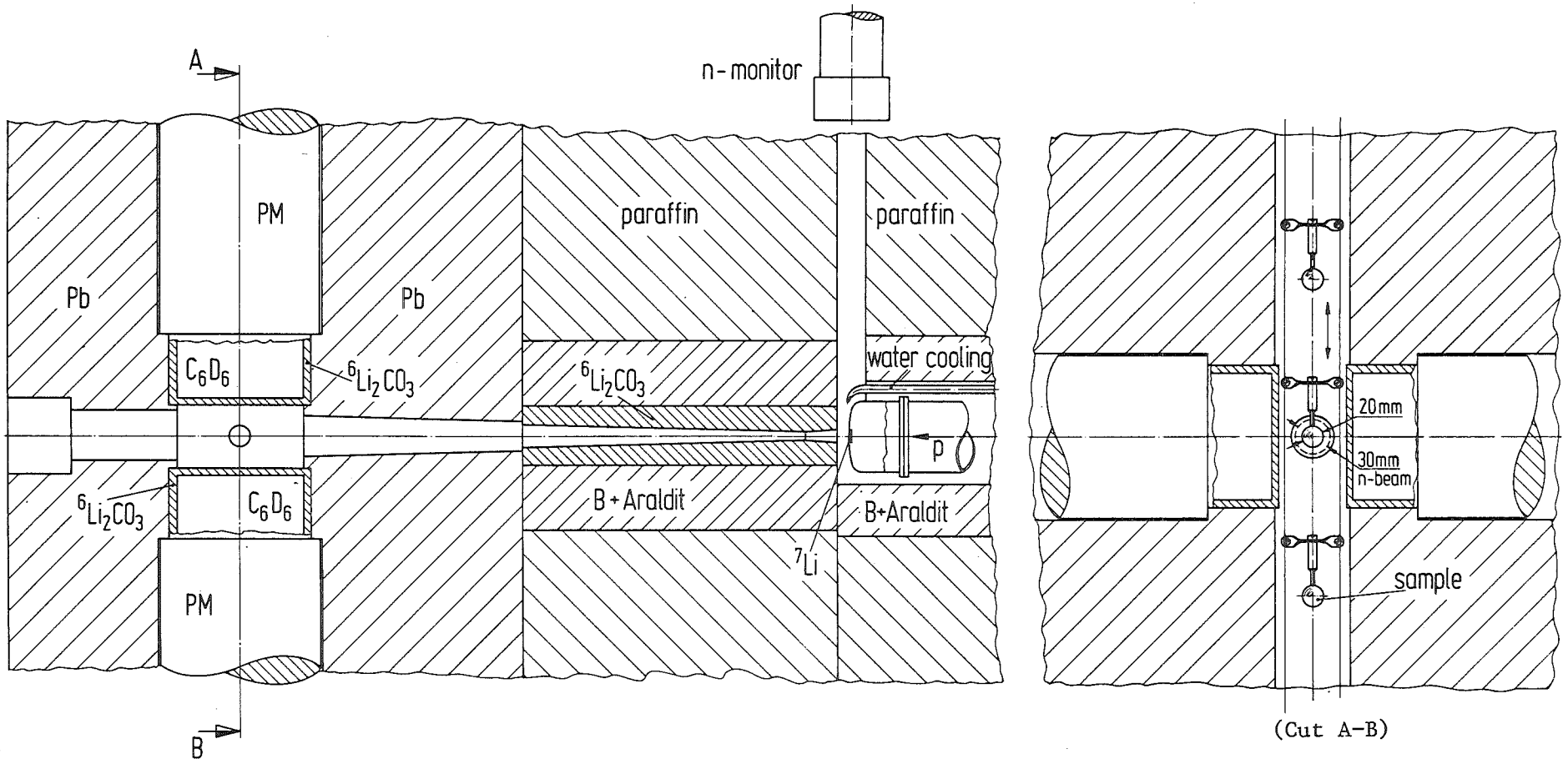


Fig. 8 Experimental set-up of the neutron capture measurements.

## III. CAPTURE CROSS SECTION MEASUREMENT

The capture cross section of the neon isotopes was measured relative to the standard gold cross section /9/. The capture events were counted by detecting the $\gamma$-ray cascades following neutron capture, with the same two $C_6D_6$ scintillators used in the transmission measurement (Section II) The neutron energies were measured by time-of-flight, and the energy ranges 5-200 keV and 170-400 keV were covered. All three isotopic samples were enriched: 99.8% $^{20}Ne$, 95.4% $^{21}Ne$, 99.8% $^{22}Ne$. The total measuring time was about 2 months.

On the automatic sample changer, Fig.8, 6 spherical(20mm diameter, 0.5mm wall thickness) stainless steel containers were placed: 3 with the neon isotopes; 1 empty container; 1 with the gold standard (a 1mm thick disk of of 20mm diameter perpendicular to the neutron beam; 1 with a 20mm diameter graphite sphere, to be used for the background correction. The neon gas was brought into the containers by cooling them with liquid helium; after returning to room temperature, the gas was under pressures of up to 300 atmospheres. The flight path was 60 cm and the total time resolution achieved 1.2ns; at 30 keV neutron energy this led to an energy resolution of 0.7 keV (of which 0.5 keV are due to the flight path uncertainty caused by the 2 cm diameter of the sample).

The experimental set-up for this type of measurement had been previously used at the Karlsruhe Van de Graaff accelerator to measure cross sections of 100 mb and more, with an accuracy of about 2 mb. This sensitivity was comparable to that obtained with an electron linear accelerator ( LINAC ), but was apparently not sufficient for our problem, because the neon cross sections were expected to be very small, only a few mb. If the cross sections were that small ( as indeed they turned out to be) only an upper limit of the cross section would be obtained, and any resonances eventually present could be masked by the background. For this reason, several modifications (III.2) were made in the experimental set-up, which allowed the cross sections to be measured with an accuracy of better than 1 mb.

## III.1. Detection of capture events

For the detection of the γ-rays following neutron capture we had a choice between 3 kinds of detectors: large liquid scintillator tank, Moxon-Rae detector, or Maier-Leibnitz detector. The use of the tank was precluded by its low count rate, due to the required minimum flight path of 150 cm ( compared to the 60 cm we used ) and the corresponding reduction of the accelerator frequency.

We applied the Maier-Leibnitz pulse height weighting technique /10/, described below, to our scintillator detectors; this allowed the ratio no. of captures in neon / no. of captures in gold, to be determined as

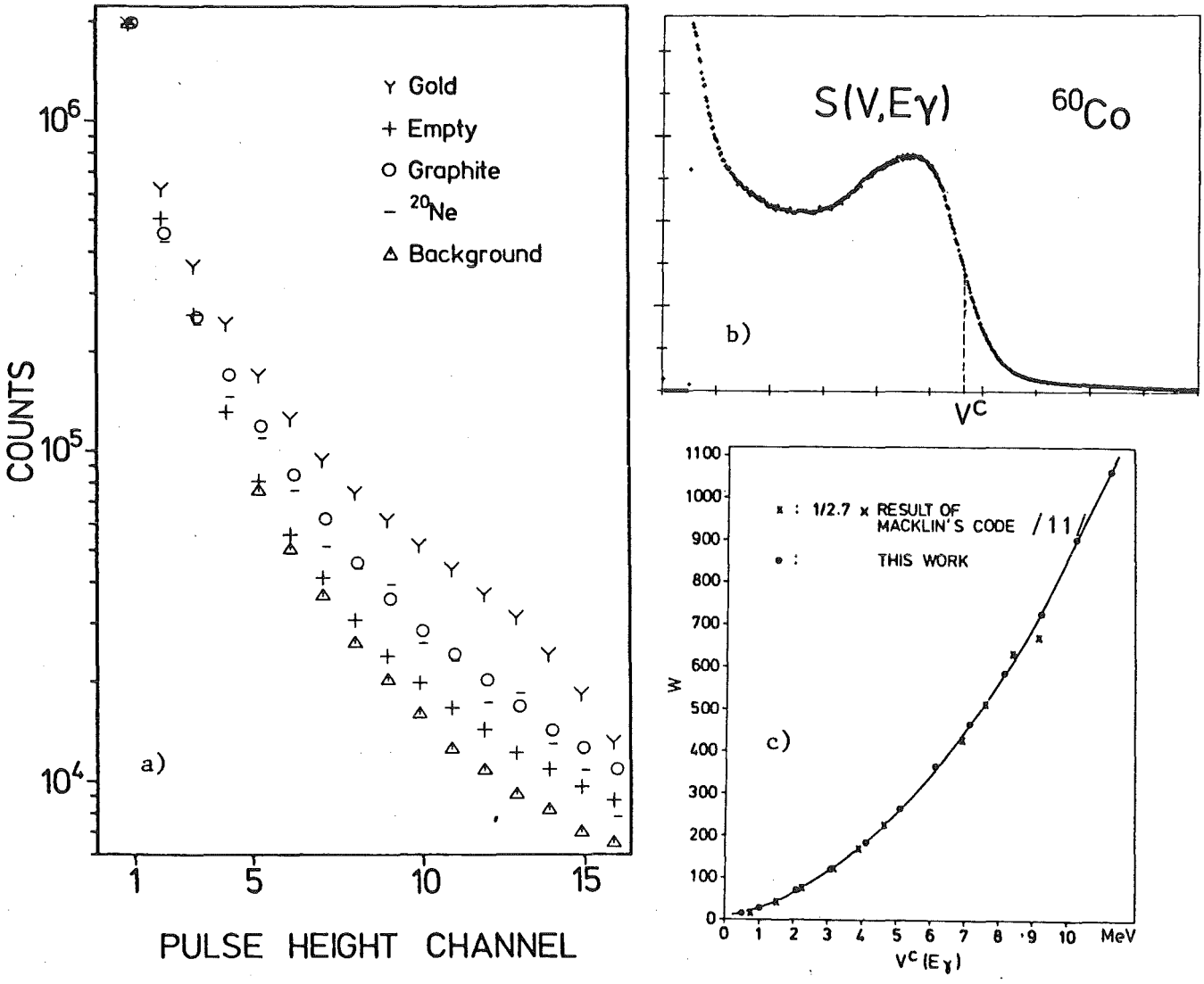


Fig. 9 a) Average pulse height spectra after background subtraction, normalized to a common count rate in channel 1.

b) Pulse height spectrum of a $^{60}Co$ source.

c) Weighting function; $V^c(E_\gamma)$ is the pulse height, at the Compton edge, of the $S(V,E_\gamma)$ spectrum from a gamma-source of energy $E_\gamma$.

a function of only the binding energies, independent of the details of the $\gamma$-cascades. A Moxon-Rae detector would also achieve this, but its efficiency (~1% ) is much lower than that of the scintillators (~20% ), which would require a prohibitively long measuring time. Reducing the flight path would worsen the energy resolution and prevent an effective shielding against the background.

The Maier-Leibnitz weighting technique can be described as follows. Let B be the excitation energy of the compound nucleus, and $E^i_\gamma$ the energies of the $\gamma$-rays in the cascade. Suppose the $\gamma$-ray detection efficiency, $\varepsilon$, is proportional to the $\gamma$-ray energy: $\varepsilon = kE^i_\gamma$.
Then, if we can neglect the probability of detecting more than one $\gamma$-ray per cascade, the probability of detecting the capture event is $\Sigma\ \varepsilon(E^i_\gamma) = \Sigma\ k\ E^i_\gamma = kB$, proportional to B.
Let $S(V,E_\gamma)$ be the detector pulse height (V) distribution produced by a monoenergetic source of $\gamma$-rays of energy $E_\gamma$ , normalized so that $\int S(V,E_\gamma)dV = P(E_\gamma)$ = probabilityof detecting the $\gamma$-ray. If the $P(E_\gamma)$ and the $S(V,E_\gamma)$ curves are known, it is possible to find a weighting function, w(V), such that the weighted detection probability, or efficiency, $\int w(v)\ S(V,E_\gamma)\ dV = f(E_\gamma)$, f being an arbitrary function. For an efficiency linear in $E_\gamma$ the function f is chosen proportional to $E_\gamma$.
The $P(E_\gamma)$ and the $S(V,E_\gamma)$ curves were for our two detectors by F. Hensley/12/, and the resulting weighting function is shown in Fig.9c.
For the implementation of this weighting procedure, the pulse height of each event must be recorded. It is found /12/ that a coarse resolution in V corresponding to 0.5 MeV in $E_\gamma$, is sufficient for a good accuracy of this weighting technique, because the pulse height distributions for our samples ( Fig. 9a ) are all smooth functions of V and have nearly the same shape. This is due to the fact that 1) At any neutron energy, the cascade $\gamma$-rays have a broad distribution of energies (shown in Fig.16 for gold ) with no sharp peaks, and 2) The scintillator pulse height spectrum for any $\gamma$-ray energy ( shown in Fig.9b for $E_\gamma$~1.3 MeV) is also a smooth curve (no photoelectric peak).

In our measurements the pulse height of each event was analysed and recorded in a 16 channel spectrum. The pulse height calibration with respect to $\gamma$-ray energy was done using the relation /13/ between the Compton edge pulse height, $V^C(E_\gamma)$and $E^\gamma$ : $V^C(E_\gamma) \propto E_\gamma/(1+E_\gamma/2m_ec^2)$. This expression was checked between 0.4 keV and 2.3 MeV with a set of monoenergetic $\gamma$-sources.

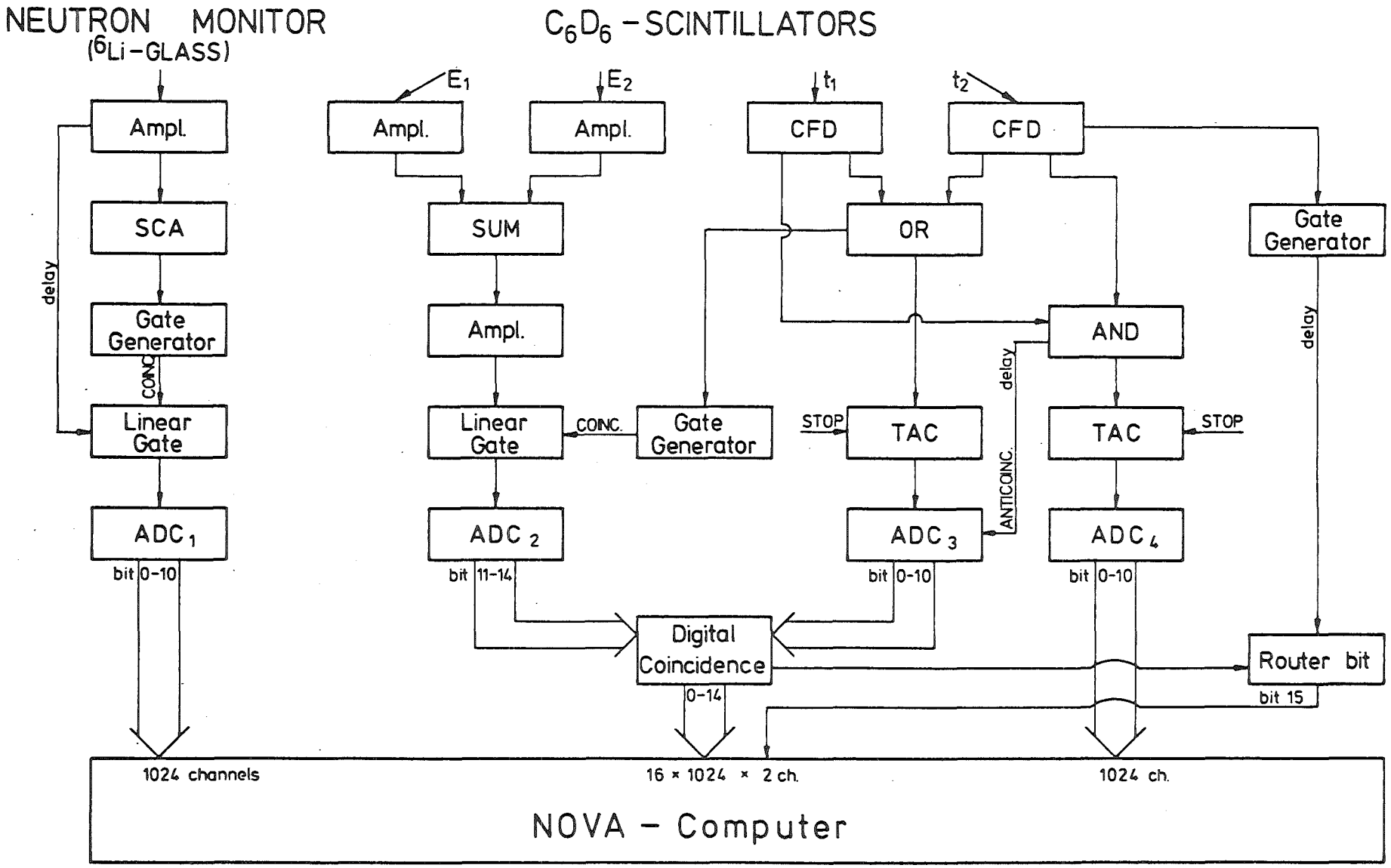


Fig. 10. Data acquisition electronics for the neutron capture measurements.

## III.2. Optimization of the experimental set-up

The experimental set-up (Fig. 8) was essentially the same as used by B. Leugers /14/. After an unsuccessful attempt at measuring the $^{20}Ne$ capture cross section, several improvements were made in the lead shielding, neutron collimation and gas containers.

A new collimator was built that produces a neutron beam of only 30 mm diameter at the sample position, the sample's diameter being 20 mm. The mounting and sealing of the spherical gas containers was redesigned by D. Erbe/15/, dispensing with the bulky and massive gas valves, thus reducing the sample mass by more than a factor 10 and thereby also reducing the scattered neutron background. With these reductions in sample size and neutron beam diameter, the two detectors could be placed closer to the sample, with a gain of 40 % in solid angle, and therefore also in count rate.

An important fraction of the background was caused by neutrons scattered in the sample, thermalized in the $C_6D_6$ scintillator, and subsequently captured in its residual $^1H$ ( the scintillator has a ratio D/H=72) or in the lead shielding. By surrounding the scintillators with a 4 mm thick layer of $^6Li_2CO_3$ , this background was reduced by 60%, which increased the signal/background ratio, and hence the sensitivity, by a factor 2.5 .

Compared to the previous set up, the statistical error on the measured cross sections is reduced by about 40% for the same measuring time.

## III.3. Electronics and data acquisition

Fig.10 shows the electronics. For each detector, the two-dimensional (time-of-flight versus pulse height) spectrum consisted of 16 TOF spectra each with 1024 channels, corresponding to the 16 channels into which the pulse height signals were analysed by ADC 2 . This ADC was operated in anticoincidence with the AND unit, so that the detector in which an event occurred could be identified by the router bit without ambiguity. Coincident events, which were thus rejected from the two-dimensional spectrum, were analysed by ADC 4, and recorded separately in a 1024 channel TOF spectrum (with no pulse height information). 1024 additional channels were used to store the neutron monitor spectrum (Fig. 5b).

Digital ratemeters allowed a permanent control of all relevant count rates. As for the transmission experiment, the 6 samples were cyclically measured for about 10 minutes each, and the data from each of these short runs ( 34×1024 channels ) were sequentially written on magnetic tape.

III.4. Data analysis

Because the neon cross sections are very small, of the order of 1mb only, the neon signal is very weak: about 95% of the count rate is due to the steel container, and must be accurately subtracted. For this reason, extreme care was taken in the summing of the short 10 minute runs: all of them were individually inspected,and the ratios count rate/neutron fluence and signal/background computed, in order to detect any variations of these ratios which, for each sample, should not vary with time.

Only series of runs showing no variation over several hours were summed and normalized to the same neutron flux. Such variations may have several causes: 1) lost timing signals from the accelerator, 2) proton beam not centered on the $^{7}Li$ target, 3) slight changes in the position of the shield blocks after a replacement of the target, which had a lifetime around 30 hours.

The final TOF spectrum was obtained by weighting the count rate of each TOF channel of the two-dimensional sum spectrum, with the weighting function, w, of Fig.9c :

$$Z(t) = \sum_{n=1}^{16} z_n(t)\, w(n)$$

where t is the TOF channel, and $z_n(t)$ is the count rate in the n-th pulse height channel. Fig.11a shows these final weighted spectra for the gold, graphite, empty and $^{22}Ne$ samples.

Since the weight, w(n), increases with pulse height while the measured count rate decreases (Fig.9a), this weighting procedure leads to a larger statistical error than would be obtained without weighting, or if the weighting did not have to be applied independently to each TOF channel. The later possibility could be implemented if the shape of the pulse height spectra changed only slightly with neutron energy (i.e. TOF channel). This is the case for the gold sample, but not for the empty container which, due to its prominent resonances in our energy range, shows important changes in the pulse height spectrum for energy intervals as small as 1 keV.

The extraction of the neon cross section can be described as follows. Let GOLD and NEON be the TOF spectra ( after subtraction of the empty container ) of the gold and neon samples. Before the $\gamma$-flash (to the right of the $\gamma$-peak (Fig.11b) in the TOF spectra ) the count rate would be zero if there were no incoming neutrons. This is not the case,

because part of the neutrons scattered by the samples are captured in the lead shielding, or are thermalized and captured in the residual $^1H$ of the scintillator, the resulting $\gamma$-rays being detected by the photomultipliers. This background, which has a time dependent component from capure in the lead shielding, is not accounted for by the subtraction of the empty container spectrum, and must also be subtracted from GOLD and NEON; this can be done by means of the graphite TOF spectrum, as described later in this section.

After these corrections, the GOLD and NEON spectra contain only events due to neutron capture. Neglecting the small correction for pile-up events (described below), the Maier Leibnitz weighting procedure ensures that the count rates are proportional to the binding energies:

$$GOLD = k\, B_{Au} N_{Au}\, \phi\, \sigma_{Au} \quad , \quad NEON = k\, B_{Ne}\, N_{Ne}\, \phi\sigma$$

where B are the binding energies and N are sample masses in nuclei per unit surface; $\phi$ is the time-integrated neutron flux.

Therefore the neon cross section for each time-of-flight channel, labeled by its corresponding neutron energy $E_n$ , is

$$\sigma(E_n) = \sigma_{Au}(E_n)\, \frac{N_{Au}\, B_{Au}}{N_{Ne}\, B_{Ne}}\, \frac{NEON(E_n)}{GOLD(E_n)} \qquad (6)$$

The cross section of the $^7Li(p,n)$ reaction which produces the neutrons is a smooth function of proton energy /16/; the gold and graphite cross sections are also smooth curves (except for some weak structure in $\sigma_{Au}$). The gold and graphite TOF spectra, after subtraction of the container spectrum, will then contain no structure apart from random fluctuations, described by the Poisson distribution. These spectra are used only as normalization quantities; in the background correction (III.4.b), a fraction of the graphite spectrum is subtracted from the gold and neon spectra, but the statistical fluctuations of the actually subtracted background are already incorporated in the uncorrected spectra. Therefore, the statistical fluctuations of the gold and graphite spectra ( after subtraction of the container) were smoothed out by a polinomial fit procedure, so that only the spectra of the empty container and of the neon samples contribute to the statistical uncertainty of $\sigma$ .

The same procedure could not be applied for the subtraction of the empty container spectrum, because the cross section of iron has many resonances in the neutron energy range measured; the fluctuations in its TOF spectrum therefore cannot be described by a simple Poisson distribution.

a)

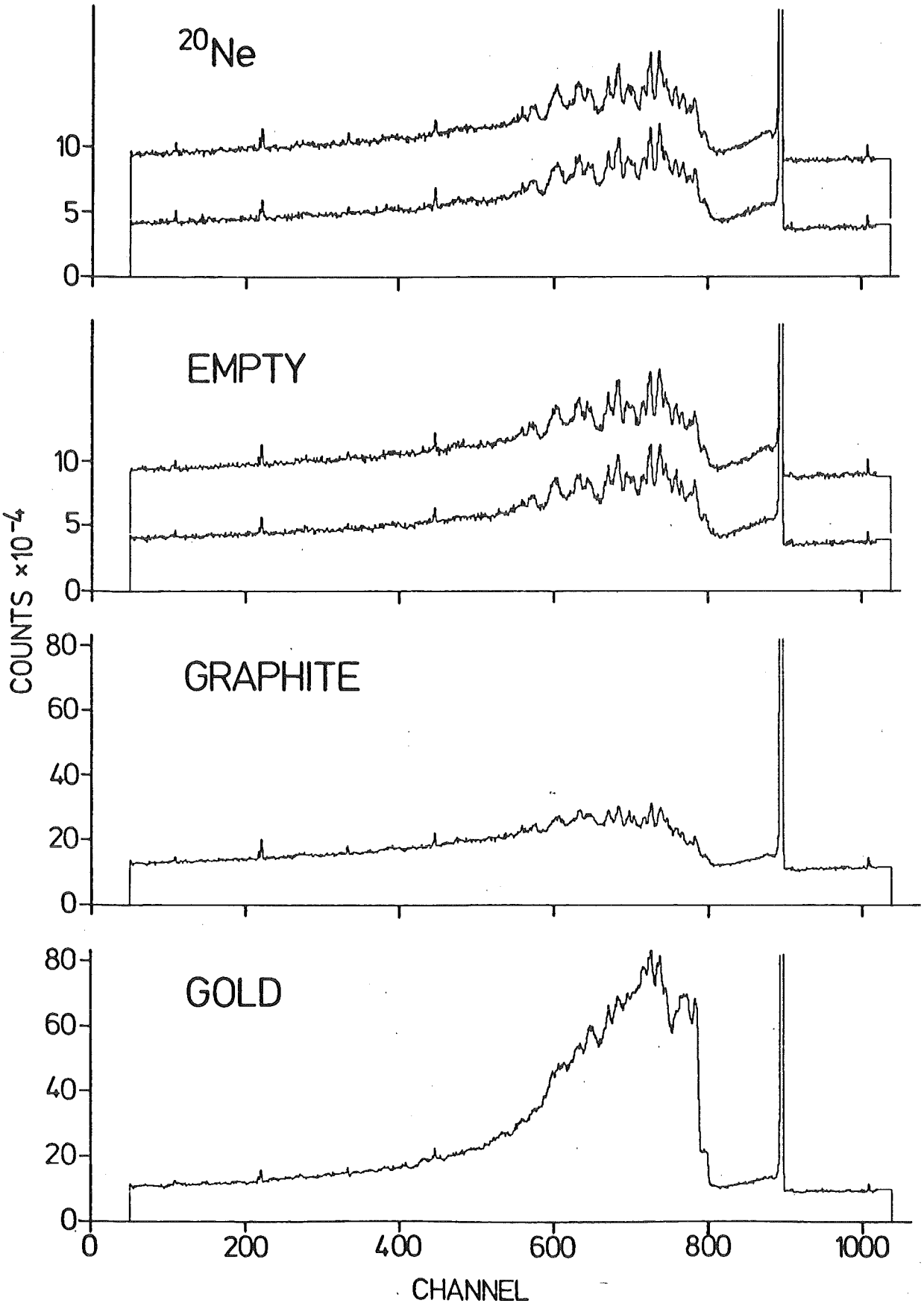


Fig 11a. Weighted TOF spectra before subtraction of the room and container backgrounds. For EMPTY and $^{20}$Ne the spectra from both detectors are plotted independently (detector 2 is shifted upwards).

b)

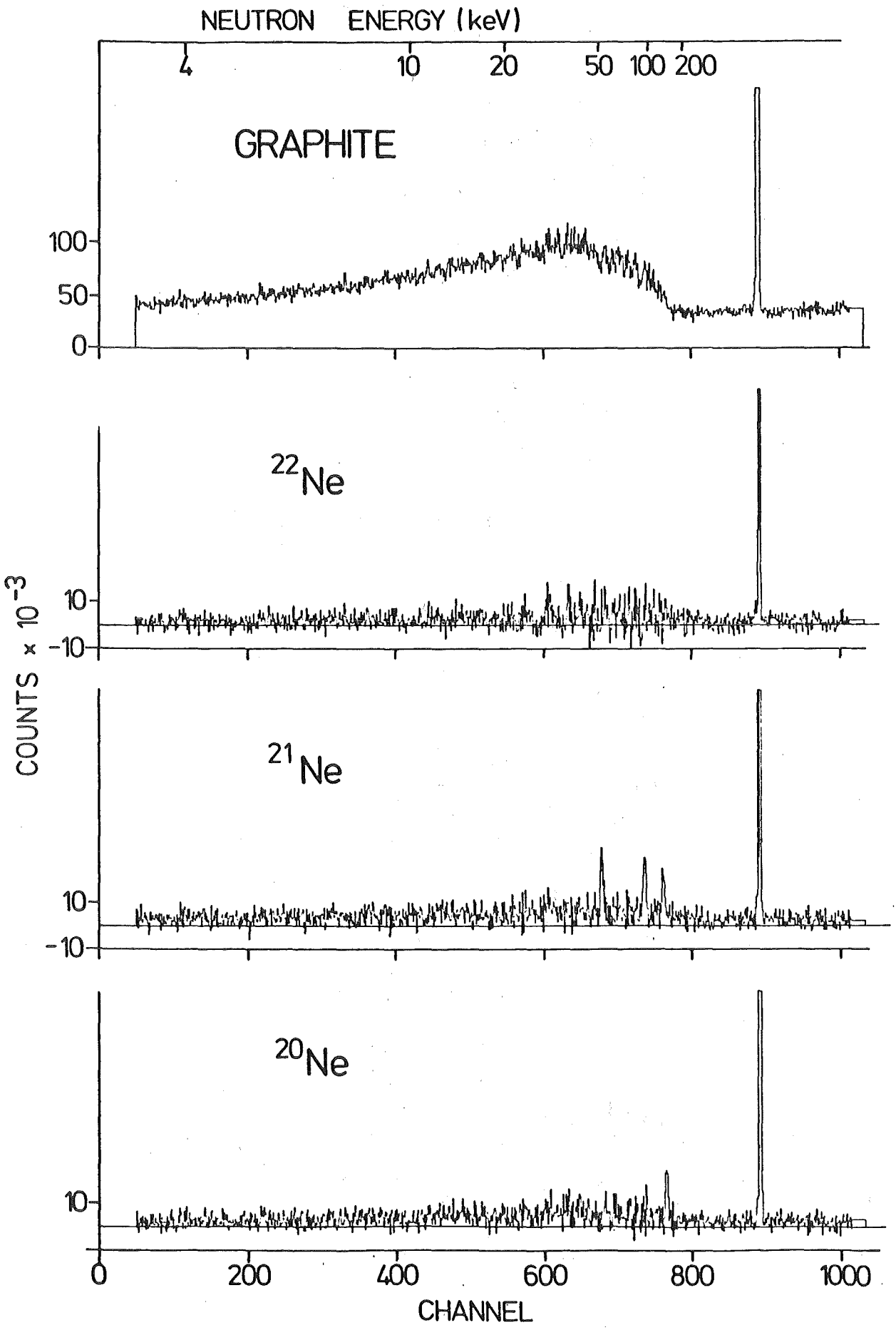


Fig. 11b. Weighted TOF spectra after subtraction of room and container background.

III.4.a. Room background and sample container background

The background count rate to be subtracted is $z_o + m(EMPTY - z_o)$, where EMPTY is the count rate of the empty container, $z_o$ is the time independent room background, always present even if no sample is in the neutron beam, m is the ratio ( sample container mass / empty container mass ). The room background was measured by performing short runs with no sample in the beam.The m-values were determined to an accuracy of 0.05% , by a separate measurement in which all the containers were empty. The weight ratio of containers yields a less accurate m-value, because the comparatively massive valves are not touched by the neutron beam.

In order to account for the effect of the divergence of the neutron beam on the count rates, the distances target-sample were measured with a precision of 0.2 mm, and all the TOF spectra were normalized to a common flight path. This correction amounted to less than 1% of the count rate for all samples, with an associated relative error <0.1% .

The TOF spectra of the three neon isotopes, after subtraction of this background, is shown in Fig.11b. The estimated total uncertainty due to these corrections leads to a systematic error on the final cross sections of about 6% .

III.4.b. Scattered neutron background

After subtraction of the empty container the neon TOF spectrum, NEON , contains a background (sketched in Fig.12 ) which is caused by scattered neutrons, due to :

a) thermalized neutrons captured in the hydrogen of the scintillators and in the lead shielding (time independent).

b) fast neutrons captured in the lead shielding and in the aluminum walls of the scintillator containers (time dependent).

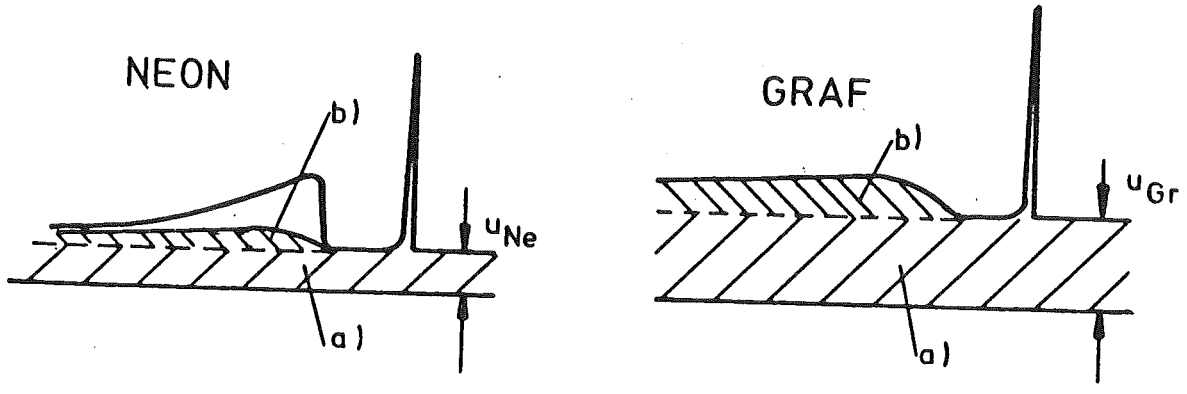


Fig. 12. Background from scattered neutrons.

To estimate this correction,the spectrum of the graphite sample was used. After subtraction of the container spectrum, the graphite spectrum, GRAF in Fig.12, contains only events due to the effects a) and b) because the capture cross section of graphite is practically zero. If the spectrum of effect b) has the same shape in both NEON and GRAF, the correction consists of just subtracting $(u_{Ne}/u_{Gr})\times$GRAF from NEON.

On the other hand, for both NEON and GRAF the count rate from effect a), $u_{Ne}$ and $u_{Gr}$, is proportional to the number of scattered neutrons, $N\int\sigma_T(E)\phi(E)dE$ , where we approximated the scattering cross section by the total, $\sigma_T$. The total cross section of graphite (Fig.5c) is known /17/, and we measured (Section II) that of the neon is. If the neutron flux, $\phi(E)$, were known, we could then calculate the expected ratios $\alpha_{Ne} = u_{Ne}/u_{Gr}$ , and compare them with the values obtained from the measured TOF spectra. In fact, since $\alpha$ is a ratio of two integrals where $\phi(E)$ appears only as a weighting function of $\sigma_T(E)$, only the shape of $\phi(E)$ is needed. This we can get from the measured gold TOF spectrum and its known capture cross section : $\phi(E) \propto GOLD(E)/\sigma_{Au}(E)$.
For $^{20}$ $^{21}$ $^{22}$Ne, we find $\alpha_{20}=0.048$ $\alpha_{21}=0.058$ $\alpha_{22}=0.029$.
The experimental values are 0.060, 0.073, 0.031, respectively, all slightly higher than expected but with the correct relative values. The statistical uncertainty of $\alpha$ is <4% .

The decision wether the calculated or the measured $\alpha$-value should be used for the correction has a noticeable effect on the cross section, because this background represents a large fraction of the total count rate from which it must be subtracted. We now show that the calculated value is the one that should be used.

We can apply the same argument to the GOLD spectrum. The calculated $\alpha$-value is 0.126;the experimental value is 0.358.This discrepancy is much larger than the statistical uncertainty, and is readily explained by the fact that, in the region to the right of the $\gamma$-peak where $\alpha$ is measured, some low energy neutrons ($E_n$=2.2 to 2.5keV) are still arriving from the previous neutron pulse. At this energy gold has a large capture cross section ($\sigma$ = 3 b) and the excess count rate should be due to these capture events.

This also explains the fact that for the neon isotopes the experimental $\alpha$-values are larger than the calculated ones; this excess is smaller than for gold because the ratio $\sigma_{n,\gamma}/\sigma_T$ is also smaller. Using the calculated $\alpha$-values for neon and gold we can compute, for $^{22}$Ne for example, the neon capture cross section in this 2.2 - 2.5keV energy range :
3 b × (0.031-0.029)/(0.358-0.126) = 26 mb; if we take into account the experimental error on $\alpha$, this is in reasonable agreement with the values

measured at higher energies. The calculated α-values, however, are affected by the uncertainty in the quantities entering in their computation, $\sigma_T$ and N; the resulting error on α could be of up to 5% . Fortunately, the range of acceptable values for α can be independently obtained, and even reduced, by the following argument.

Consider the $^{22}$Ne cross sections that are obtained for two different α-values (Fig.13); for readability, each experimental point represents an average over many channels. At neutron energies above 20 keV the cross sections are nearly equal; at lower energies they differ widely. That above 20 keV the cross section is less sensitive to the value used for α, is due to the decreasing fraction of the total count rate that is due to this background.

The experimental value, α = 0.031, leads to negative cross sections, which means that it is too high, as expected. The value α=0.026 is too low, because it leads to a σ(E) curve that is too steep: in this energy range, where no resonances are present, the cross section is due mainly to direct capture (III.5) which is proportional to $E^{-1/2}$. The true σ(E) curve should lie somewhere between the two full lines, that means between σ = constant and $\sigma \propto E^{-1/2}$. The corresponding α-values, obtained by a least squares fit to the experimental points, are 0.0289 and 0.0265. The resulting cross sections differ by less than 10% for neutron energies above 20 keV.

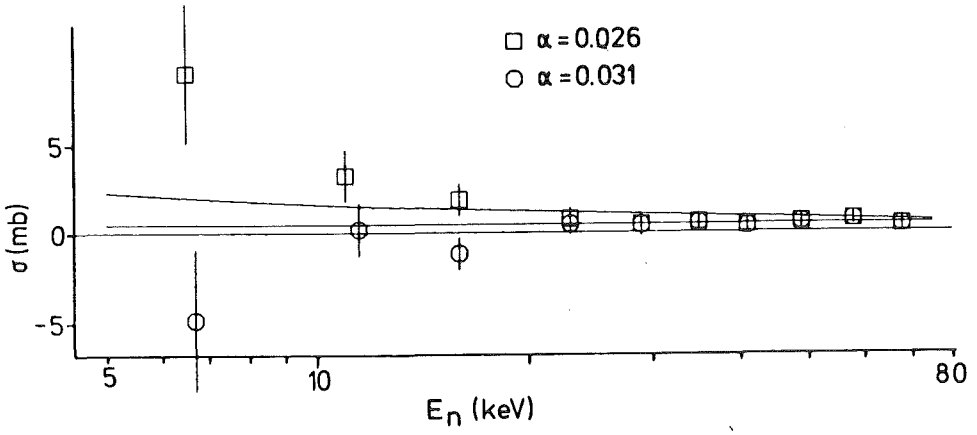


Fig. 13. Effect of the neutron background on the $^{22}$Ne cross section.

A 5% error on $\alpha_{Au}$ results in a systematic error on the neon cross section of about 2% at neutron energies below 10 keV, and much less at higher energies (0.1% at 150 keV).

We have assumed that the TOF spectrum of the time dependent component of this background, b) in Fig.12, has the same shape for NEON and GRAF; this would be exact if the ratio $\sigma_T$(Ne)/$\sigma_T$(graphite) did not depend on

neutron energy. Nevertheless, this is certainly a good approximation: the cross sections ratio does not vary by more than 50%, and it has been experimentally verified ( with a $^{23}Na$ sample ) that even a very strong resonance in the scattering cross section does not produce any detectable time delayed peak in the spectrum.

III.4.c.Correction for pile-up events

The cross section is calculated with the assumption that, for each detector and after applying the weighting function, the count rate is proportional to the binding energy; this would be the case if only one $\gamma$-ray per cascade were detected (III.1). However, given the large solid angle of the detectors seen by the sample, there is a relatively large probability for two (or more) $\gamma$-rays of the same cascade to be simultaneously detected in the same detector; the pulse height of the resulting signal will then be equal to the sum of the pulse heights from each $\gamma$-ray. Since the two detectors are placed symetrically to the sample ( and assuming an isotropic distribution for the cascade $\gamma$-rays),the probabilities of detecting a pile-up event or a coincident event (Fig.14) are equal.

$k_i$ = coincident event
$p_i$ = pile-up event

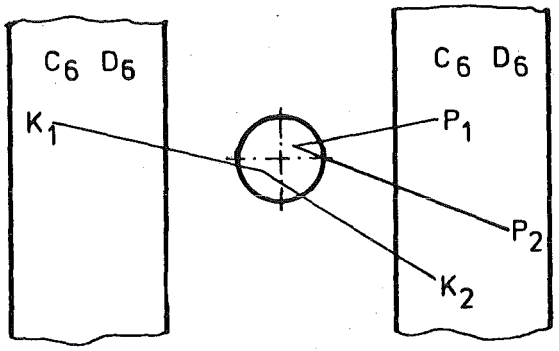


Fig. 14. Coincident and pile-up events.

The coincident events were registered separately, and were rejected from the two-dimensional spectra (III.3). After weighting, since the pulse height distributions of the $k_i$ and $p_i$ are of course the same, these missing events would be exactly compensated by the pile-up events if the weighting function were proportional to the pulse height, which it is not - it grows faster (Fig.9c).

The magnitude of the systematic error thus introduced depends on the cascade multiplicity and on the average $\gamma$-ray energy, and it can be estimated in the following way.

Let $Z_o(t,E)$ be the correct two-dimensional spectrum, i.e., that which

would be obtained if there were no pile-up events ( and therefore also no coincidences ). The total number of events in $Z_o(t,E)$ is the measured one in the two-dimensional spectrum, $Z(t,E)$, plus the coincident events. This number of coincidences we know from the measured coincident spectra;the spectrum $Z_o(t,E)$ was measured for the gold and empty container samples in a separate run, with the detectors operating in coincidence with each other. Fig.15 shows for the gold sample, after subtraction of the container spectrum, the dependence of $Z_o$ and $Z$ on the pulse height. As expected, for any TOF channel, $Z_o$ falls off faster than $Z$ for increasing values of E ( because $Z_o$ contains no pile-up events ); there was no significant change in the spectrum shape for different TOF channels.

After normalizing $Z_o$ and $Z$ to the same total number of counts and applying the weighting function, we find $Z/Z_o = 1.031$, which means that the gold count rate was overestimated by 3% .

The corresponding $Z_o(t,E)$ neon spectra would have taken too long to measure; but their average cascade multiplicity are lower than that of gold,so their excess count rate is less than 3% .Therefore the resulting systematic uncertainty on $\sigma$ is less than 3% .

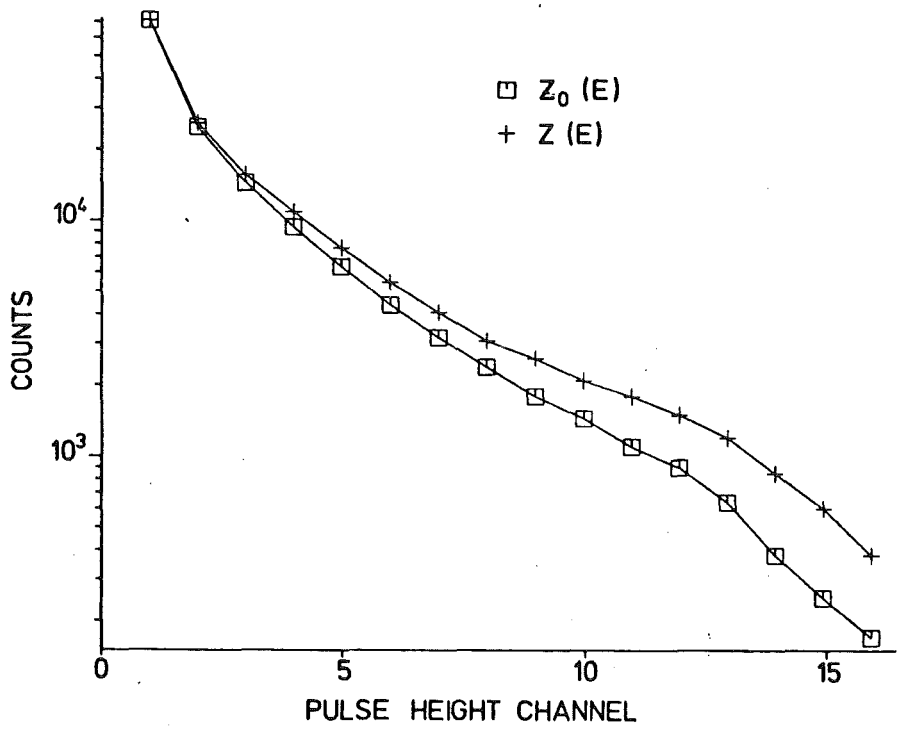


Fig. 15 Gold sample pulse height spectrum with (Z) and without ($Z_o$) pile-up events. The curves are normalized to a common count rate in channel 1.

III.4.d. Lower threshold correction

In a γ-ray cascade there may be transitions with $E_n$ < 90 keV, which corresponds to the lower threshold of the linear gate (Fig.10) analysing the pulse height of the events; these events are therefore lost. The γ-ray energy spectrum of the Au (n,γ) reaction is shown in Fig.16 for a neutron energy of 30 keV/18/. About 12% of all γ-rays are below our 90keV threshold; the corresponding missing counts, however, are a much smaller fraction of the total counts because we used the Maier-Leibnitz weighting method, where higher energy γ-rays have a much heavier weight. The correction for the gold spectrum amounts to less than 1% of the weighted count rate. For the neon samples the fraction of γ-rays of energy < 90 keV should be smaller than for gold, because these low energy γ-rays are due mainly to intra-band transitions, and the neon isotopes have a lower density of excited states than gold. Therefore the resulting error on σ should be smaller than 1 % .

The 90 keV threshold was chosen high enough that the maximum pulse height /19/ of a recoil event ( a head-on collision between a 200 keV neutron and a proton in the scintillator ) was below our threshold; with a 60 keV threshold these recoil events produce already a large background.

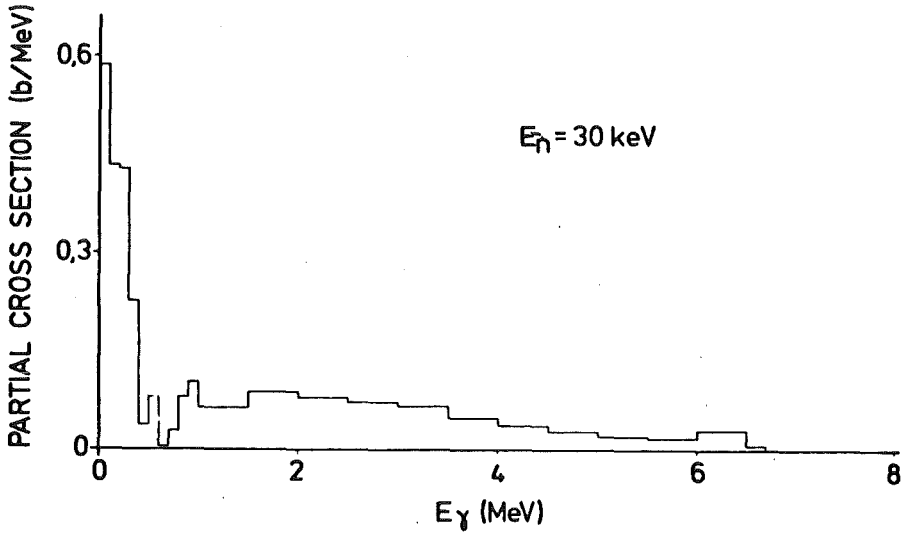


Fig. 16 Energy distribution of capture gamma-rays in gold

III.4.e. Multiple scattering, self-shielding, self-absorption

Multiple scattering of a neutron inside the sample changes the effective sample thickness seen by the neutron. Nuclei in the rear side of the sample see a lower neutron flux, because some of the incident neutrons have been captured or scattered and thus removed

from the beam. Self absorption of capture γ-rays in the sample lowers the detector count rate.

For the gold sample the influence of the first two effects was calculated as a function of neutron energy, with the computer code SESH /20/; the correction factor, f(E), by which the final cross section must be multiplied is largest at neutron energies close to 50 keV: f(50keV)=1.07.

For the neon samples, the self shielding is completely negligible because, with a capture cross section of the order of a few mb and a thickness of 0.01 nuclei/b, the fraction of neutrons that are captured is $< 10^{-4}$.

Multiple scattering is also negligible because all neon samples have a transmission coefficient > 98% and, due to their spherical geometry, the thickness of material crossed by a neutron is very little affected by a scattering event.

The effect of the self absorption of capture γ-rays in the gold would be very cumbersome to calculate accurately, because of the geometry of the problem - the sample (a 1 mm thick disk) is placed perpendicularly to the beam, and the detectors are very close to it. The count rate loss due to this effect has been determined /21/ by an experiment in which the count rates from gold samples of varying thickness (from 0.2 to 1.5 mm) were measured. For our 1mm thickness the correction for γ-ray self absorption amounts to (6±1)% .

III.4.f. Sample thickness

The sample thickness (number of nuclei per unit surface), N in eq.(6), is calculated in a straightforward way for the gold sample. For the spherical neon and graphite samples, N was calculated as follows.

Consider the volume between two cylinders along the beam axis ( Fig.17 ) of radius h and h+dh. This volume element has a length $l = 2\,(R^2 - h^2)^{1/2}$. and an area $2\pi h\,dh$ exposed to the beam; its thickness is $n_s = \rho l(h)$ nuclei/cm$^2$ where $\rho = Z/V$, Z is the total number of nuclei in the sample, $V = (4/3)\pi R^3$ .

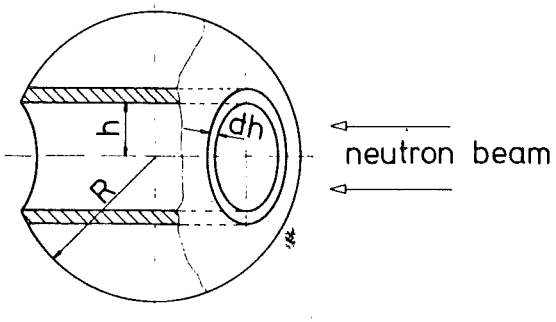


Fig. 17.
The effective sample thickness is calculated as the average over hollow cylinders with wall thickness dh.

The effective thickness is the average $n_s$ for all the volume elements, weighted by their exposed areas: the result is $N = (4/3)\rho R$.

The energy resolution is also affected by the uncertainty in flight path due to the 2 cm diameter of the sample. For 3 different neutron energies, Table 1 shows the energy resolution resulting from this flight path uncertainty, as well as that resulting from the 1.2 ns total time resolution measured at the γ-peak.

Table 1.

| Neutron energy ( keV ) | Energy resolution (keV) Δl | Δt | total |
|---|---|---|---|
| 6 | 0.1 | 0.02 | 0.10 |
| 50 | 1.1 | 0.54 | 1.2 |
| 180 | 3.4 | 3.2 | 4.7 |

## III.5. Differential and Maxwell averaged cross sections

### III.5.a. Differential cross section

The energy ranges 5-200 keV and 170-400 keV were covered by independent runs. The cross sections obtained for the three neon isotopes between 5 and 200 keV are shown in Fig.18, where the error bars represent only the statistical uncertainty.

The two resonances observed in the transmission measurement, at at 137 keV for $^{21}$Ne, and 147 keV for $^{20}$Ne (Fig. 7), are here also clearly observed. Two additional resonances in $^{21}$Ne - at 52 and 98 keV - are here observed that were not detected in the total cross section. All these four resonances show up clearly in the TOF spectra of both detectors, as shown in Fig.19 for $^{21}$Ne. Because of the poor statistics, each experimental point plotted in Fig.18 represents an average over several TOF channels.

For the runs at higher energies, only about two weeks of good data could be obtained, and the uncertainty on the extracted cross section is larger. An upper limit of about 1mb was found for the average cross sections between 200 and 400 keV. The two strong resonances, at 265 keV

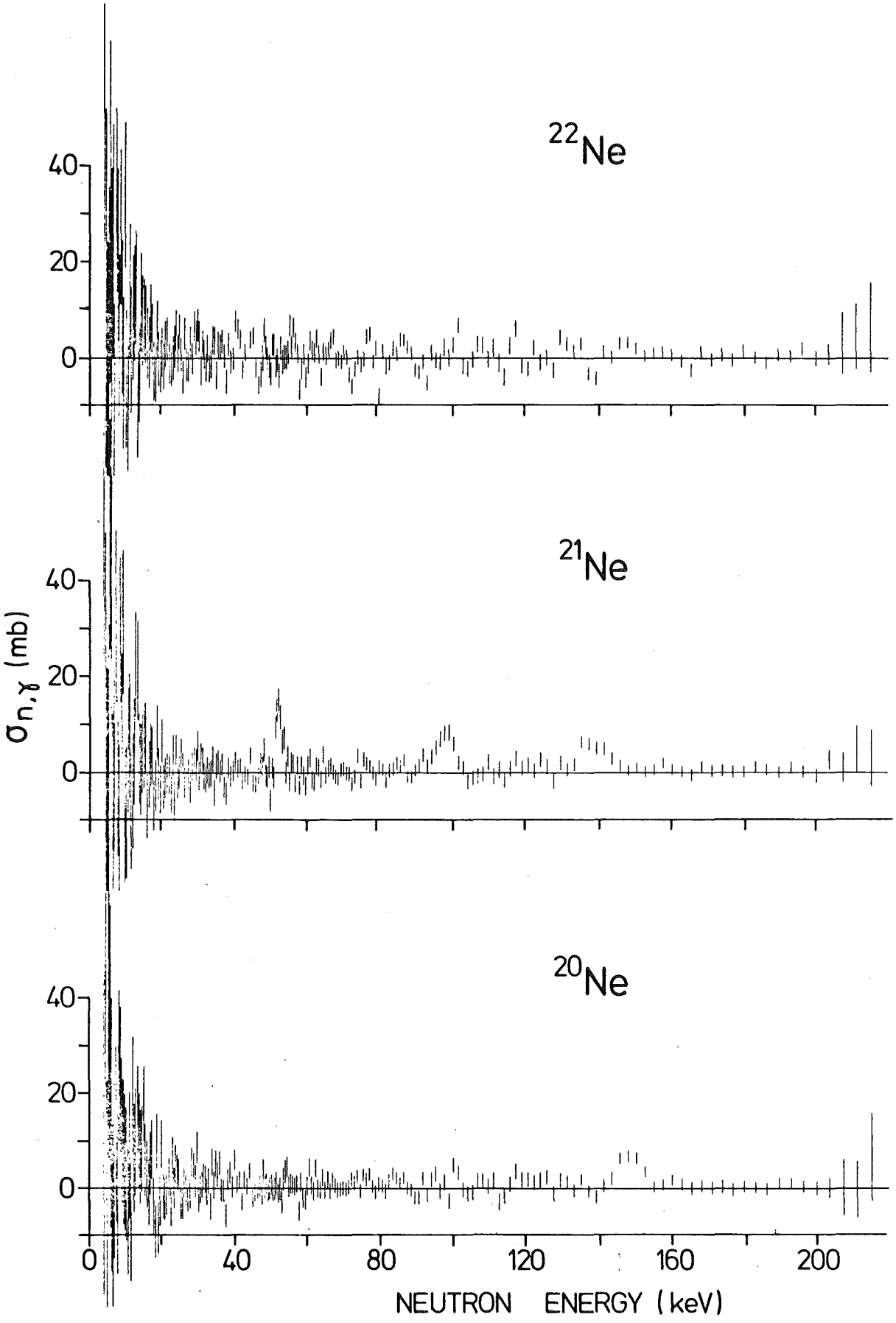


Fig. 18. Measured capture cross sections.

and 304 keV, in the total cross section of $^{22}Ne$ (Fig. 7) are not seen the capture measurement, confirming that the capture cross section must indeed be very small.

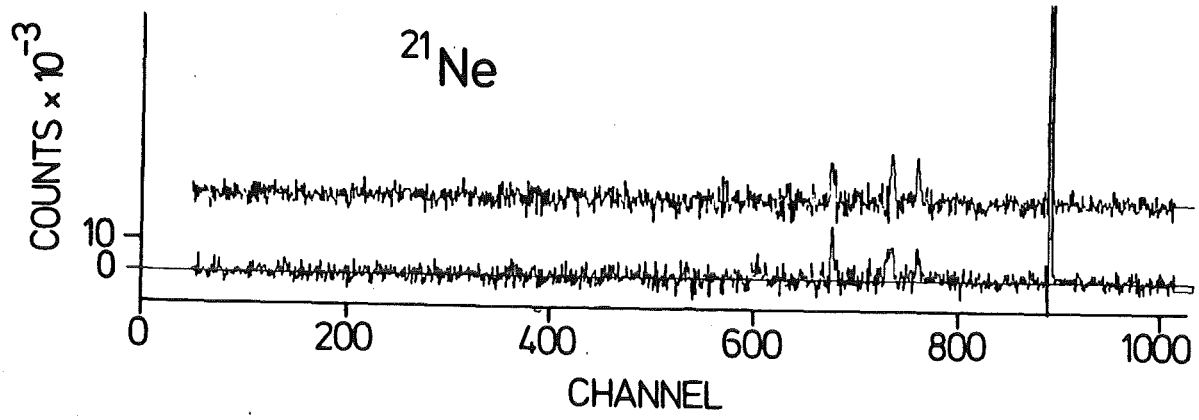


Fig. 19. $^{21}Ne$ TOF spectrum for both detectors after subtraction of all backgrounds.

III.5.b. Maxwellian average cross section

The neutron capture rate for a nuclear species, A, in a monoenergetic neutron flux is $dN_A/dt = -N_A N_n v \sigma$ , where $N_A$ and $N_n$ are the density of A nuclei and of neutrons, and v the neutron velocity. In the interior of a star, considered as a non-degenerate non-relativistic gas in thermal equilibrium at temperature T, the relative velocity, v, between neutrons and nuclei has a Maxwellian distribution /22/

$$\Phi_T(v)\, dv = (m/2\pi kT)^{3/2}\, 4\pi v^2 \exp(-E/kT)\, dv, \quad \text{or} \quad \Phi_T(E)\, dE = 2\sqrt{\pi}(kT)^{-3/2}\, E^{1/2} \exp(-E/kT)\, dE \tag{7}$$

where $E=mv^2/2$ , $m=(M_n M_A)/(M_n+M_A)$.

The capture rate is then $dN_A/dt = -N_A N_n \langle \sigma v \rangle_T$

where $$\langle \sigma v \rangle_T = \frac{\int_o^\infty dE\ \Phi(E)\sigma(E)}{\int_o^\infty \Phi(E)\, dE} \tag{8}$$

The Maxwellian average cross section at temperature T, $\langle \sigma \rangle_T$ ,

is defined by

$$dN_A/dt = -N_A\, N_n\, v_T\, \langle \sigma \rangle_T$$

where $v_T = (2kT/m)^{1/2}$ = most probable neutron velocity. Therefore

$$\langle \sigma \rangle_T = \frac{\langle \sigma v \rangle_T}{v_T}$$

Solving the integrals in (8), one finds /23/,

$$\langle \sigma \rangle_T = \frac{2}{\sqrt{\pi}} (kT)^{-2} \int_0^\infty dE \cdot E \cdot \sigma(E) \cdot e^{-E/kT} \qquad (9)$$

Since our data cover the energy range 5 - 200 keV, we calculated the contribution of the measured cross sections to $\langle \sigma \rangle_T$ according to eq.(8), replacing the integration limits, 0 and ∞, by 5 and 200keV, and approximating the integrals by discrete sums over the experimental points.

Fig.20 shows the maxwellian energy distribution for a temperature of kT = 30 keV (T=3.5 $10^8$ K), and the neutron energy distribution in our measurements. The neutrons of energy $E_n$ > 200 keV make a negligible contribution to $\langle \sigma \rangle_T$. Those in the range 0-5 keV, for which we have no data, represent less than 5 % of the total neutrons; therefore, the resonances eventually present in this energy range would increase the $\langle \sigma \rangle_T$ values in Table 2 by at most a few % .

The estimated uncertainty in $\langle \sigma \rangle_T$ associated with the corrections listed below, amounts to less than 10% .

| | |
|---|---|
| Container subtraction | 6% |
| Pulse height weighting | 0.5% |
| Self shielding and multiple scattering | 2% |
| Self absorption | 1% |
| Pile-up events | 2% |
| Lower threshold | 1% |

It has been mentioned in the previous section (III.4.d) that, for neutron energies below 20 keV, the systematic error from the correction of the scattered neutron background is very large. The total estimated uncertainties given in Table 2 correspond to the two limiting cases for $E_n$ < 20 keV : $\sigma(E) \propto E^{-1/2}$ and $\sigma(E)$ = constant. The third column gives the contribution of the statistical uncertainty. One finds that most uncertainties are negligible compared to that due to the statistics and to the effect of scattered neutrons.

Table 2.

| Isotope | $\langle \sigma \rangle_{30\ keV}$ ( mb ) |
|---|---|
| $^{20}Ne$ | 1.46 ± 0.6 (0.35) |
| $^{21}Ne$ | 1.64 ± 0.8 (0.35) |
| $^{22}Ne$ | 0.93 ± 0.6 (0.40) |

A lower limit for the capture cross section is set by the direct capture process : the potential-scattered wave function of the incident neutron is not orthogonal to the single-particle excited states of the final nucleus, and thus there is a non zero matrix element for transitions from the entrance channel directly to single particle states, without formation of a compound nucleus. An approximate expression for the cross section of such a transition to a s.p. state, i, is /24/

$$\sigma_i = \frac{0.062}{a\ E_n} \left(\frac{Z}{A}\right)^2 \frac{2F+1}{2I+1} S^i\ y^2 \left(\frac{y+3}{y+2}\right)^2 \qquad (10)$$

where $E_n$ is in MeV, I and F are the spins of initial and final states, $a = 1.35\ A^{1/3}$ fm is the nuclear radius, $y^2 = 2ME_\gamma a^2/h^2$ ( M = neutron mass, $E_\gamma$ = transition energy ), $S^i$ is the spectroscopic factor of state i. The total direct capture cross section is $\Sigma\sigma_i$, i running over all s.p. states.

A fairly complete set of spectroscopic factors has been published /25,26/ only for $^{23}Ne$, product nucleus of the $^{22}Ne(n,\gamma)$ reaction; these were measured through the (d,p) reaction. Using the expression above at $E_n$=30 keV, one finds $\Sigma\sigma_i$=0.55 mb. The neutron capture cross section of $^{22}Ne$ could therefore be entirely due to this direct capture process.

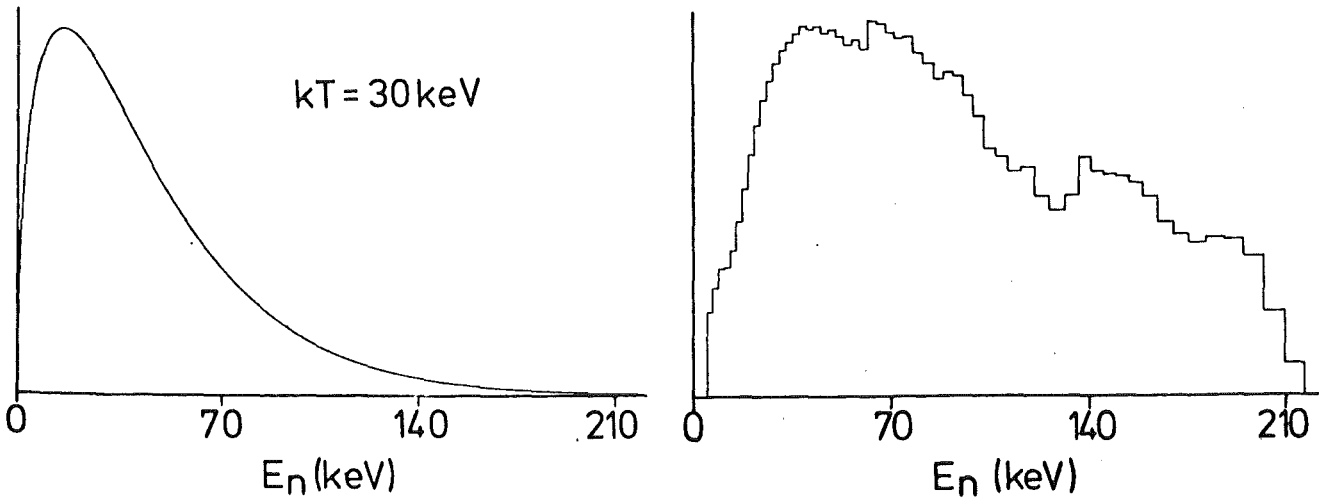


Fig. 20. a) Energy distribution in a thermal bath at kT=30 keV.
b) Neutron energy spectrum in our measurements.

## IV. ASTROPHYSICS

In this section the production and absorption of neutrons in the s-process is calculated, using the distribution of neutron fluences derived from the standard treatment of this process.We then examine the constraints that the requirement of neutron balance imposes on the site proposed by Iben /3,27/ for the operation of the s-process: the He burning shell of a pulsating red giant with the $^{22}Ne(\alpha,n)$ reaction as the neutron source.

### IV.1. The s-process and the σN curve

The equation governing the abundance of any isotope A, during the s-process is

$$\frac{dN_A}{dt} = \phi(t)\ \sigma_{A-1}\ N_{A-1}(t) - [\phi(t)\ \sigma_A + \lambda_\beta]N_A(t) \qquad (11)$$

where $\phi(t)$ is the neutron flux, $\lambda_\beta$ the β-decay rate if A is unstable, σ the neutron capture cross section, averaged over the Maxwellian energy distribution at the temperature T(t). The abundances are expressed in number of nuclei per $10^6$ Si atoms in the solar system.

Three simplifying assumptions/28/ are made:

1) The isotopes on the s-process path are either stable or decay instantly to their daughter nucleus, that is, $\lambda_\beta >> \phi\sigma$ or $\lambda_\beta << \phi\sigma$ . This is corrected for by taking averaged values of σ for the isobars arising at branching points.

2) The temperature is constant during the s-process. This is justified because at the temperatures considered ( kT~30 keV ), the capture cross sections scale about the same way with energy, so that changes in T

affect only the amount of synthesized material, the relative abundances remaining unchanged.

3) As s-process seed only $^{56}Fe$ is considered. This is certainly a good approximation, because the neighbour nuclei in the Fe peak are much less abundant and have a smaller cross section, than $^{56}Fe$.The lighter elements with abundances comparable to $^{56}Fe$ have much smaller cross sections and their contribution to the synthesis of the heavy elements is negligible.

Equation (11) becomes then, introducing the time integrated neutron flux $\tau = \int_0^t \phi(t)dt$ as a new variable,

$$\frac{dN_A}{d\tau} = \sigma_{A-1} N_{A-1} - \sigma_A N_A \qquad (12)$$

Since at time t=0 only $^{56}Fe$ is present, the curve $\sigma N_A(A)$ is a monotonically decreasing function of A, the slope of the curve becoming less steep for increasing values of the total neutron exposure $\tau$.

Let $N^{\bullet}\psi_A(\tau)$ be the $\sigma_A N_A$ value obtained by exposing $N^{\bullet}$ seed nuclei to a neutron exposure $\tau$; Clayton et al./29/ showed that the observed solar $\sigma N(A)$ curve for the s-only isotopes cannot be obtained by such a single neutron exposure. If a total of $N^{\bullet}$ seed nuclei have a distribution of neutron exposures $\rho(\tau)$ - with $\rho(\tau)$ normalized, $\int\rho(\tau)d\tau=1$ - that is, if $N^{\bullet}\rho(\tau)d\tau$ is the number of seeds that had a neutron exposure between $\tau$ and $\tau+d\tau$ ,then the resulting $\sigma N(A)$ curve is given by

$$\sigma_A N_A = \int_0^\infty d\tau \;\; \rho(\tau) \; \psi_A(\tau) \qquad (13)$$

The function $\rho(\tau)$, which describes the neutron exposure history of the s-process seeds, can then be deduced by fitting the $\sigma N(A)$ curve given by (13) to the observed solar $\sigma N$ values of the s-only isotopes. A reasonable fit was obtained /30/ for

$$\rho(\tau) = \frac{N^{\bullet}_{56}}{\tau_o} e^{-\tau/\tau_o} \qquad \text{with } N^{\bullet}_{56} = 5.8\ 10^3, \;\; \tau_o = 0.17 \qquad (14)$$

The expression (13) can be evaluated analytically for an exponential $\rho(\tau)$ distribition, and the resulting $\sigma N$ curve is given /31/ by

$$\sigma_A N_A = \frac{N^{\bullet}_{56}}{\tau_o} \prod_{i=56}^{A} \frac{\tau_o \sigma_i}{1+\tau_o \sigma_i} \qquad (15)$$

For the $\rho(\tau)$ in eq.(14) the total amount of seed nuclei, $N^{\bullet}_{56}$, is much less than the solar system $^{56}Fe$ abundance ( $N^{\odot}_{56} = 8.25\ \ 10^5$ ). Thus, in order to produce the observed heavy element abundances, only a few percent

of the solar system $^{56}$Fe had to undergo the s-process. Since initially only $^{56}$Fe nuclei were present, each heavier nucleus, A, created in the s-process results from the capture of (A-56) neutrons. The total number of neutrons captured in the s-process is then

$$n_c = \sum_{A=56}^{200} (A-56)\, N_A \qquad (16)$$

Expressions (15) and (16) take no account of the α-decays of the Pb and Bi isotopes, at the end of the β-stability valley. But the abundance of the heaviest isotopes, with A>200, is so small that their contribution to $n_c$ can be altogether neglected.

As more accurate neutron capture cross section data became available, especially for the isotopes closest to the $^{56}$Fe seed, it was recognized that a second term in eq.(14) was needed. The best fit to the observed curve, shown in Fig.21 , is obtained /32/ for the distribution

$$\rho(\tau) = \rho_1(\tau) + \rho_2(\tau) = \frac{s_1 N_{56}^{\odot}}{\tau_{01}}\, e^{-\tau/\tau_{01}} + \frac{s_2 N_{56}^{\odot}}{\tau_{02}}\, e^{-\tau/\tau_{02}} \qquad (17)$$

where $N_{56}^{\odot}$ is the solar $^{56}$Fe abundance, and $s_1=(2.7\pm0.2)\%$ , $\tau_{01}=0.056\pm0.005$, $s_2=(0.092\pm0.015)\%$ , $\tau_{02}=0.24\pm0.010$ The first term, $\rho_1(\tau)$, requires a larger ($s_1>s_2$) total amount of Fe seeds than $\rho_2(\tau)$, but with a much smaller number of seeds being exposed to large neutron fluences ($\tau_{01}<\tau_{02}$). As a result, $\rho_1(\tau)$ produces almost no isotopes that are more than a few mass units away from the Fe seed.

## IV.2. Exponential neutron exposure and thermal pulses

The contribution of the first term in eq.(17) to the production of isotopes of mass number A>85 being negligible, the second term alone accounts for the synthesis of the s-nuclides in the mass range 85< A <200. As already noted in I.1, this is precisely the mass range in which the operation of the s-process, in the convective He shell of thermally pulsing red giants, is found to reproduce the solar system σN(A) curve /7/. This is no mere coincidence. It has been shown /33,34/ that the empirically determined exponential neutron exposure distribution, ρ(τ), is a consequence of the following pulsed neutron irradiation model, of which the 7 $M_{\odot}$ star model of Iben /3/ represents a good approximation:

Consider a He shell undergoing short thermal pulses at long time intervals, its mass, M, remaining constant between pulses. At the beginning of each

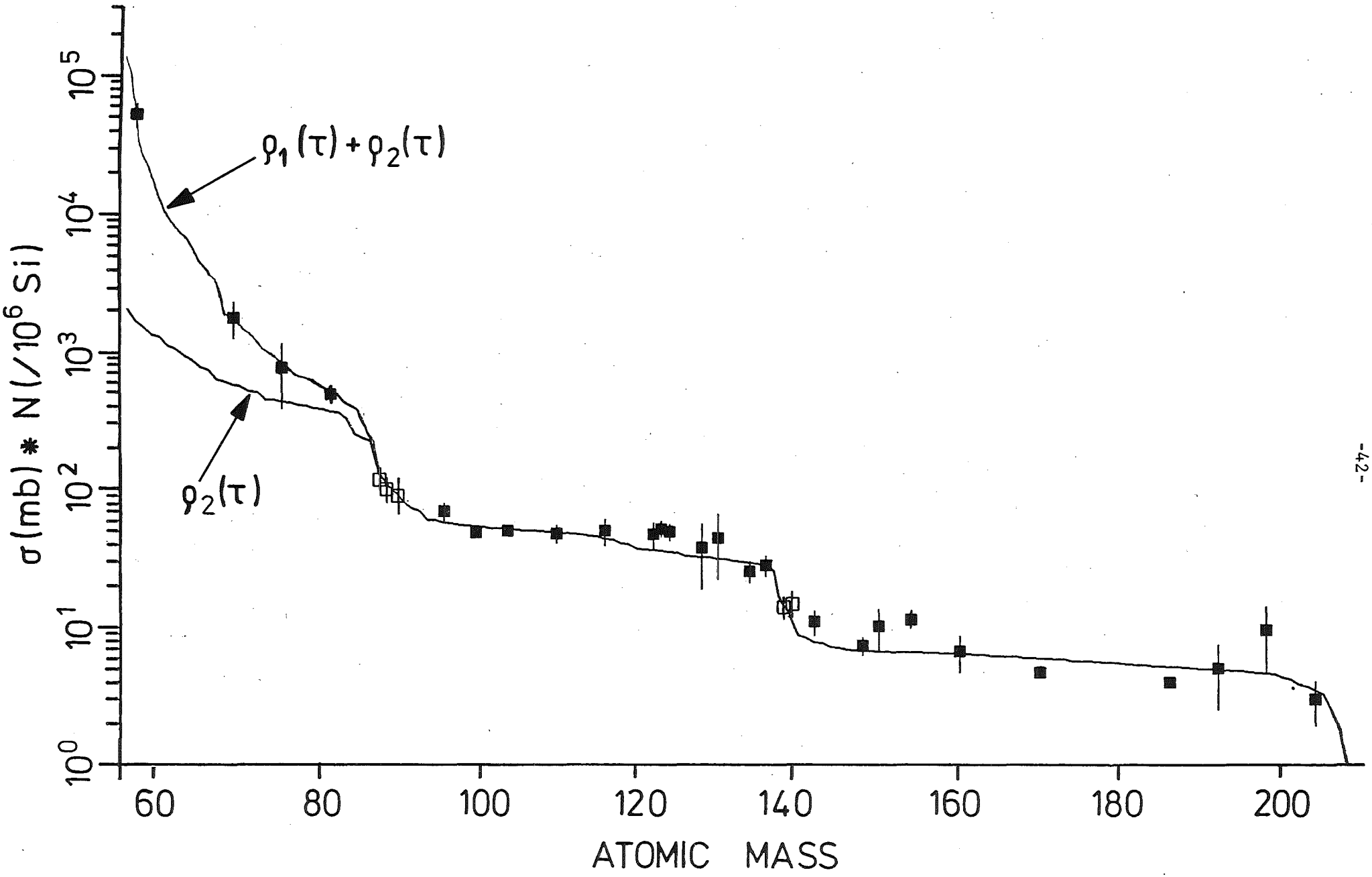


Fig. 21 Calculated solar system σN curve along the s-process path obtained with expression (17). The empirical values for s-only isotopes are represented by solid squares. Open squares denote neutron magic nuclei which are predominantly of s-origin. The error bars include only the cross section uncertainty.

pulse a small amount of matter, (1-r)M , is added to the shell, and the amount (1-r)M is extracted at the end of the pulse. During each pulse a certain number, $\Delta\tau$, of neutrons is released,in Iben's star model through the reaction $^{22}Ne(\alpha,n)$. In the matter introduced at the beginning of each pulse, let $N_A^{\bullet}$ be the abundance of nuclear species A, that is, the number of nuclei A per gram of matter; let $N_A$ be the abundance of A at the end of the pulse, after the $\Delta\tau$ neutrons have been captured. After enough pulses a steady state will be reached, where during the pulse each nuclear species looses as many nuclei by neutron capture as it gains by neutron capture on its progenitor or as new matter introduced in the shell by the convective cell. $N_A$ will then be the same from pulse to pulse.

Take an individual nucleus of $^{56}Fe$, the s-process seed, present in the He shell during pulse number p. The probability that it entered the shell at pulse ( p-i ) is proportional to r , since a constant amount of $^{56}Fe$ per pulse is being added to and extracted from the shell, and r is the mass fraction of the shell that remains after each pulse. Or, since each pulse releases $\Delta\tau$ neutrons, the probability that it has had a neutron exposure of $\tau$ neutrons is proportional to

$$r^{\tau/\Delta\tau} = e^{\ln(r)\ \tau/\Delta\tau} = e^{\ \tau/\tau_0} \quad \text{with } \tau_0 = \Delta\tau/\ln(r^{-1})$$

## IV.3. The s-process neutron balance

The numerical difficulties in the calculation of the evolution of realistic models of pulsating stars /7,35/ prevent a reliable demonstration that the s-isotopes are synthesized by these objects with solar system relative abundances.

An alternative approach, which we take here, is to assume that the operation of the s-process in this environment does indeed produce the observed solar $\sigma N$ curve and, using the standard treatment of the s-process, to determine what conditions should be satisfied by the star model.

We assume that the heavy s-nuclides of the solar system with $A > 85$ were produced in such a pulsing He shell, during each pulse the same amount of fresh matter being brought into the He burning region and the same number of neutrons being produced, so that $^{56}Fe$ had a neutron exposure given by the second term of eq.(17).

At each pulse, along with $^{56}Fe$ other light elements are introduced in the He burning region; hence, they are exposed to the same neutron flux as $^{56}Fe$. Although their contribution to the synthesis of heavy isotopes (A>56) is very small, they nevertheless absorb a considerable fraction of the available neutrons.Each of these light elements is also an s-process seed, building heavier isotopes, A, to abundances given by eq.(15) :

$$\sigma_A N_A(\text{seed}) = \frac{N^{\bullet}_{\text{seed}}}{\tau_o} \prod_{i=\text{seed}}^{A} \frac{\tau_o \sigma_i}{1+\tau_o \sigma_i} \qquad (18)$$

For each heavier isotope, A, thus produced, ( A-seed ) neutrons are captured by its progenitors following the seed.Therefore the s-process progeny of a species 'seed' captures a total number of neutrons

$$n_c(\text{seed}) = \sum_{A=\text{seed}}^{200} (A-\text{seed})\, N_A(\text{seed}) \qquad (19)$$

The total number of neutrons captured during the s-process is $\Sigma n_c(i)$, where i runs over all seeds. We assume that the elements from C to Fe initially present had the same relative abundances as in the solar system ( an assumption discussed below ). As we know the total amount of $^{56}Fe$ processed, $N^{\bullet}_{56} = s_2 N^{\odot}_{56}$ , we know also that fraction of the light isotopes, $N^{\bullet}_{A} = s_2 N^{\odot}_{A}$ , and with (18) and (19) we can compute $\Sigma n_c(i)$. The neutron source is the $^{22}Ne$. Its abundance, $N^{\bullet}_{22}$ , prior to the onset of the $^{22}Ne(\alpha,n)^{25}Mg$ reaction is, since all the C, N and O end up as $^{22}Ne$, $( N_C + N_N + N_O + N_{22} )^{\text{solar}}$, or $N^{\odot}_{CNO}$ for short. A fraction, f, of the $^{22}Ne$ undergoes the $(\alpha,n)$ reaction. The number of neutrons produced is $fN_{CNO}$ ; an amount $(1-f)N_{CNO}$ of $^{22}Ne$ and $fN_{CNO}$ of $^{25}Mg$ are left to act as s-process seeds. One might object that this Ne and Mg left behind as ashes of $^{22}Ne(\alpha,n)$ should not be treated like the other seeds because they are progressively created during the pulse, instead of being brought in with a definite concentration by the convective cell. During the pulse in which they are created, these Ne and Mg will indeed not see the same flux as the Fe seed, but it will already be the case for the next pulse.The argument of the preceding section still holds, except for very small exposures, $\tau<\Delta\tau$ .

Under the conditions /7/ prevailing in the He shell(density~1500 $g/cm^3$, abundance by mass of elements heavier than oxygen > 0.1% ) the neutron half life against capture is much shorter than the free neutron half life. We can therefore write the neutron balance condition

(number of neutrons produced) = (number of neutrons captured)

$$\text{or} \quad f N^{\bullet}_{22} = f\, s_2\, N^{\odot}_{CNO} = n_c(^{56}\text{Fe}) + n_c(^{22}\text{Ne}) + n_c(^{25}\text{Mg}) + n_c(\text{others}) \qquad (20)$$

from which we can extract f since it is the only unknown quantity.

A condition for the validity of this model where $^{22}$Ne is the only neutron source, is that this equation should yield a value $f < 1$.

The solar abundances /6/ and the cross sections used for the isotopes between $^{19}$F and $^{56}$Fe are listed in Table 3 . Where available, experimental $\langle \sigma \rangle_T$ values have been used and the respective uncertainties are given in column 3; otherwise semi-empirical values /32,36/ were adopted. For $f = 80\%$ are also listed :

1) the number of neutrons captured by each seed, $n_c(A)$, given by eq.(19)

2) the ratio, $N^s/N^{\odot}$, of the abundance to which each isotope A is built. This ratio summarizes all contributions, given by eq.(18), from all seeds of mass below A to its solar abundance. Values $N^s/N^{\odot} > 1$ would mean that a larger abundance was built by the s-process than is observed today. No such overproduction occurs, all ratios are <15% .

Abundant isotopes like $^{36}$Ar,$^{40}$Ca,$^{54}$Fe,$^{58}$Ni which are outside the s-process path have also been included, to ensure that all significant neutron sinks are taken into account. Since our main concern is the absorption of neutrons, not the final isotopic abundances, no attempt was made to treat branching points ($^{39}$Ar,$^{55}$Fe) correctly.

For this value of f=80% it is clear that the neutron balance condition (20) is not satisfied: the number of neutrons produced is $fN^{\bullet}_{22} = fs_2N^{\odot}_{CNO} =$ $= 0.80\times0.00092\times3.223\ 10^7 = 2.372\ 10^4$, while $\Sigma n_c = 2.671\ 10^4$. That is, more neutrons would be captured than were produced. The parameter f must therefore be >80% .

For any seed A, $n_c(A)$ is proportional to $N^{\bullet}_A$, as can be seen from eqs.(18) and (19). The only seeds whose abundances depend on f are $^{22}$Ne and $^{25}$Mg. Since $N^{\bullet}_{22} \propto (1-f)$ and $N^{\bullet}_{25} \propto f$, we can write

$$n_c(^{22}\text{Ne}) = (1-f)C_{22} \quad , \quad n_c(^{25}\text{Mg}) = f\, C_{25}$$

From the $n_c$ values shown in Table 3 for a particular f, we get

$$C_{22} = 9280.5 \quad , \quad C_{25} = 18725.1$$

TABLE 3. Neutron absorption by the light elememts for

$f = 80\ \%$ and $\rho(\tau) = (0.00092\ N^{@}_{56}/0.24)\ \exp(-\tau/0.24)$

| Isotope | σ | Δσ | $N^{@}$ | $n_c$ | $N^s/N^{@}$ |
|---|---|---|---|---|---|
| | (mb) | | (/$10^6$ Si) | (/$10^6$ Si) | (%) |
| $^{12}C$ | | | 1.11E+07 | | |
| $^{13}C$ | | | 1.23E+05 | | |
| $^{14}N$ | | | 2.31E+06 | | |
| $^{15}N$ | | | 8.50E+03 | | |
| $^{16}O$ | | | 1.84E+07 | | |
| $^{17}O$ | | | 6.90E+03 | | |
| $^{19}F$ | 0.25 | | 7.80E+02 | 0.1 | 0.02 |
| $^{20}Ne$ | 1.46 | 0.6 | 2.31E+06 | 755.9 | 0.07 |
| $^{21}Ne$ | 1.64 | 0.8 | 7.00E+03 | 2.4 | 5.72 |
| $^{22}Ne$ | 0.93 | 0.6 | 2.82E+05 | 1856.1 | 1.76 |
| $^{23}Na$ | 2.70 | | 6.00E+04 | 39.5 | 1.18 |
| $^{24}Mg$ | 4.20 | 0.5 | 8.34E+05 | 628.4 | 0.07 |
| $^{25}Mg$ | 6.43 | 0.7 | 1.07E+05 | 14980.1 | 8.94 |
| $^{26}Mg$ | 0.09 | | 1.18E+05 | 4.4 | 12.33 |
| $^{27}Al$ | 4.30 | | 8.50E+04 | 67.7 | 0.23 |
| $^{28}Si$ | 2.40 | | 9.22E+05 | 587.0 | 0.07 |
| $^{29}Si$ | 5.40 | | 4.70E+04 | 40.0 | 0.40 |
| $^{30}Si$ | 1.50 | | 3.09E+04 | 18.2 | 0.64 |
| $^{31}P$ | 7.90 | | 6.50E+03 | 8.5 | 0.41 |
| $^{32}S$ | 3.90 | | 4.75E+05 | 509.1 | 0.05 |
| $^{33}S$ | 8.30 | | 3.80E+03 | 4.9 | 2.10 |
| $^{34}S$ | 2.90 | | 2.11E+04 | 21.7 | 0.50 |
| $^{35}Cl$ | 11.00 | | 3.58E+03 | 5.7 | 0.59 |
| $^{36}Ar$ | 8.00 | | 8.93E+04 | 113.1 | 0.05 |
| $^{37}Cl$ | 2.80 | | 1.16E+03 | 1.2 | 4.72 |
| $^{38}Ar$ | 2.60 | | 1.67E+04 | 26.4 | 0.19 |
| $^{39}K$ | 16.00 | 2 | 3.25E+03 | 10.4 | 0.15 |
| $^{40}Ca$ | 6.70 | 0.7 | 6.06E+04 | 178.5 | 0.05 |
| $^{41}K$ | 15.00 | | 2.41E+02 | 1.0 | 4.14 |
| $^{42}Ca$ | 15.60 | 3 | 4.00E+02 | 1.7 | 1.91 |
| $^{43}Ca$ | 62.00 | 7 | 9.10E+01 | 0.4 | 1.99 |
| $^{44}Ca$ | 15.30 | 3 | 1.29E+03 | 5.1 | 0.47 |
| $^{45}Sc$ | 52.00 | | 3.10E+01 | 0.1 | 5.29 |
| $^{46}Ti$ | 20.00 | | 1.90E+02 | 0.7 | 1.87 |
| $^{47}Ti$ | 46.00 | | 1.75E+02 | 0.6 | 0.82 |
| $^{48}Ti$ | 14.00 | | 1.77E+03 | 4.9 | 0.23 |
| $^{49}Ti$ | 23.00 | | 1.32E+02 | 0.4 | 1.58 |
| $^{50}Ti$ | 2.70 | | 1.28E+02 | 0.3 | 5.50 |
| $^{51}V$ | 22.00 | 8 | 2.53E+02 | 1.2 | 0.30 |
| $^{52}Cr$ | 12.00 | | 1.06E+04 | 50.1 | 0.03 |
| $^{53}Cr$ | 24.00 | | 1.21E+03 | 6.6 | 0.14 |
| $^{54}Cr$ | 7.20 | | 3.02E+02 | 1.7 | 1.21 |
| $^{55}Mn$ | 28.00 | | 9.30E+03 | 71.8 | 0.02 |
| $^{54}Fe$ | 28.00 | 10 | 5.24E+04 | 331.2 | 0.03 |
| $^{58}Ni$ | 27.00 | 10 | 3.24E+04 | 250.1 | 0.02 |
| $^{56}Fe$ | 13.20 | 2 | 8.25E+05 | 6147.8 | 0.02 |

TOTAL NEUTRONS CAPTURED : 2.671E+04

For convenience, we adopt a new unit for $\Sigma n_c$ : neutrons per $^{56}Fe$ seed, instead of neutrons per $10^6$ Si atoms. since the number of $^{56}Fe$ seeds is $s_2 N^{\odot}_{56} = 759 /10^6$ Si, only multiplication by a factor 1/759 is involved. Using Table 3, equation (20) can then be written

$$f\ 39.07 = 8.10 + (1-f)\ 12.23 + f\ 24.67 + 4.91 \qquad (21)$$

which gives $f = 0.948$ : the neutron balance is satisfied if, during each pulse, 95 % of the $^{22}Ne$ present in the He shell produce neutrons by the $(\alpha,n)$ reaction.

The effect of the uncertainties in the quantities entering in the calculations is shown in Fig.22 , where the left and right hand sides of the neutron balance equation (21), $fN_{CNO}$ and $\Sigma n_c$ , are plotted as a function of f.

The lines labeled $+\Delta\tau_o$ and $-\Delta\tau_o$ give the values of $\Sigma n_c$ corresponding to the upper and lower limits of the exposure parameter, $\tau_{02} = 0.240 \pm 0.010$ . The other parameter of the neutron exposure distribution, $s_2$ , plays no role in determinig $\Sigma n_c$ because we are expressing it in units of exposed $^{56}Fe$ seeds, $s_2 N^{\odot}_{56}$ . The number of neutrons captured by any seed A is proportional to $s_2 N^{\odot}_A$ ; expressed in our unit this is independent of $s_2$. The only other significant source of uncertainty of $\Sigma n_c$ is the uncertainty in $\sigma_{25}$, the capture cross section of $^{25}Mg$; since almost all the $^{22}Ne$, with an abundance equal to $N_{CNO}$, undergoes the $^{22}Ne(\alpha,n)^{25}Mg$ reaction, this $^{25}Mg$ has a very large abundance in the He shell and is by far the largest

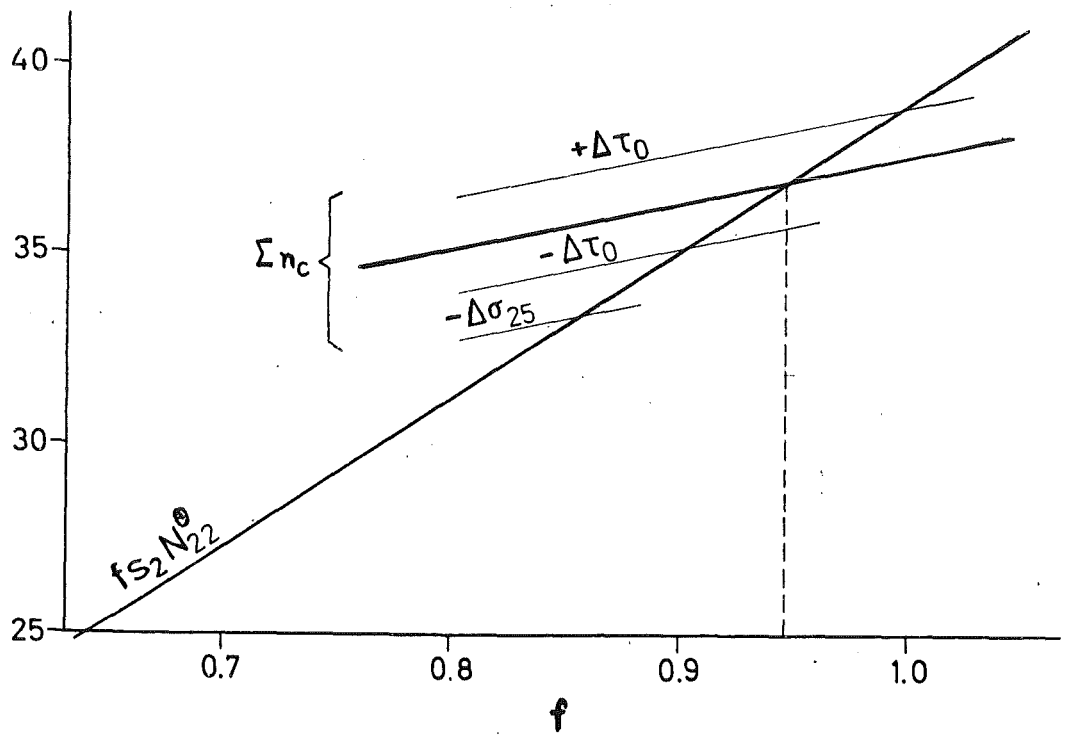


Fig. 22. Uncertainty on f .

neutron absorber (Table 3). The capture cross sections of the Mg isotopes have been measured by Macklin et al./37,38/ who give $\sigma_{25}$=(6.4+0.7) mb. The line labeled $-\sigma_{25}$ shows the value of $\Sigma n_c$ when both lower limits are used for $\tau_{02}$ and $\sigma_{25}$ ; in this case f = 86% .

It is fortunate that such a large fraction of the $^{22}Ne$ should produce neutrons and that $\sigma_{25}$ has been accurately measured,so that the very large $\Delta\sigma/\sigma$ of most isotopes results in only a small additional error in $\Sigma n_c$. If every cross section except $\sigma_{25}$ and $\sigma_{56}$ in Table 3 is increased by 50%, the total neutron absorption increases by less than 10% . As an additive error propagation is unlikely we conservatively obtain f = ( 95 ± 10 )% .

The main assumptions on which this result is based are :

1) The relative abundances of the isotopes between C and Fe in the H shell of the red giant are the same as in the solar system.

In trying to justify this assumption we will consider the simplest sequence of events in which our star could synthesyze the heavy s-process isotopes of the solar system. We suppose that our star was born in a large, homogeneous cloud containing all the elements up to Fe. During the pulsating phase of its life, matter is progressively s-processed in the He shell, convected to the surface, expelled by stellar winds and remixed into the cloud, from which the sun condensed later. A fraction representing about 0.1% of the solar material comes from our red giant, where the heavy s-nuclides have been synthesized. Since most of the fresh Fe is destroyed during the s-process and very little is produced by lighter seeds, the solar Fe abundance differs by at most 0.1% from that of the original cloud. The CNO isotopes also, are not produced in the s-process, and therefore their abundance, $N^{\bullet}_{CNO}$ , exceeds $N^{⓪}_{CNO}$ by at most 0.1% .Within this scenario the terms $fs_2N^{⓪}_{CNO}$ and $n_c(^{56}Fe)$ in the neutron balance equation (20) are then justified.

Since $N^{\bullet}_{CNO} \sim N^{⓪}_{CNO}$,the terms $n_c(^{25}Mg)$ and $n_c(^{22}Ne)$ are also justified. Almost all of $n_c(^{25}Mg)$ represents in fact neutrons captured by the $^{25}Mg$ created by $^{22}Ne(\alpha,n)$, and this $^{25}Mg$ has an abundance $fN_{CNO}$ , much larger than that of the fresh Mg convected down from the H shell. Almost all of the $^{22}Ne$ responsible for $n_c(^{22}Ne)$ is also due to the C,N,O isotopes.

Only the last term of (20), $n_c$(others), must still be examined. From column 6 of Table 3 it is clear that the s-process itself is not responsible for more than a few % of the solar abundance of these species, and their contribution to the absorption of neutrons is less

than 15% of the total; moreover, column 6 also shows that among these, the largest neutron absorbers ($^{20}$Ne,$^{24}$Mg,$^{28}$Si,$^{32}$S) all emerge with an abundance smaller than 0.1% of the solar system's, so that practically no error is introduced by taking $N_A^{\bullet} = N_A^{\odot}$ . In this idealized picture, the r-process nuclei must still be accounted for; their production in a supernova requires an amount of heavy seeds comparable to that produced in the s-process. Since the latter involved around 0.1% of the solar system $^{56}$Fe, its solar abundance was also only little affected by the r-process.

2) The $^{22}$Ne(α,n) reaction is the sole neutron source and, apart from $^{22}$Ne, no other nuclei react with α particles, so that only neutron capture has to be considered in calculating the final abundances.
This assumption may be justified by noting that, at the relevant temperature of kT ~ 30 keV, the (α,n) cross section for nuclei heavier than $^{22}$Ne are orders of magnitude smaller /39/, while at the same time the abundance of $^{22}$Ne in the fresh matter brought down with each pulse is much larger than for all other elements. Other possible reactions, mainly (α,γ), have even smaller cross sections. However, if 95% of the $^{22}$Ne burns by (α,n) a large concentration of $^{25}$Mg will build up. Although at kT=30 keV its (α,n) cross section/39/ is 1200 smaller than that of $^{22}$Ne, it may produce a considerable number of neutrons if the pulse lasts long enough.

## IV.4. The s-process temperature

We now try to determine wether the condition f=95% can be fulfilled under the conditions prevailing in the He shell.
The rate at which $^{22}$Ne undergoes the (α,n) reaction is /40/

$$\lambda = N_A \langle \sigma_{\alpha,n} v \rangle \rho \frac{X}{A} \qquad (22)$$

where $N_A$ is Avogadro's number, ρ is the density, and X,A, are the mass fraction and atomic mass of α-particles in the He burning region. In Iben's star model /7/ one finds $\rho = 1600$ g/cm$^3$ and X >90% . At kT = 30 keV $N_A\langle\sigma v\rangle = 0.48\ 10^9$ s$^{-1}$cm$^3$mole$^{-1}$ can be taken from Fowler et al./39/. This gives $\lambda = 1.8\ 10^7$ s$^{-1}$. The fraction of $^{22}$Ne surviving after a time Δt is $\exp(-\lambda\Delta t)=0.3\%$ for an interval of 1 year. Since the high temperature convective period of the thermal pulse lasts /35/ from 0.5 to 8 years, depending on the core mass, there is more than enough time to burn 95% of the $^{22}$Ne. In addition, under these conditions the $^{25}$Mg(α,n) reaction cannot

constitute a significant neutron source.

We have, however, neglected all other reactions on $^{22}Ne$, mainly $(\alpha,\gamma)$. The reaction rate ratio, $\lambda^n/\lambda^\gamma$ of $(\alpha,n)$ and $(\alpha,\gamma)$ on $^{22}Ne$ is shown in Fig.23 as a function of temperature, calculated according to /39/. From this curve, a lower limit for the temperature in the He burning region can be inferred :

In the extreme case in which all the $^{22}Ne$ is burned by $(\alpha,n)$ and $(\alpha,\gamma)$, none being left to capture neutrons, one has $f^n + f^\gamma = 1$, $f^n$ and $f^\gamma$ being the fraction consumed by $(\alpha,n)$ and $(\alpha,\gamma)$ respectively, and of course $f^n/f^\gamma = \lambda^n/\lambda^\gamma$ . For the value $f^n = 94.8\%$ deduced from the neutron balance equation, $f^\gamma = 1-f^n = 5.2$, or $f^n/f^\gamma = 18.2$ . Since it is unreasonable to expect that no neutrons at all are captured by $^{22}Ne$, $f^\gamma$ must be $<5.2\%$, and therefore $\lambda^n/\lambda^\gamma > 18.2$, a condition satisfied only if $kT > 35$ keV.

In our derivation of the value of f we assumed the abundance of $^{22}Ne$ to be $N_{CNO}+N_{22}$ , thus neglecting the $^{22}Ne$ produced in the s-process itself by neutron capture on lighter isotopes, $^{19}F$, $^{20,21}Ne$. Taking into account this additional amount of fuel for the $^{22}Ne(\alpha,n)$ neutron source will cause the value of f to decrease.

The amount of $^{22}Ne$ thus produced is obtained using eq. (18) and the

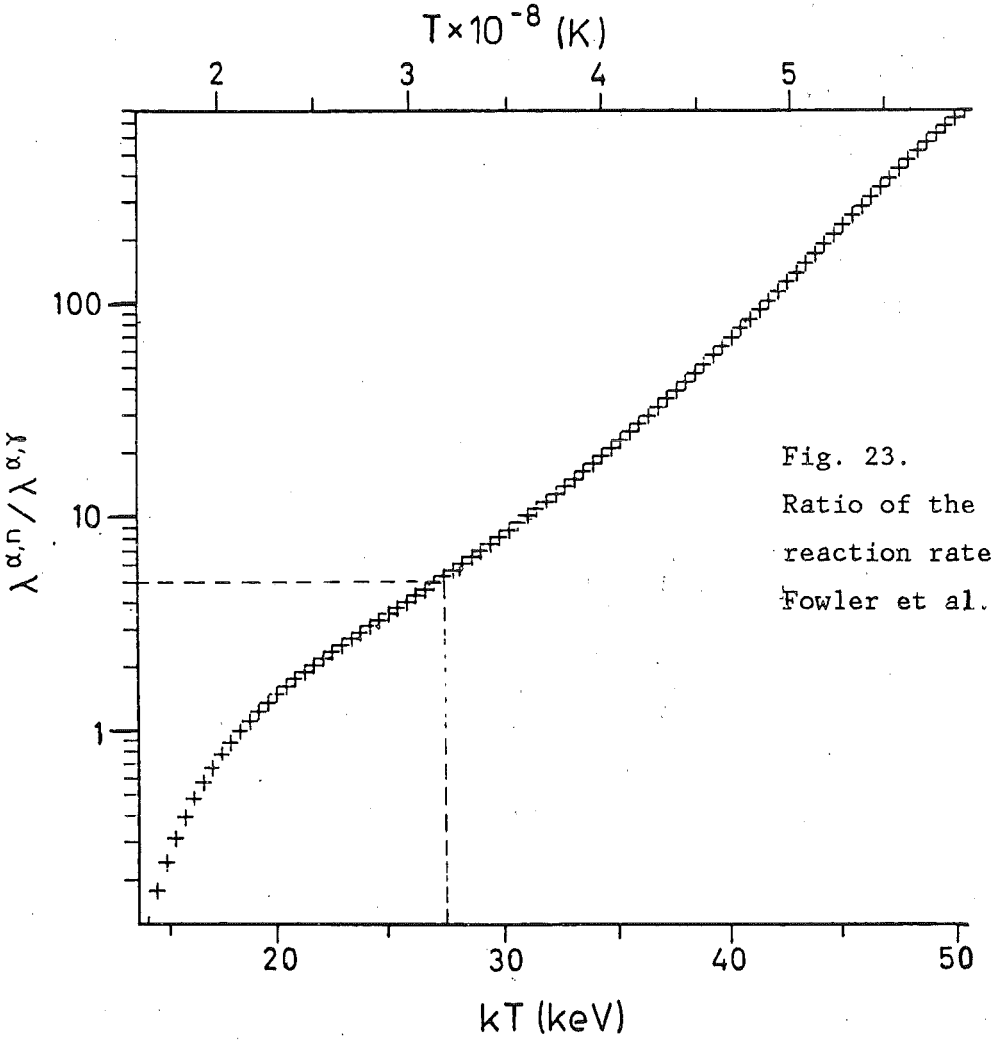


Fig. 23.
Ratio of the $(\alpha,n)$ and $(\alpha,\gamma)$ reaction rates, after Fowler et al. /39/.

abundance of these seeds, $s_2N_{20}$ (the contribution of $^{19}F$ and $^{21}Ne$ is about 100 times smaller). The left hand side of the neutron balance equation (20) is thereby increased by 1.5% . In the right hand side, the constant $C_{22}$ increases by the same factor since it is proportional to the $^{22}Ne$ abundance. The constant $C_{25}$ increases by practically the same factor, because most of the $^{25}Mg$ is due to the $^{22}Ne(\alpha,n)$ reaction. The last term, $\Sigma n_c$(others) decreases because the part of $n_c(^{20}Ne)$ due to its progeny with A>22 is now incorporated into $C_{22}$ ; the contribution of $n_c(20)$ to this last term is obtained from eq.(19) by cutting the summation at A=22. One gets then $\Sigma n_c$(others) =3.73 ( we have neglected the small change in $\Sigma n_c$ caused by $^{22}Ne(\alpha,\gamma)$, which transforms some $^{22}Ne$ into $^{26}Mg$).

Eq. (20) now yields $f^n = 89.6\%$ . Therefore $f^n/f^\gamma > 8.6$ , and from Fig. 23, kT > 31 keV. A pleasant feature of the curve in Fig. 23 is that it is so steep ( the ordinate scale is logarithmic ), which makes the temperature little sensitive to $\lambda^n/\lambda^\gamma$. If we allow for the 10% uncertainty in $f^n$, its lower limit is $f^n=80\%$ , and therefore $f^n/f^\gamma > 4$ and kT > 28 keV.

It should be stressed that this result is based on the experimentally determined solar abundances, not on the model dependent physical conditions in the He shell where the s-process is conjectured to take place.
The only detailed model of pulsating red giants is that of Iben, for which the time dependence of temperature and neutron flux during a thermal pulse have been calculated by Cosner et al./41/. Their numerical results are consistent with our lower limit for the average s-process temperature : it is found that more than 90% of the neutrons are released while the temperature is above 28 keV (at the onset of convection the temperature rises sharply from 14 keV to 34 keV, and during the pulse it decreases monotonically back to its 14 keV interpulse value).

Within the approximations used here, we conclude that the bulk of the solar system s-nuclides (85<A<200) could indeed have been created in the He burning shell of a pulsating red giant. The lower limit that we find for the temperature, kT > 28 keV, is well within the temperature range in the He shell, and comfortably below the value deduced by B. Leugers /14/ from the analysis of the s-process branching at $^{79}Se$, who reported kT = 35.5 keV.

## APPENDIX 1

### TOTAL CROSS SECTIONS

a) Low energy run (5 - 350 keV)

$^{20}Ne$

| $E_n$ keV | σ b | Δσ b | $E_n$ | σ | Δσ | $E_n$ | σ | Δσ |
|---|---|---|---|---|---|---|---|---|
| 5.1 | 2.19 | 0.2 | 6.1 | 2.87 | 0.2 | 6.9 | 2.45 | 0.2 |
| 7.7 | 3.10 | 0.2 | 8.4 | 2.77 | 0.2 | 9.2 | 1.80 | 0.2 |
| 9.9 | 2.68 | 0.2 | 10.7 | 2.79 | 0.2 | 11.5 | 2.78 | 0.2 |
| 12.2 | 2.77 | 0.2 | 13.0 | 2.47 | 0.2 | 13.8 | 2.17 | 0.2 |
| 14.5 | 2.50 | 0.2 | 15.3 | 2.59 | 0.2 | 16.1 | 2.49 | 0.2 |
| 16.8 | 2.15 | 0.2 | 17.6 | 2.31 | 0.2 | 18.4 | 2.65 | 0.2 |
| 19.2 | 2.11 | 0.2 | 19.9 | 2.57 | 0.2 | 20.7 | 2.38 | 0.2 |
| 21.5 | 2.27 | 0.2 | 22.3 | 2.47 | 0.2 | 23.1 | 2.23 | 0.2 |
| 23.9 | 2.34 | 0.2 | 24.7 | 2.33 | 0.2 | 25.5 | 1.95 | 0.2 |
| 26.2 | 2.45 | 0.2 | 27.0 | 2.30 | 0.2 | 27.8 | 2.04 | 0.2 |
| 28.6 | 2.33 | 0.2 | 29.4 | 2.29 | 0.2 | 30.2 | 2.47 | 0.2 |
| 31.0 | 2.55 | 0.2 | 31.8 | 2.26 | 0.2 | 32.7 | 2.57 | 0.2 |
| 33.5 | 2.48 | 0.2 | 34.3 | 2.55 | 0.2 | 35.1 | 2.21 | 0.2 |
| 35.9 | 2.24 | 0.2 | 36.7 | 2.34 | 0.2 | 37.6 | 2.42 | 0.2 |
| 38.4 | 2.11 | 0.2 | 39.2 | 2.16 | 0.2 | 40.1 | 2.58 | 0.2 |
| 40.9 | 2.19 | 0.2 | 41.8 | 2.33 | 0.2 | 42.6 | 2.31 | 0.2 |
| 43.5 | 2.31 | 0.2 | 44.3 | 2.26 | 0.2 | 45.2 | 2.31 | 0.2 |
| 46.0 | 2.51 | 0.2 | 46.9 | 2.22 | 0.2 | 47.8 | 2.20 | 0.2 |
| 48.6 | 2.41 | 0.2 | 49.5 | 2.22 | 0.2 | 50.4 | 2.20 | 0.2 |
| 51.2 | 2.45 | 0.2 | 52.1 | 2.45 | 0.2 | 53.0 | 2.54 | 0.2 |
| 53.9 | 1.94 | 0.2 | 54.8 | 2.21 | 0.2 | 55.7 | 2.12 | 0.2 |
| 56.5 | 2.23 | 0.2 | 57.4 | 2.43 | 0.2 | 58.3 | 2.42 | 0.2 |
| 59.3 | 2.33 | 0.2 | 60.2 | 1.92 | 0.2 | 61.1 | 2.27 | 0.2 |
| 62.0 | 2.23 | 0.2 | 62.9 | 2.47 | 0.2 | 63.8 | 2.38 | 0.2 |
| 64.8 | 1.97 | 0.2 | 65.8 | 2.51 | 0.2 | 66.8 | 2.34 | 0.2 |
| 67.7 | 2.41 | 0.2 | 68.6 | 2.39 | 0.2 | 69.5 | 2.09 | 0.2 |
| 70.4 | 2.49 | 0.2 | 71.4 | 2.25 | 0.2 | 72.4 | 2.04 | 0.2 |
| 73.4 | 2.21 | 0.2 | 74.4 | 2.31 | 0.2 | 75.5 | 2.18 | 0.2 |
| 76.4 | 2.57 | 0.2 | 77.3 | 2.36 | 0.2 | 78.3 | 2.40 | 0.2 |
| 79.2 | 1.96 | 0.2 | 80.2 | 2.07 | 0.2 | 81.2 | 2.49 | 0.2 |
| 82.2 | 2.26 | 0.2 | 83.3 | 2.35 | 0.2 | 84.3 | 2.30 | 0.2 |
| 85.4 | 1.98 | 0.2 | 86.5 | 2.27 | 0.2 | 87.7 | 2.23 | 0.2 |
| 88.6 | 2.23 | 0.2 | 89.6 | 2.15 | 0.2 | 90.6 | 2.27 | 0.2 |
| 91.6 | 2.08 | 0.2 | 92.6 | 2.21 | 0.2 | 93.6 | 1.99 | 0.2 |
| 94.7 | 2.26 | 0.2 | 95.8 | 2.24 | 0.2 | 96.8 | 2.21 | 0.2 |
| 97.9 | 1.86 | 0.2 | 99.1 | 2.40 | 0.2 | 100.2 | 2.11 | 0.2 |
| 101.4 | 2.15 | 0.2 | 102.6 | 2.37 | 0.2 | 103.8 | 1.95 | 0.2 |
| 105.0 | 2.16 | 0.2 | 106.3 | 2.35 | 0.2 | 107.3 | 2.02 | 0.2 |
| 108.3 | 2.29 | 0.2 | 109.4 | 2.22 | 0.2 | 110.4 | 2.17 | 0.2 |
| 111.5 | 2.09 | 0.2 | 112.6 | 1.90 | 0.2 | 113.7 | 2.17 | 0.2 |
| 114.9 | 2.11 | 0.2 | 116.0 | 2.10 | 0.2 | 117.2 | 2.26 | 0.2 |
| 118.3 | 2.06 | 0.2 | 119.5 | 2.04 | 0.2 | 120.8 | 2.02 | 0.2 |
| 122.0 | 1.98 | 0.2 | 123.2 | 1.92 | 0.2 | 124.5 | 2.14 | 0.2 |
| 125.8 | 2.07 | 0.2 | 127.1 | 2.22 | 0.2 | 128.5 | 2.27 | 0.2 |
| 129.8 | 2.05 | 0.2 | 131.2 | 1.99 | 0.2 | 132.6 | 1.87 | 0.2 |

| | | | | | | | | |
|---|---|---|---|---|---|---|---|---|
| 134.0 | 1.86 | 0.2 | 135.4 | 2.06 | 0.2 | 136.9 | 2.20 | 0.2 |
| 138.4 | 2.03 | 0.2 | 139.5 | 1.94 | 0.2 | 140.7 | 2.52 | 0.4 |
| 141.1 | 2.28 | 0.4 | 141.5 | 2.57 | 0.4 | 141.8 | 2.28 | 0.4 |
| 142.2 | 2.28 | 0.4 | 142.6 | 2.10 | 0.4 | 143.0 | 2.14 | 0.4 |
| 143.4 | 2.34 | 0.4 | 143.8 | 2.18 | 0.4 | 144.2 | 2.42 | 0.4 |
| 144.6 | 2.13 | 0.4 | 145.0 | 2.03 | 0.4 | 145.4 | 2.99 | 0.4 |
| 145.8 | 2.85 | 0.4 | 146.2 | 3.71 | 0.4 | 146.6 | 5.38 | 0.4 |
| 147.1 | 7.97 | 0.4 | 147.5 | 8.98 | 0.4 | 147.9 | 7.66 | 0.4 |
| 148.3 | 5.57 | 0.4 | 148.7 | 3.17 | 0.4 | 149.1 | 2.94 | 0.4 |
| 149.6 | 2.57 | 0.4 | 150.0 | 2.06 | 0.4 | 150.4 | 2.25 | 0.4 |
| 150.8 | 1.78 | 0.4 | 151.3 | 2.37 | 0.4 | 151.7 | 2.41 | 0.4 |
| 152.1 | 1.81 | 0.4 | 152.6 | 1.95 | 0.4 | 153.0 | 2.06 | 0.4 |
| 153.4 | 1.94 | 0.4 | 153.9 | 1.48 | 0.4 | 154.3 | 2.09 | 0.4 |
| 154.8 | 1.55 | 0.4 | 155.2 | 2.46 | 0.4 | 155.6 | 2.19 | 0.4 |
| 156.1 | 1.68 | 0.4 | 156.5 | 1.95 | 0.4 | 157.0 | 1.97 | 0.4 |
| 157.5 | 1.78 | 0.4 | 157.9 | 2.01 | 0.4 | 158.4 | 1.98 | 0.4 |
| 158.8 | 2.38 | 0.4 | 159.3 | 2.36 | 0.4 | 159.8 | 2.19 | 0.4 |
| 160.2 | 1.76 | 0.4 | 160.7 | 2.21 | 0.4 | 161.2 | 1.95 | 0.4 |
| 161.6 | 1.95 | 0.4 | 162.1 | 2.24 | 0.4 | 162.6 | 1.81 | 0.4 |
| 163.1 | 1.96 | 0.4 | 163.6 | 2.28 | 0.4 | 164.0 | 2.05 | 0.4 |
| 164.5 | 2.08 | 0.4 | 165.0 | 1.78 | 0.4 | 165.5 | 2.08 | 0.3 |
| 166.0 | 2.15 | 0.4 | 166.5 | 2.06 | 0.4 | 167.0 | 2.15 | 0.3 |
| 167.5 | 2.16 | 0.4 | 168.0 | 1.89 | 0.4 | 168.5 | 1.88 | 0.3 |
| 169.0 | 2.05 | 0.3 | 169.5 | 2.19 | 0.3 | 170.0 | 1.97 | 0.3 |
| 170.5 | 2.24 | 0.3 | 171.0 | 2.24 | 0.3 | 171.6 | 1.71 | 0.3 |
| 172.1 | 2.48 | 0.3 | 172.6 | 2.46 | 0.3 | 173.1 | 1.66 | 0.3 |
| 173.7 | 2.21 | 0.3 | 174.2 | 2.14 | 0.3 | 174.7 | 1.79 | 0.3 |
| 175.2 | 2.00 | 0.3 | 175.8 | 1.70 | 0.3 | 176.3 | 1.93 | 0.3 |
| 176.9 | 1.53 | 0.3 | 177.4 | 1.53 | 0.3 | 178.0 | 2.18 | 0.3 |
| 178.5 | 1.58 | 0.3 | 179.1 | 1.70 | 0.3 | 179.6 | 2.13 | 0.3 |
| 180.2 | 1.87 | 0.3 | 180.7 | 2.00 | 0.3 | 181.3 | 2.09 | 0.3 |
| 181.9 | 2.23 | 0.3 | 182.4 | 1.77 | 0.3 | 183.0 | 1.97 | 0.3 |
| 183.6 | 1.58 | 0.3 | 184.1 | 1.53 | 0.3 | 184.7 | 1.66 | 0.3 |
| 185.3 | 1.91 | 0.3 | 185.9 | 1.93 | 0.3 | 186.5 | 1.93 | 0.3 |
| 187.1 | 1.73 | 0.3 | 187.6 | 2.45 | 0.3 | 188.2 | 1.84 | 0.3 |
| 188.8 | 1.85 | 0.3 | 189.4 | 2.43 | 0.3 | 190.0 | 1.76 | 0.3 |
| 190.7 | 2.31 | 0.3 | 191.3 | 1.47 | 0.3 | 191.9 | 1.91 | 0.3 |
| 192.5 | 1.75 | 0.3 | 193.1 | 2.35 | 0.3 | 193.7 | 2.25 | 0.3 |
| 194.3 | 1.63 | 0.3 | 195.0 | 1.62 | 0.3 | 195.6 | 1.51 | 0.3 |
| 196.2 | 1.73 | 0.3 | 196.9 | 1.98 | 0.3 | 197.5 | 2.05 | 0.3 |
| 198.2 | 1.77 | 0.3 | 198.8 | 1.94 | 0.3 | 199.4 | 1.78 | 0.3 |
| 200.1 | 1.57 | 0.3 | 200.8 | 2.12 | 0.3 | 201.4 | 1.72 | 0.3 |
| 202.1 | 1.76 | 0.3 | 202.7 | 1.81 | 0.3 | 203.4 | 1.75 | 0.3 |
| 204.1 | 1.51 | 0.3 | 204.8 | 1.71 | 0.3 | 205.4 | 1.73 | 0.3 |
| 206.1 | 1.86 | 0.3 | 206.8 | 1.83 | 0.3 | 207.5 | 1.34 | 0.3 |
| 208.2 | 1.89 | 0.3 | 208.9 | 2.22 | 0.3 | 209.6 | 1.07 | 0.3 |
| 210.3 | 1.55 | 0.3 | 211.0 | 1.40 | 0.3 | 211.7 | 1.78 | 0.3 |
| 212.4 | 1.81 | 0.3 | 213.1 | 1.82 | 0.3 | 213.8 | 1.36 | 0.3 |
| 214.6 | 1.80 | 0.3 | 215.3 | 2.02 | 0.3 | 216.0 | 1.81 | 0.3 |
| 216.8 | 1.77 | 0.3 | 217.5 | 1.78 | 0.3 | 218.2 | 1.90 | 0.3 |
| 219.0 | 1.86 | 0.3 | 219.7 | 1.60 | 0.3 | 220.5 | 1.42 | 0.3 |
| 221.2 | 1.51 | 0.3 | 222.0 | 1.83 | 0.3 | 222.8 | 1.54 | 0.3 |
| 223.5 | 1.74 | 0.3 | 224.3 | 1.67 | 0.3 | 225.1 | 1.55 | 0.3 |
| 225.9 | 1.59 | 0.3 | 226.7 | 1.54 | 0.3 | 227.4 | 1.91 | 0.3 |
| 228.2 | 1.53 | 0.3 | 229.0 | 1.42 | 0.3 | 229.8 | 1.69 | 0.3 |
| 230.6 | 1.73 | 0.3 | 231.5 | 1.45 | 0.3 | 232.3 | 1.63 | 0.3 |

| | | | | | | | | |
|---|---|---|---|---|---|---|---|---|
| 233.1 | 1.30 | 0.3 | 233.9 | 1.32 | 0.3 | 234.7 | 1.34 | 0.3 |
| 235.6 | 1.58 | 0.3 | 236.4 | 1.51 | 0.3 | 237.2 | 1.60 | 0.3 |
| 238.1 | 1.49 | 0.3 | 238.9 | 1.09 | 0.3 | 239.8 | 1.32 | 0.3 |
| 240.7 | 1.70 | 0.3 | 241.5 | 1.51 | 0.3 | 242.4 | 1.95 | 0.3 |
| 243.3 | 1.38 | 0.3 | 244.1 | 1.54 | 0.3 | 245.0 | 1.11 | 0.3 |
| 245.9 | 1.67 | 0.3 | 246.8 | 1.99 | 0.3 | 247.7 | 1.42 | 0.3 |
| 248.6 | 1.21 | 0.3 | 249.5 | 1.64 | 0.3 | 250.4 | 1.70 | 0.3 |
| 251.3 | 1.45 | 0.3 | 252.3 | 1.76 | 0.3 | 253.2 | 1.14 | 0.3 |
| 254.1 | 1.74 | 0.3 | 255.1 | 1.61 | 0.3 | 256.0 | 1.54 | 0.3 |
| 256.9 | 1.28 | 0.3 | 257.9 | 1.32 | 0.4 | 258.9 | 1.98 | 0.4 |
| 259.8 | 1.90 | 0.4 | 260.8 | 1.86 | 0.4 | 261.8 | 1.88 | 0.4 |
| 262.7 | 1.64 | 0.4 | 263.7 | 2.21 | 0.4 | 264.7 | 2.05 | 0.4 |
| 265.7 | 2.29 | 0.4 | 266.7 | 1.89 | 0.4 | 267.7 | 2.29 | 0.4 |
| 268.7 | 1.88 | 0.4 | 269.8 | 1.73 | 0.4 | 270.8 | 1.56 | 0.4 |
| 271.8 | 1.87 | 0.4 | 272.9 | 1.99 | 0.4 | 273.9 | 0.90 | 0.4 |
| 275.0 | 1.45 | 0.4 | 276.0 | 1.85 | 0.4 | 277.1 | 2.07 | 0.4 |
| 278.1 | 1.96 | 0.4 | 279.2 | 1.50 | 0.4 | 280.3 | 1.62 | 0.4 |
| 281.4 | 1.87 | 0.4 | 282.5 | 1.23 | 0.4 | 283.6 | 1.92 | 0.4 |
| 284.7 | 1.25 | 0.4 | 285.8 | 1.79 | 0.4 | 286.9 | 1.50 | 0.4 |
| 288.0 | 2.07 | 0.4 | 289.2 | 1.65 | 0.4 | 290.3 | 2.02 | 0.4 |
| 291.4 | 1.35 | 0.4 | 292.6 | 2.49 | 0.4 | 293.8 | 2.48 | 0.4 |
| 294.9 | 2.09 | 0.4 | 296.1 | 1.77 | 0.4 | 297.3 | 2.31 | 0.4 |
| 298.5 | 2.37 | 0.4 | 299.6 | 2.61 | 0.4 | 300.8 | 2.30 | 0.4 |
| 302.1 | 1.86 | 0.4 | 303.3 | 2.26 | 0.4 | 304.5 | 2.52 | 0.4 |
| 305.7 | 2.56 | 0.4 | 307.0 | 1.52 | 0.4 | 308.2 | 1.93 | 0.4 |
| 309.5 | 2.21 | 0.4 | 310.7 | 1.61 | 0.4 | 312.0 | 2.29 | 0.4 |
| 313.3 | 2.32 | 0.5 | 314.5 | 2.33 | 0.5 | 315.8 | 1.94 | 0.5 |
| 317.1 | 1.81 | 0.5 | 318.4 | 1.94 | 0.5 | 319.8 | 1.57 | 0.5 |
| 321.1 | 2.37 | 0.5 | 322.4 | 2.17 | 0.5 | 323.8 | 2.15 | 0.5 |
| 325.1 | 1.12 | 0.5 | 326.5 | 1.90 | 0.5 | 327.8 | 1.15 | 0.5 |
| 329.2 | 1.74 | 0.5 | 330.6 | 1.69 | 0.5 | 332.0 | 0.54 | 0.5 |
| 333.4 | 1.26 | 0.6 | 334.8 | 1.52 | 0.6 | 336.2 | 1.42 | 0.6 |
| 337.6 | 1.04 | 0.6 | 339.1 | 1.90 | 0.6 | 340.5 | 0.98 | 0.7 |
| 342.0 | 0.88 | 0.8 | 343.4 | 1.52 | 0.9 | 344.9 | 2.44 | 1.0 |
| 346.4 | 1.70 | 1.3 | 347.9 | 0.77 | 1.7 | 349.4 | -2.22 | 2.2 |
| 350.9 | 2.75 | 2.6 | 352.4 | -1.56 | 2.7 | 353.9 | 1.25 | 2.8 |

$^{21}$NE

| | | | | | | | | |
|---|---|---|---|---|---|---|---|---|
| 5.1 | 4.27 | 2.2 | 5.8 | 4.13 | 2.6 | 6.4 | 3.21 | 2.4 |
| 6.9 | 2.38 | 2.3 | 7.4 | 4.80 | 2.2 | 8.0 | 4. 9 | 2.1 |
| 8.5 | 3.19 | 2.1 | 9.0 | 4.79 | 2.2 | 9.6 | 1.51 | 2.3 |
| 10.1 | 3.58 | 2.3 | 10.6 | 2.04 | 2.3 | 11.2 | 2.44 | 2.4 |
| 11.7 | 1.51 | 2.3 | 12.3 | 2.37 | 2.4 | 12.8 | 3.07 | 2.2 |
| 13.4 | 4.81 | 2.3 | 13.9 | 2.33 | 2.3 | 14.4 | 3.54 | 2.2 |
| 15.0 | 3.50 | 2.3 | 15.5 | 3.66 | 2.3 | 16.1 | 3.43 | 2.1 |
| 16.6 | 1.04 | 2.2 | 17.2 | 2.30 | 2.2 | 17.7 | 2.19 | 2.2 |
| 18.3 | 3.64 | 2.1 | 18.8 | 3.73 | 2.1 | 19.4 | 3.01 | 2.1 |
| 20.0 | 5.47 | 2.1 | 20.5 | 4.67 | 2.1 | 21.1 | 4.56 | 2.0 |
| 21.6 | 0.94 | 2.0 | 22.2 | 3.08 | 2.0 | 22.8 | 4.21 | 2.0 |
| 23.3 | 3.28 | 2.0 | 23.9 | 6.85 | 2.0 | 24.5 | 3.75 | 2.0 |
| 25.0 | 1.88 | 2.0 | 25.6 | 1.20 | 1.9 | 26.2 | 3.03 | 2.0 |
| 26.7 | 0.78 | 1.9 | 27.3 | 2.82 | 1.9 | 27.9 | -0.20 | 1.9 |
| 28.5 | 0.12 | 1.9 | 29.1 | -0.64 | 1.9 | 29.6 | 0.96 | 2.0 |
| 30.2 | 3.07 | 1.9 | 30.8 | 2.91 | 1.9 | 31.4 | 7.02 | 2.0 |

| | | | | | | | | |
|---|---|---|---|---|---|---|---|---|
| 32.0 | 4.33 | 1.9 | 32.6 | 3.56 | 1.9 | 33.2 | 4.99 | 2.0 |
| 33.8 | 5.41 | 2.0 | 34.3 | 3.52 | 1.9 | 35.0 | 1.20 | 2.0 |
| 35.5 | 1.09 | 2.0 | 36.1 | 2.41 | 2.0 | 36.7 | 3.82 | 2.0 |
| 37.4 | 0.58 | 2.0 | 38.0 | 3.00 | 2.0 | 38.6 | 0.24 | 2.0 |
| 39.2 | 4.60 | 2.0 | 39.8 | 3.69 | 2.1 | 40.4 | 3.15 | 2.1 |
| 41.0 | 2.18 | 2.0 | 41.6 | 3.77 | 2.0 | 42.2 | 4.21 | 2.0 |
| 42.9 | 3.26 | 2.0 | 43.5 | 0.73 | 2.1 | 44.1 | 4.82 | 2.1 |
| 44.7 | 3.32 | 2.1 | 45.4 | 2.19 | 2.0 | 46.0 | 5.20 | 2.0 |
| 46.7 | 5.78 | 2.0 | 47.3 | 6.39 | 2.1 | 47.9 | 4.47 | 2.1 |
| 48.6 | 7.29 | 2.1 | 49.2 | 3.24 | 2.1 | 49.8 | 2.34 | 2.1 |
| 50.5 | 1.49 | 2.1 | 51.2 | 6.34 | 2.1 | 51.8 | 5.58 | 2.0 |
| 52.5 | 2.96 | 2.2 | 53.2 | 5.09 | 2.1 | 53.8 | 2.35 | 2.1 |
| 54.4 | 3.88 | 2.1 | 55.1 | 3.36 | 2.1 | 55.8 | 4.85 | 2.1 |
| 56.4 | 3.73 | 2.1 | 57.1 | 4.58 | 2.1 | 57.8 | 3.70 | 1.9 |
| 58.5 | 2.17 | 2.0 | 59.3 | 4.15 | 2.2 | 59.9 | 1.78 | 2.2 |
| 60.6 | 1.62 | 2.2 | 61.2 | 1.60 | 2.1 | 61.9 | 4.93 | 2.1 |
| 62.6 | 3.50 | 2.1 | 63.3 | 4.59 | 2.1 | 64.0 | 6.39 | 2.1 |
| 64.7 | 0.96 | 2.1 | 65.4 | 4.84 | 2.1 | 66.1 | 3.23 | 2.1 |
| 66.9 | 1.74 | 2.0 | 67.7 | 6.00 | 2.0 | 68.4 | 3.04 | 2.2 |
| 69.1 | 4.01 | 2.2 | 69.8 | 1.67 | 2.2 | 70.4 | 6.42 | 2.2 |
| 71.1 | 2.41 | 2.2 | 71.8 | 6.35 | 2.2 | 72.5 | 3.95 | 2.1 |
| 73.2 | 1.76 | 2.1 | 74.0 | 1.55 | 2.1 | 74.7 | 5.58 | 2.1 |
| 75.5 | 2.47 | 2.1 | 76.2 | 5.16 | 2.1 | 77.0 | 4.38 | 2.1 |
| 77.8 | 3.12 | 2.1 | 78.6 | 4.06 | 2.0 | 79.4 | 1.49 | 2.0 |
| 80.2 | 2.47 | 2.0 | 81.0 | 6.00 | 2.0 | 81.9 | 6.00 | 2.0 |
| 82.8 | 5.65 | 2.0 | 83.6 | 7.15 | 2.2 | 84.3 | 2.97 | 2.2 |
| 85.1 | 2.47 | 2.2 | 85.8 | 0.77 | 2.2 | 86.5 | 3.16 | 2.2 |
| 87.3 | 6.37 | 2.2 | 88.0 | 4.09 | 2.2 | 88.8 | 2.27 | 2.1 |
| 89.6 | 3.42 | 2.1 | 90.4 | 5.49 | 2.1 | 91.2 | 4.20 | 2.1 |
| 92.0 | 2.32 | 2.1 | 92.8 | 4.93 | 2.1 | 93.6 | -0.62 | 2.1 |
| 94.5 | 3.74 | 2.1 | 95.3 | 1.17 | 2.0 | 96.2 | 5.92 | 2.1 |
| 97.1 | 5.84 | 2.0 | 97.9 | -1.14 | 2.0 | 98.9 | 4.28 | 2.0 |
| 99.8 | 4.75 | 2.0 | 100.7 | 3.97 | 2.0 | 101.6 | 5.64 | 2.0 |
| 102.6 | 3.92 | 2.0 | 103.5 | 4.10 | 2.0 | 104.5 | 3.70 | 2.0 |
| 105.5 | 5.41 | 2.0 | 106.5 | 2.81 | 2.0 | 107.6 | 2.67 | 1.9 |
| 108.6 | 3.56 | 1.9 | 109.6 | 4.60 | 2.2 | 110.4 | 4.42 | 2.2 |
| 111.2 | 5.39 | 2.2 | 112.1 | 0.87 | 2.2 | 112.9 | 3.57 | 2.2 |
| 113.7 | 5.17 | 2.2 | 114.6 | 5.59 | 2.2 | 115.4 | 3.63 | 2.2 |
| 116.3 | 2.28 | 2.2 | 117.2 | 3.07 | 2.2 | 118.0 | 3.27 | 2.2 |
| 118.9 | 6.20 | 2.2 | 119.8 | 4.39 | 2.1 | 120.8 | 3.88 | 2.1 |
| 121.7 | 4.16 | 2.1 | 122.6 | 3.46 | 2.1 | 123.6 | 4.33 | 2.1 |
| 124.5 | 1.98 | 2.1 | 125.5 | 4.32 | 2.1 | 126.5 | 2.86 | 2.1 |
| 127.5 | 7.89 | 2.1 | 128.5 | 6.62 | 2.1 | 129.5 | 5.15 | 2.0 |
| 130.5 | 4.37 | 2.1 | 131.5 | 4.32 | 2.1 | 132.6 | 5.04 | 2.1 |
| 133.6 | 6.30 | 2.1 | 134.7 | 10.91 | 2.0 | 135.8 | 15.24 | 2.0 |
| 136.9 | 20.42 | 2.0 | 138.0 | 17.88 | 2.0 | 139.2 | 11.64 | 2.0 |
| 140.3 | 9.66 | 2.0 | 141.5 | 6.47 | 2.0 | 142.6 | 4.45 | 2.0 |
| 143.8 | 3.91 | 2.0 | 145.0 | 4.52 | 2.0 | 146.2 | 2.44 | 2.0 |
| 147.5 | 5.12 | 2.0 | 148.7 | 2.86 | 2.0 | 150.0 | 3.19 | 2.0 |
| 151.3 | 4.75 | 2.0 | 152.6 | 5.28 | 2.0 | 153.9 | 5.08 | 1.9 |
| 155.2 | 5.69 | 1.9 | 156.5 | 2.65 | 1.9 | 157.9 | 0.93 | 1.9 |
| 159.3 | 3.27 | 1.9 | 160.7 | 1.72 | 1.9 | 162.1 | 4.17 | 1.9 |
| 163.6 | 6.59 | 1.9 | 165.0 | 5.01 | 1.9 | 166.5 | 2.23 | 1.9 |
| 168.0 | 2.75 | 1.9 | 169.5 | 2.20 | 1.9 | 171.0 | 5.52 | 1.9 |
| 172.6 | 2.74 | 1.9 | 174.2 | 1.98 | 2.3 | 175.2 | 1.63 | 2.3 |
| 176.3 | 1.06 | 2.3 | 177.4 | -1.62 | 2.3 | 178.5 | -2.00 | 2.3 |

| | | | | | | | | |
|---|---|---|---|---|---|---|---|---|
| 179.6 | 0.95 | 2.3 | 180.7 | 6.82 | 2.3 | 181.9 | 6.67 | 2.3 |
| 183.0 | 9.36 | 2.3 | 184.1 | 7.74 | 2.3 | 185.3 | 4.32 | 2.3 |
| 186.5 | 6.83 | 2.3 | 187.6 | 5.86 | 2.3 | 188.8 | 5.85 | 2.3 |
| 190.0 | 5.77 | 2.3 | 191.3 | 4.37 | 2.3 | 192.5 | 8.29 | 2.3 |
| 193.7 | 5.85 | 2.3 | 195.0 | 4.05 | 2.3 | 196.2 | 0.84 | 2.3 |
| 197.5 | 5.22 | 2.2 | 198.8 | 3.35 | 2.3 | 200.1 | 3.34 | 2.3 |
| 201.4 | 3.62 | 2.3 | 202.7 | 2.55 | 2.2 | 204.1 | 4.43 | 2.2 |
| 205.4 | 3.32 | 2.2 | 206.8 | 1.91 | 2.3 | 208.2 | 4.17 | 2.2 |
| 209.6 | 0.14 | 2.2 | 211.0 | -1.93 | 3.2 | 211.7 | 0.88 | 3.2 |
| 212.4 | 2.27 | 3.2 | 213.1 | 3.70 | 3.2 | 213.8 | 0.45 | 3.2 |
| 214.6 | 3.10 | 3.2 | 215.3 | 6.36 | 3.2 | 216.0 | 6.18 | 3.2 |
| 216.8 | 4.18 | 3.2 | 217.5 | 6.16 | 3.2 | 218.2 | 4.45 | 3.2 |
| 219.0 | 4.63 | 3.2 | 219.7 | 4.96 | 3.2 | 220.5 | -0.58 | 3.2 |
| 221.2 | -2.97 | 3.2 | 222.0 | 4.41 | 3.2 | 222.8 | 4.68 | 3.2 |
| 223.5 | 4.23 | 3.2 | 224.3 | 2.54 | 3.2 | 225.1 | 0.17 | 3.2 |
| 225.9 | 1.00 | 3.2 | 226.7 | 2.19 | 3.2 | 227.4 | 5.96 | 3.2 |
| 228.2 | 0.97 | 3.2 | 229.0 | 1.35 | 3.2 | 229.8 | 0.18 | 3.2 |
| 230.6 | 3.11 | 3.2 | 231.5 | 1.14 | 3.2 | 232.3 | 5.44 | 3.2 |
| 233.1 | -2.13 | 3.2 | 233.9 | 4.22 | 3.2 | 234.7 | 3.73 | 3.2 |
| 235.6 | 5.90 | 3.2 | 236.4 | 3.96 | 3.2 | 237.2 | 3.42 | 3.2 |
| 238.1 | 5.78 | 3.2 | 238.9 | 5.06 | 3.2 | 239.8 | 3.86 | 3.2 |
| 240.7 | 4.74 | 3.2 | 241.5 | 1.22 | 3.2 | 242.4 | 3.55 | 3.2 |
| 243.3 | 0.15 | 3.3 | 244.1 | 2.75 | 3.2 | 245.0 | 1.36 | 3.2 |
| 245.9 | 4.93 | 3.3 | 246.8 | 2.98 | 3.2 | 247.7 | 0.59 | 3.3 |
| 248.6 | 6.11 | 3.2 | 249.5 | 4.64 | 3.3 | 250.4 | 2.92 | 3.3 |
| 251.3 | -1.38 | 3.3 | 252.3 | 0.05 | 3.3 | 253.2 | -2.35 | 3.3 |
| 254.1 | 2.88 | 3.3 | 255.1 | 1.34 | 3.3 | 256.0 | 2.15 | 3.3 |
| 256.9 | 1.93 | 3.3 | 257.9 | 0.09 | 3.3 | 258.9 | 2.97 | 3.3 |

$^{22}$NE

| | | | | | | | | |
|---|---|---|---|---|---|---|---|---|
| 5.1 | 2.83 | 0.2 | 6.1 | 2.82 | 0.3 | 6.9 | 1.81 | 0.2 |
| 7.7 | 1.67 | 0.2 | 8.4 | 1.75 | 0.2 | 9.2 | 1.63 | 0.2 |
| 9.9 | 1.32 | 0.2 | 10.7 | 2.12 | 0.2 | 11.5 | 2.30 | 0.2 |
| 12.2 | 2.04 | 0.3 | 13.0 | 1.94 | 0.2 | 13.8 | 1.54 | 0.2 |
| 14.5 | 1.88 | 0.2 | 15.3 | 1.88 | 0.2 | 16.1 | 1.82 | 0.2 |
| 16.8 | 1.47 | 0.2 | 17.6 | 1.94 | 0.2 | 18.4 | 1.92 | 0.2 |
| 19.2 | 1.44 | 0.2 | 19.9 | 2.20 | 0.2 | 20.7 | 1.85 | 0.2 |
| 21.5 | 1.78 | 0.2 | 22.3 | 1.52 | 0.2 | 23.1 | 1.65 | 0.2 |
| 23.9 | 1.52 | 0.2 | 24.7 | 1.45 | 0.2 | 25.5 | 1.31 | 0.2 |
| 26.2 | 1.81 | 0.2 | 27.0 | 1.23 | 0.2 | 27.8 | 1.53 | 0.2 |
| 28.6 | 1.41 | 0.2 | 29.4 | 1.29 | 0.2 | 30.2 | 1.57 | 0.2 |
| 31.0 | 1.76 | 0.2 | 31.8 | 1.52 | 0.2 | 32.7 | 1.85 | 0.2 |
| 33.5 | 1.93 | 0.2 | 34.3 | 1.46 | 0.2 | 35.1 | 1.46 | 0.2 |
| 35.9 | 1.27 | 0.2 | 36.7 | 1.50 | 0.2 | 37.6 | 1.53 | 0.2 |
| 38.4 | 1.45 | 0.2 | 39.2 | 1.48 | 0.2 | 40.1 | 1.38 | 0.2 |
| 40.9 | 1.45 | 0.2 | 41.8 | 1.58 | 0.2 | 42.6 | 1.49 | 0.2 |
| 43.5 | 1.47 | 0.2 | 44.3 | 1.49 | 0.2 | 45.2 | 1.57 | 0.2 |
| 46.0 | 1.55 | 0.2 | 46.9 | 1.74 | 0.2 | 47.8 | 1.28 | 0.2 |
| 48.6 | 1.67 | 0.2 | 49.5 | 1.26 | 0.2 | 50.4 | 1.54 | 0.2 |
| 51.2 | 1.42 | 0.2 | 52.1 | 1.63 | 0.2 | 53.0 | 2.02 | 0.2 |
| 53.9 | 1.33 | 0.2 | 54.8 | 1.29 | 0.2 | 55.7 | 1.69 | 0.2 |
| 56.5 | 1.48 | 0.2 | 57.4 | 1.58 | 0.2 | 58.3 | 1.49 | 0.2 |
| 59.3 | 1.51 | 0.2 | 60.2 | 1.16 | 0.2 | 61.1 | 1.10 | 0.2 |
| 62.0 | 1.32 | 0.2 | 62.9 | 1.61 | 0.2 | 63.8 | 1.31 | 0.2 |

| | | | | | | | | |
|---|---|---|---|---|---|---|---|---|
| 64.8 | 1.05 | 0.2 | 65.8 | 1.40 | 0.2 | 66.8 | 1.27 | 0.2 |
| 67.7 | 1.30 | 0.2 | 68.6 | 1.49 | 0.2 | 69.5 | 1.23 | 0.2 |
| 70.4 | 1.62 | 0.2 | 71.4 | 1.41 | 0.2 | 72.4 | 1.51 | 0.2 |
| 73.4 | 0.92 | 0.2 | 74.4 | 1.52 | 0.2 | 75.5 | 1.32 | 0.2 |
| 76.4 | 1.66 | 0.2 | 77.3 | 1.25 | 0.2 | 78.3 | 1.32 | 0.2 |
| 79.2 | 1.26 | 0.2 | 80.2 | 1.37 | 0.2 | 81.2 | 1.73 | 0.2 |
| 82.2 | 1.40 | 0.2 | 83.3 | 1.30 | 0.2 | 84.3 | 1.40 | 0.2 |
| 85.4 | 1.16 | 0.2 | 86.5 | 1.29 | 0.2 | 87.7 | 1.36 | 0.2 |
| 88.6 | 1.29 | 0.2 | 89.6 | 1.55 | 0.2 | 90.6 | 1.16 | 0.2 |
| 91.6 | 1.34 | 0.2 | 92.6 | 1.50 | 0.2 | 93.6 | 1.04 | 0.2 |
| 94.7 | 1.35 | 0.2 | 95.8 | 1.41 | 0.2 | 96.8 | 1.43 | 0.2 |
| 97.9 | 0.57 | 0.2 | 99.1 | 1.40 | 0.2 | 100.2 | 1.12 | 0.2 |
| 101.4 | 1.28 | 0.2 | 102.6 | 1.54 | 0.2 | 103.8 | 1.04 | 0.2 |
| 105.0 | 1.50 | 0.2 | 106.3 | 1.43 | 0.2 | 107.3 | 0.90 | 0.2 |
| 108.3 | 1.05 | 0.2 | 109.4 | 1.18 | 0.2 | 110.4 | 1.22 | 0.2 |
| 111.5 | 0.67 | 0.2 | 112.6 | 1.11 | 0.2 | 113.7 | 0.82 | 0.2 |
| 114.9 | 1.00 | 0.2 | 116.0 | 1.13 | 0.2 | 117.2 | 1.13 | 0.2 |
| 118.3 | 1.12 | 0.2 | 119.5 | 1.02 | 0.2 | 120.8 | 1.19 | 0.2 |
| 122.0 | 1.20 | 0.2 | 123.2 | 1.08 | 0.2 | 124.5 | 1.08 | 0.2 |
| 125.8 | 1.00 | 0.2 | 127.1 | 0.95 | 0.2 | 128.5 | 1.56 | 0.2 |
| 129.8 | 0.99 | 0.2 | 131.2 | 1.06 | 0.2 | 132.6 | 1.13 | 0.2 |
| 134.0 | 0.92 | 0.2 | 135.4 | 0.88 | 0.2 | 136.9 | 0.88 | 0.2 |
| 138.4 | 1.14 | 0.3 | 139.5 | 1.00 | 0.3 | 140.7 | 1.11 | 0.3 |
| 141.8 | 1.01 | 0.3 | 143.0 | 0.93 | 0.3 | 144.2 | 0.96 | 0.3 |
| 145.4 | 0.98 | 0.3 | 146.6 | 0.77 | 0.3 | 147.9 | 0.62 | 0.3 |
| 149.1 | 0.76 | 0.2 | 150.4 | 1.18 | 0.2 | 151.7 | 1.09 | 0.2 |
| 153.0 | 0.83 | 0.2 | 154.3 | 0.94 | 0.2 | 155.6 | 0.59 | 0.2 |
| 157.0 | 0.93 | 0.2 | 158.4 | 0.95 | 0.2 | 159.8 | 0.57 | 0.2 |
| 161.2 | 0.78 | 0.2 | 162.6 | 1.09 | 0.2 | 164.0 | 1.30 | 0.2 |
| 165.5 | 0.56 | 0.2 | 167.0 | 1.05 | 0.2 | 168.5 | 0.95 | 0.2 |
| 170.0 | 0.81 | 0.2 | 171.6 | 1.07 | 0.2 | 173.1 | 0.89 | 0.2 |
| 174.7 | 0.83 | 0.2 | 176.3 | 0.57 | 0.2 | 178.0 | 0.53 | 0.2 |
| 179.6 | 1.01 | 0.2 | 181.3 | 0.97 | 0.2 | 183.0 | 0.58 | 0.2 |
| 184.7 | 0.50 | 0.2 | 186.5 | 0.46 | 0.2 | 188.2 | 0.57 | 0.2 |
| 190.0 | 0.58 | 0.2 | 191.9 | 0.90 | 0.2 | 193.7 | 0.40 | 0.2 |
| 195.6 | 0.56 | 0.2 | 197.5 | 0.78 | 0.2 | 199.4 | 0.51 | 0.2 |
| 201.4 | 0.40 | 0.2 | 203.4 | 0.42 | 0.2 | 205.4 | 0.37 | 0.2 |
| 207.5 | 0.17 | 0.2 | 209.6 | 0.22 | 0.2 | 211.7 | 0.31 | 0.2 |
| 213.8 | 0.22 | 0.2 | 216.0 | 0.73 | 0.2 | 218.2 | 0.44 | 0.2 |
| 220.5 | -0.07 | 0.3 | 222.0 | 0.15 | 0.3 | 223.5 | 0.15 | 0.3 |
| 225.1 | -0.37 | 0.3 | 226.7 | 0.45 | 0.3 | 228.2 | 0.22 | 0.3 |
| 229.8 | 0.36 | 0.3 | 231.5 | 0.02 | 0.3 | 233.1 | -0.08 | 0.3 |
| 234.7 | 0.23 | 0.3 | 236.4 | 0.53 | 0.3 | 238.1 | 0.11 | 0.3 |
| 239.8 | 0.42 | 0.3 | 241.5 | 0.16 | 0.3 | 243.3 | 0.17 | 0.3 |
| 245.0 | 0.45 | 0.3 | 246.8 | 0.35 | 0.3 | 248.6 | 0.47 | 0.3 |
| 250.4 | 0.50 | 0.3 | 252.3 | 0.97 | 0.3 | 254.1 | 1.22 | 0.3 |
| 256.0 | 1.73 | 0.3 | 257.9 | 2.10 | 0.4 | 258.9 | 3.35 | 0.4 |
| 259.8 | 3.50 | 0.4 | 260.8 | 5.28 | 0.4 | 261.8 | 6.53 | 0.4 |
| 262.7 | 7.36 | 0.4 | 263.7 | 9.06 | 0.4 | 264.7 | 9.89 | 0.4 |
| 265.7 | 9.82 | 0.4 | 266.7 | 8.50 | 0.4 | 267.7 | 7.18 | 0.4 |
| 268.7 | 5.77 | 0.4 | 269.8 | 4.53 | 0.4 | 270.8 | 3.88 | 0.4 |
| 271.8 | 3.28 | 0.4 | 272.9 | 2.63 | 0.4 | 273.9 | 2.48 | 0.4 |
| 275.0 | 2.49 | 0.4 | 276.0 | 2.66 | 0.4 | 277.1 | 2.24 | 0.4 |
| 278.1 | 2.65 | 0.4 | 279.2 | 2.63 | 0.4 | 280.3 | 3.19 | 0.4 |
| 281.4 | 3.52 | 0.4 | 282.5 | 3.81 | 0.4 | 283.6 | 4.67 | 0.4 |
| 284.7 | 4.05 | 0.4 | 285.8 | 4.56 | 0.4 | 286.9 | 5.25 | 0.4 |

| | | | | | | | | |
|---|---|---|---|---|---|---|---|---|
| 288.0 | 6.46 | 0.5 | 289.2 | 7.01 | 0.5 | 290.3 | 7.65 | 0.5 |
| 291.4 | 7.81 | 0.5 | 292.6 | 9.10 | 0.5 | 293.8 | 10.05 | 0.5 |
| 294.9 | 8.81 | 0.5 | 296.1 | 9.79 | 0.5 | 297.3 | 11.01 | 0.5 |
| 298.5 | 10.15 | 0.5 | 299.6 | 10.91 | 0.5 | 300.8 | 10.45 | 0.5 |
| 302.1 | 9.59 | 0.5 | 303.3 | 10.33 | 0.5 | 304.5 | 10.14 | 0.5 |
| 305.7 | 9.38 | 0.5 | 307.0 | 8.64 | 0.5 | 308.2 | 8.64 | 0.5 |
| 309.5 | 8.91 | 0.5 | 310.7 | 7.55 | 0.5 | 312.0 | 8.04 | 0.5 |
| 313.3 | 7.45 | 0.5 | 314.5 | 7.04 | 0.5 | 315.8 | 7.22 | 0.6 |
| 317.1 | 6.44 | 0.6 | 318.4 | 5.86 | 0.6 | 319.8 | 6.00 | 0.6 |
| 321.1 | 6.18 | 0.6 | 322.4 | 5.35 | 0.6 | 323.8 | 5.70 | 0.6 |
| 325.1 | 4.10 | 0.6 | 326.5 | 5.00 | 0.6 | 327.8 | 4.87 | 0.6 |
| 329.2 | 4.76 | 0.6 | 330.6 | 4.29 | 0.6 | 332.0 | 3.07 | 0.6 |
| 333.4 | 4.15 | 0.7 | 334.8 | 3.33 | 0.7 | 336.2 | 3.98 | 0.7 |
| 337.6 | 3.25 | 0.7 | 339.1 | 3.80 | 0.8 | 340.5 | 3.19 | 0.8 |
| 342.0 | 2.84 | 0.9 | 343.4 | 4.11 | 1.0 | 344.9 | 3.60 | 1.2 |
| 346.4 | 2.60 | 1.6 | 347.9 | 2.22 | 2.0 | 349.4 | -3.39 | 2.7 |
| 350.9 | 5.52 | 3.2 | 352.4 | -4.64 | 3.2 | 353.9 | -7.59 | 3.3 |

b) High energy run (130 - 800 keV)

$^{20}Ne$

| | | | | | | | | |
|---|---|---|---|---|---|---|---|---|
| 133.3 | 2.82 | 0.7 | 134.4 | 2.80 | 0.3 | 135.6 | 1.37 | 0.3 |
| 136.7 | 2.18 | 0.3 | 137.9 | 2.54 | 0.3 | 139.0 | 2.53 | 0.3 |
| 140.2 | 2.27 | 0.3 | 141.4 | 1.99 | 0.3 | 142.7 | 2.20 | 0.3 |
| 143.9 | 1.79 | 0.3 | 145.2 | 2.34 | 0.3 | 146.4 | 5.28 | 0.3 |
| 147.7 | 9.12 | 0.3 | 149.0 | 3.07 | 0.3 | 150.3 | 1.99 | 0.3 |
| 151.7 | 1.89 | 0.3 | 153.0 | 2.30 | 0.3 | 154.4 | 2.07 | 0.3 |
| 155.8 | 1.89 | 0.3 | 157.2 | 2.27 | 0.3 | 158.6 | 2.24 | 0.3 |
| 160.1 | 1.84 | 0.3 | 161.5 | 1.80 | 0.3 | 163.0 | 1.64 | 0.3 |
| 164.6 | 2.06 | 0.3 | 166.1 | 2.03 | 0.3 | 167.6 | 1.22 | 0.3 |
| 169.2 | 1.65 | 0.3 | 170.3 | 2.04 | 0.3 | 171.3 | 2.16 | 0.3 |
| 172.4 | 2.17 | 0.3 | 173.5 | 1.89 | 0.3 | 174.6 | 2.65 | 0.3 |
| 175.7 | 2.46 | 0.3 | 176.9 | 1.71 | 0.3 | 178.0 | 1.98 | 0.3 |
| 179.1 | 2.48 | 0.3 | 180.3 | 1.64 | 0.3 | 181.5 | 1.91 | 0.3 |
| 182.6 | 2.26 | 0.3 | 183.8 | 2.05 | 0.3 | 185.0 | 2.07 | 0.3 |
| 186.2 | 2.44 | 0.3 | 187.5 | 1.76 | 0.3 | 188.7 | 1.81 | 0.3 |
| 190.0 | 1.92 | 0.3 | 191.2 | 1.53 | 0.3 | 192.5 | 2.45 | 0.3 |
| 193.8 | 2.00 | 0.3 | 195.1 | 1.81 | 0.3 | 196.4 | 2.36 | 0.3 |
| 197.7 | 2.01 | 0.3 | 199.1 | 1.68 | 0.3 | 200.4 | 2.08 | 0.3 |
| 201.8 | 2.20 | 0.3 | 203.2 | 2.13 | 0.3 | 204.6 | 1.66 | 0.3 |
| 206.0 | 1.43 | 0.4 | 206.7 | 1.94 | 0.4 | 207.4 | 2.10 | 0.4 |
| 208.1 | 1.55 | 0.4 | 208.8 | 2.04 | 0.4 | 209.5 | 2.39 | 0.4 |
| 210.3 | 2.53 | 0.4 | 211.0 | 1.34 | 0.4 | 211.7 | 2.06 | 0.4 |
| 212.5 | 1.47 | 0.4 | 213.2 | 1.55 | 0.4 | 214.0 | 2.10 | 0.4 |
| 214.7 | 2.08 | 0.4 | 215.5 | 1.97 | 0.4 | 216.2 | 1.51 | 0.4 |
| 217.0 | 2.03 | 0.4 | 217.8 | 1.36 | 0.4 | 218.5 | 1.84 | 0.4 |
| 219.3 | 1.86 | 0.4 | 220.1 | 1.78 | 0.4 | 220.9 | 1.91 | 0.4 |
| 221.7 | 1.39 | 0.4 | 222.5 | 1.72 | 0.4 | 223.3 | 1.88 | 0.4 |
| 224.1 | 1.80 | 0.4 | 224.9 | 1.29 | 0.4 | 225.7 | 2.06 | 0.4 |
| 226.5 | 1.47 | 0.4 | 227.3 | 1.57 | 0.4 | 228.1 | 1.18 | 0.4 |
| 229.0 | 2.20 | 0.4 | 229.8 | 1.19 | 0.4 | 230.6 | 1.60 | 0.4 |
| 231.5 | 1.69 | 0.4 | 232.3 | 2.23 | 0.4 | 233.2 | 1.31 | 0.4 |
| 234.0 | 2.41 | 0.4 | 234.9 | 1.23 | 0.4 | 235.8 | 1.74 | 0.4 |

| | | | | | | | | |
|---|---|---|---|---|---|---|---|---|
| 236.6 | 2.00 | 0.4 | 237.5 | 1.12 | 0.4 | 238.4 | 1.38 | 0.4 |
| 239.3 | 1.16 | 0.4 | 240.1 | 1.84 | 0.4 | 241.0 | 1.71 | 0.4 |
| 241.9 | 2.25 | 0.4 | 242.8 | 1.65 | 0.4 | 243.8 | 2.07 | 0.4 |
| 244.7 | 1.57 | 0.4 | 245.6 | 2.34 | 0.4 | 246.5 | 1.38 | 0.4 |
| 247.4 | 1.37 | 0.4 | 248.4 | 1.82 | 0.4 | 249.3 | 1.95 | 0.4 |
| 250.3 | 2.47 | 0.4 | 251.2 | 1.79 | 0.4 | 252.2 | 1.35 | 0.4 |
| 253.1 | 2.02 | 0.4 | 254.1 | 1.88 | 0.4 | 255.1 | 1.64 | 0.4 |
| 256.0 | 1.59 | 0.4 | 257.0 | 1.53 | 0.4 | 258.0 | 1.42 | 0.3 |
| 259.0 | 1.77 | 0.3 | 260.0 | 1.23 | 0.3 | 261.0 | 1.76 | 0.3 |
| 262.0 | 2.37 | 0.3 | 263.0 | 2.66 | 0.3 | 264.1 | 2.50 | 0.3 |
| 265.1 | 2.32 | 0.3 | 266.1 | 2.27 | 0.3 | 267.2 | 2.17 | 0.3 |
| 268.2 | 2.22 | 0.3 | 269.3 | 1.51 | 0.3 | 270.3 | 2.41 | 0.3 |
| 271.4 | 2.03 | 0.3 | 272.5 | 1.83 | 0.3 | 273.6 | 1.87 | 0.3 |
| 274.6 | 1.55 | 0.3 | 275.7 | 1.26 | 0.3 | 276.8 | 2.03 | 0.3 |
| 277.9 | 1.09 | 0.3 | 279.0 | 1.70 | 0.3 | 280.2 | 1.79 | 0.3 |
| 281.3 | 1.79 | 0.3 | 282.4 | 1.71 | 0.3 | 283.6 | 1.99 | 0.3 |
| 284.7 | 2.35 | 0.3 | 285.9 | 1.96 | 0.3 | 287.0 | 2.38 | 0.3 |
| 288.2 | 1.79 | 0.3 | 289.4 | 1.65 | 0.3 | 290.5 | 1.90 | 0.3 |
| 291.7 | 1.83 | 0.3 | 292.9 | 2.07 | 0.3 | 294.1 | 1.87 | 0.3 |
| 295.3 | 2.43 | 0.3 | 296.6 | 1.94 | 0.3 | 297.8 | 1.85 | 0.3 |
| 299.0 | 2.43 | 0.3 | 300.3 | 1.96 | 0.3 | 301.5 | 2.34 | 0.3 |
| 302.8 | 2.00 | 0.3 | 304.0 | 2.38 | 0.3 | 305.3 | 2.12 | 0.3 |
| 306.6 | 2.34 | 0.3 | 307.9 | 2.27 | 0.3 | 309.2 | 1.96 | 0.3 |
| 310.5 | 2.09 | 0.3 | 311.8 | 1.53 | 0.3 | 313.1 | 1.93 | 0.3 |
| 314.4 | 2.02 | 0.3 | 315.8 | 1.76 | 0.3 | 317.1 | 2.04 | 0.3 |
| 318.5 | 1.94 | 0.3 | 319.8 | 1.70 | 0.3 | 321.2 | 1.95 | 0.3 |
| 322.6 | 1.59 | 0.3 | 324.0 | 1.56 | 0.3 | 325.4 | 1.44 | 0.3 |
| 326.8 | 1.26 | 0.3 | 328.2 | 1.58 | 0.3 | 329.6 | 1.21 | 0.3 |
| 331.1 | 1.23 | 0.3 | 332.5 | 1.24 | 0.3 | 334.0 | 1.22 | 0.3 |
| 335.4 | 1.95 | 0.3 | 336.9 | 1.34 | 0.3 | 338.4 | 1.34 | 0.3 |
| 339.9 | 1.45 | 0.3 | 341.4 | 1.07 | 0.3 | 342.9 | 1.13 | 0.3 |
| 344.4 | 1.46 | 0.3 | 346.0 | 1.03 | 0.3 | 347.5 | 1.42 | 0.3 |
| 349.1 | 1.41 | 0.3 | 350.6 | 1.15 | 0.3 | 352.2 | 1.18 | 0.3 |
| 353.8 | 1.08 | 0.3 | 355.4 | 0.80 | 0.3 | 357.0 | 0.92 | 0.3 |
| 358.6 | 1.35 | 0.3 | 360.3 | 0.85 | 0.3 | 361.9 | 1.01 | 0.3 |
| 363.6 | 1.23 | 0.3 | 365.2 | 1.14 | 0.2 | 366.9 | 1.09 | 0.2 |
| 368.6 | 0.86 | 0.2 | 370.3 | 1.05 | 0.2 | 372.0 | 0.73 | 0.2 |
| 373.7 | 0.70 | 0.2 | 375.4 | 0.67 | 0.2 | 377.2 | 0.40 | 0.2 |
| 378.9 | 0.85 | 0.2 | 380.7 | 0.67 | 0.2 | 382.5 | 0.88 | 0.2 |
| 384.3 | 0.69 | 0.2 | 386.1 | 0.65 | 0.2 | 387.9 | 0.58 | 0.2 |
| 389.8 | 0.40 | 0.2 | 391.6 | 0.62 | 0.2 | 393.5 | 0.94 | 0.2 |
| 395.3 | 0.59 | 0.2 | 397.2 | 0.23 | 0.2 | 399.1 | 0.31 | 0.2 |
| 401.1 | 0.54 | 0.2 | 403.0 | 0.64 | 0.2 | 404.9 | 0.55 | 0.2 |
| 406.9 | 0.55 | 0.2 | 408.9 | 0.59 | 0.2 | 410.8 | 0.64 | 0.2 |
| 412.8 | 0.37 | 0.2 | 414.9 | 0.43 | 0.2 | 416.9 | 0.19 | 0.3 |
| 418.9 | 0.72 | 0.3 | 421.0 | 1.66 | 0.3 | 423.1 | 1.94 | 0.3 |
| 425.2 | 1.67 | 0.3 | 427.3 | 1.03 | 0.3 | 429.4 | 0.89 | 0.3 |
| 431.5 | 1.17 | 0.3 | 433.7 | 0.78 | 0.3 | 435.8 | 1.15 | 0.3 |
| 438.0 | 1.63 | 0.3 | 440.2 | 0.88 | 0.3 | 442.4 | 1.20 | 0.3 |
| 444.7 | 1.31 | 0.3 | 446.9 | 1.17 | 0.3 | 449.2 | 1.50 | 0.3 |
| 451.5 | 1.17 | 0.3 | 453.8 | 1.84 | 0.3 | 456.1 | 1.84 | 0.3 |
| 458.4 | 1.82 | 0.2 | 460.8 | 2.38 | 0.2 | 463.2 | 2.69 | 0.2 |
| 465.6 | 3.10 | 0.2 | 468.0 | 3.02 | 0.2 | 470.4 | 3.21 | 0.2 |
| 472.9 | 3.72 | 0.2 | 475.3 | 3.70 | 0.2 | 477.8 | 3.88 | 0.2 |
| 480.3 | 4.29 | 0.2 | 482.9 | 4.71 | 0.2 | 485.4 | 4.65 | 0.2 |
| 488.0 | 4.87 | 0.2 | 490.6 | 5.05 | 0.2 | 493.2 | 5.46 | 0.2 |

| | | | | | | | | |
|---|---|---|---|---|---|---|---|---|
| 495.8 | 5.75 | 0.2 | 498.5 | 5.96 | 0.2 | 501.1 | 6.24 | 0.2 |
| 503.8 | 5.97 | 0.2 | 506.6 | 6.19 | 0.2 | 509.3 | 6.04 | 0.2 |
| 512.1 | 6.09 | 0.2 | 514.9 | 6.11 | 0.2 | 517.7 | 6.09 | 0.2 |
| 520.5 | 6.34 | 0.2 | 523.3 | 6.20 | 0.2 | 526.2 | 6.29 | 0.2 |
| 529.1 | 6.02 | 0.2 | 532.0 | 6.10 | 0.2 | 535.0 | 6.16 | 0.2 |
| 538.0 | 5.98 | 0.2 | 541.0 | 6.03 | 0.2 | 544.0 | 6.07 | 0.2 |
| 547.0 | 6.07 | 0.2 | 550.1 | 5.91 | 0.2 | 553.2 | 5.93 | 0.2 |
| 556.4 | 5.56 | 0.2 | 559.5 | 5.60 | 0.2 | 562.7 | 5.32 | 0.2 |
| 565.9 | 5.26 | 0.2 | 569.1 | 5.29 | 0.2 | 572.4 | 5.18 | 0.2 |
| 575.7 | 5.29 | 0.2 | 579.0 | 5.39 | 0.2 | 582.4 | 4.99 | 0.2 |
| 585.7 | 5.10 | 0.2 | 589.1 | 4.85 | 0.2 | 592.6 | 4.70 | 0.2 |
| 596.1 | 4.83 | 0.2 | 599.6 | 4.46 | 0.2 | 603.1 | 4.27 | 0.2 |
| 606.6 | 3.87 | 0.3 | 610.2 | 3.99 | 0.3 | 613.9 | 4.35 | 0.4 |
| 617.5 | 4.04 | 0.4 | 621.2 | 3.97 | 0.4 | 624.9 | 4.39 | 0.4 |
| 628.7 | 4.46 | 0.4 | 632.5 | 4.83 | 0.4 | 636.3 | 3.41 | 0.4 |
| 640.2 | 3.97 | 0.5 | 644.1 | 4.24 | 0.5 | 648.0 | 3.95 | 0.5 |
| 652.0 | 3.85 | 0.5 | 656.0 | 4.47 | 0.5 | 660.0 | 4.71 | 0.5 |
| 664.1 | 4.17 | 0.5 | 668.2 | 4.71 | 0.5 | 672.4 | 5.03 | 0.5 |
| 676.5 | 3.98 | 0.5 | 680.8 | 4.18 | 0.5 | 685.1 | 4.57 | 0.5 |
| 689.4 | 4.97 | 0.5 | 693.7 | 4.25 | 0.5 | 698.1 | 4.31 | 0.5 |
| 702.6 | 4.54 | 0.5 | 707.0 | 3.61 | 0.5 | 711.6 | 4.49 | 0.6 |
| 716.1 | 3.80 | 0.6 | 720.7 | 3.38 | 0.6 | 725.4 | 3.17 | 0.7 |
| 730.1 | 2.49 | 0.7 | 734.8 | 3.49 | 0.7 | 739.6 | 5.27 | 0.7 |
| 744.5 | 2.00 | 0.7 | 749.4 | 4.61 | 0.8 | 754.3 | 2.72 | 0.8 |
| 759.3 | 3.85 | 0.8 | 764.3 | 3.27 | 0.9 | 769.4 | 1.71 | 0.9 |
| 774.5 | 2.30 | 0.9 | 779.7 | 4.07 | 0.9 | 785.0 | 0.26 | 1.0 |
| 790.3 | 1.43 | 1.1 | 795.6 | 3.08 | 1.1 | 801.0 | 1.26 | 1.2 |

$^{21}$NE

| | | | | | | | | |
|---|---|---|---|---|---|---|---|---|
| 133.3 | 6.69 | 7.3 | 134.4 | 18.20 | 3.1 | 135.6 | 20.26 | 3.2 |
| 136.7 | 28.82 | 3.1 | 137.9 | 21.32 | 3.1 | 139.0 | 20.79 | 3.0 |
| 140.2 | 13.94 | 3.0 | 141.4 | 7.46 | 2.9 | 142.7 | 8.32 | 2.8 |
| 143.9 | 7.79 | 2.8 | 145.2 | 5.37 | 2.8 | 146.4 | 11.95 | 2.8 |
| 147.7 | 10.29 | 2.8 | 149.0 | 4.98 | 2.7 | 150.3 | 7.05 | 2.7 |
| 151.7 | 1.16 | 2.7 | 153.0 | 7.68 | 2.7 | 154.4 | 6.39 | 2.7 |
| 155.8 | 3.86 | 2.6 | 157.2 | 9.56 | 2.6 | 158.6 | 7.90 | 2.6 |
| 160.1 | 7.95 | 2.6 | 161.5 | 5.82 | 2.6 | 163.0 | 4.81 | 2.6 |
| 164.6 | 5.72 | 2.5 | 166.1 | 4.73 | 2.5 | 167.6 | 5.83 | 2.5 |
| 169.2 | 0.57 | 3.1 | 170.3 | 7.82 | 3.0 | 171.3 | 8.28 | 3.0 |
| 172.4 | 3.77 | 3.0 | 173.5 | 4.41 | 3.0 | 174.6 | 10.92 | 3.0 |
| 175.7 | 6.96 | 3.0 | 176.9 | 9.39 | 3.0 | 178.0 | 3.31 | 2.9 |
| 179.1 | 8.89 | 2.9 | 180.3 | 1.05 | 2.9 | 181.5 | 7.44 | 2.9 |
| 182.6 | 12.06 | 2.9 | 183.8 | 14.83 | 2.8 | 185.0 | 5.26 | 2.6 |
| 186.2 | 9.11 | 2.7 | 187.5 | 8.21 | 2.8 | 188.7 | 6.62 | 2.8 |
| 190.0 | 2.53 | 2.8 | 191.2 | 4.21 | 2.8 | 192.5 | 9.94 | 2.8 |
| 193.8 | 7.23 | 2.8 | 195.1 | 1.66 | 2.7 | 196.4 | 7.40 | 2.7 |
| 197.7 | 4.51 | 2.7 | 199.1 | 4.12 | 2.7 | 200.4 | 3.39 | 2.7 |
| 201.8 | 8.55 | 2.7 | 203.2 | 2.87 | 2.6 | 204.6 | 3.44 | 2.6 |
| 206.0 | 0.29 | 3.7 | 206.7 | 4.23 | 3.7 | 207.4 | 4.99 | 3.7 |
| 208.1 | 3.03 | 3.7 | 208.8 | 7.78 | 3.7 | 209.5 | 4.70 | 3.7 |
| 210.3 | 8.86 | 3.7 | 211.0 | -2.07 | 3.7 | 211.7 | 7.78 | 3.7 |
| 212.5 | 1.85 | 3.7 | 213.2 | 0.14 | 3.6 | 214.0 | 3.12 | 3.6 |
| 214.7 | 3.78 | 3.6 | 215.5 | 4.82 | 3.6 | 216.2 | 0.45 | 3.6 |
| 217.0 | 5.72 | 3.6 | 217.8 | 1.62 | 3.6 | 218.5 | 0.84 | 3.6 |

| | | | | | | | | |
|---|---|---|---|---|---|---|---|---|
| 219.3 | 3.40 | 3.6 | 220.1 | 4.47 | 3.5 | 220.9 | 2.03 | 3.5 |
| 221.7 | 0.84 | 3.5 | 222.5 | 0.66 | 3.5 | 223.3 | 3.67 | 3.5 |
| 224.1 | 9.45 | 3.5 | 224.9 | -1.72 | 3.5 | 225.7 | 5.34 | 3.5 |
| 226.5 | -1.69 | 3.5 | 227.3 | 2.94 | 3.5 | 228.1 | -0.41 | 3.4 |
| 229.0 | 5.51 | 3.5 | 229.8 | 2.31 | 3.4 | 230.6 | 0.13 | 3.4 |
| 231.5 | 4.90 | 3.4 | 232.3 | 5.87 | 3.4 | 233.2 | 5.96 | 3.4 |
| 234.0 | 9.44 | 3.4 | 234.9 | 1.32 | 3.4 | 235.8 | 4.36 | 3.4 |
| 236.6 | 4.01 | 3.4 | 237.5 | -0.92 | 3.4 | 238.4 | 2.55 | 3.4 |
| 239.3 | -1.51 | 3.4 | 240.1 | 2.79 | 3.3 | 241.0 | 4.03 | 3.3 |
| 241.9 | 0.34 | 3.3 | 242.8 | 2.65 | 3.3 | 243.8 | 9.21 | 3.3 |
| 244.7 | 8.29 | 3.3 | 245.6 | 8.42 | 3.3 | 246.5 | -2.02 | 3.3 |
| 247.4 | 1.81 | 3.3 | 248.4 | -1.72 | 3.3 | 249.3 | -1.60 | 3.3 |
| 250.3 | 7.90 | 3.3 | 251.2 | 1.13 | 3.3 | 252.2 | -0.98 | 3.3 |

$^{22}$NE

| | | | | | | | | |
|---|---|---|---|---|---|---|---|---|
| 133.3 | -5.44 | 0.9 | 134.4 | 1.96 | 0.4 | 135.6 | 0.95 | 0.4 |
| 136.7 | 2.02 | 0.4 | 137.9 | 2.04 | 0.4 | 139.0 | 1.27 | 0.4 |
| 140.2 | 2.07 | 0.4 | 141.4 | 1.15 | 0.4 | 142.7 | 1.45 | 0.4 |
| 143.9 | 0.83 | 0.4 | 145.2 | 1.24 | 0.4 | 146.4 | 1.68 | 0.4 |
| 147.7 | 1.35 | 0.4 | 149.0 | 1.93 | 0.3 | 150.3 | 1.40 | 0.3 |
| 151.7 | 0.82 | 0.3 | 153.0 | 1.80 | 0.3 | 154.4 | 1.80 | 0.3 |
| 155.8 | 1.52 | 0.3 | 157.2 | 1.45 | 0.3 | 158.6 | 1.38 | 0.3 |
| 160.1 | 1.75 | 0.3 | 161.5 | 1.39 | 0.3 | 163.0 | 0.80 | 0.3 |
| 164.6 | 1.54 | 0.3 | 166.1 | 1.08 | 0.3 | 167.6 | 0.83 | 0.3 |
| 169.2 | 1.03 | 0.4 | 170.3 | 0.96 | 0.4 | 171.3 | 1.19 | 0.4 |
| 172.4 | 1.46 | 0.4 | 173.5 | 1.69 | 0.4 | 174.6 | 2.33 | 0.4 |
| 175.7 | 1.39 | 0.4 | 176.9 | 1.36 | 0.4 | 178.0 | 1.65 | 0.4 |
| 179.1 | 1.47 | 0.4 | 180.3 | 1.15 | 0.4 | 181.5 | 0.93 | 0.4 |
| 182.6 | 1.55 | 0.4 | 183.8 | 1.88 | 0.4 | 185.0 | 1.55 | 0.3 |
| 186.2 | 1.95 | 0.3 | 187.5 | 1.51 | 0.4 | 188.7 | 1.06 | 0.4 |
| 190.0 | 1.01 | 0.4 | 191.2 | 0.63 | 0.4 | 192.5 | 0.74 | 0.3 |
| 193.8 | 1.70 | 0.4 | 195.1 | 0.92 | 0.3 | 196.4 | 1.10 | 0.3 |
| 197.7 | 1.08 | 0.3 | 199.1 | 1.35 | 0.3 | 200.4 | 1.26 | 0.3 |
| 201.8 | 1.56 | 0.3 | 203.2 | 1.26 | 0.3 | 204.6 | 1.19 | 0.3 |
| 206.0 | 0.82 | 0.5 | 206.7 | 1.77 | 0.5 | 207.4 | 1.10 | 0.5 |
| 208.1 | 0.75 | 0.5 | 208.8 | 0.26 | 0.5 | 209.5 | 1.22 | 0.5 |
| 210.3 | 1.40 | 0.5 | 211.0 | 0.05 | 0.5 | 211.7 | 0.94 | 0.5 |
| 212.5 | 0.20 | 0.5 | 213.2 | 0.48 | 0.5 | 214.0 | 0.93 | 0.5 |
| 214.7 | 0.58 | 0.5 | 215.5 | 0.45 | 0.5 | 216.2 | 0.74 | 0.5 |
| 217.0 | 1.04 | 0.5 | 217.8 | 0.38 | 0.5 | 218.5 | 0.71 | 0.5 |
| 219.3 | 0.86 | 0.5 | 220.1 | 0.97 | 0.4 | 220.9 | 0.38 | 0.4 |
| 221.7 | 0.43 | 0.4 | 222.5 | 0.63 | 0.4 | 223.3 | 1.17 | 0.4 |
| 224.1 | 0.73 | 0.4 | 224.9 | 0.62 | 0.4 | 225.7 | 1.21 | 0.4 |
| 226.5 | 0.05 | 0.4 | 227.3 | 0.94 | 0.4 | 228.1 | 0.52 | 0.4 |
| 229.0 | 1.06 | 0.4 | 229.8 | 0.68 | 0.4 | 230.6 | 0.40 | 0.4 |
| 231.5 | 0.71 | 0.4 | 232.3 | 0.65 | 0.4 | 233.2 | 0.69 | 0.4 |
| 234.0 | 1.90 | 0.4 | 234.9 | 0.65 | 0.4 | 235.8 | 0.73 | 0.4 |
| 236.6 | 0.74 | 0.4 | 237.5 | -0.15 | 0.4 | 238.4 | 0.19 | 0.4 |
| 239.3 | 0.71 | 0.4 | 240.1 | 1.01 | 0.4 | 241.0 | 1.02 | 0.4 |
| 241.9 | 0.45 | 0.4 | 242.8 | 0.35 | 0.4 | 243.8 | 1.43 | 0.4 |
| 244.7 | 1.48 | 0.4 | 245.6 | 1.13 | 0.4 | 246.5 | 0.26 | 0.4 |
| 247.4 | 0.17 | 0.4 | 248.4 | 1.15 | 0.4 | 249.3 | 0.81 | 0.4 |
| 250.3 | 1.12 | 0.4 | 251.2 | 0.94 | 0.4 | 252.2 | 1.07 | 0.4 |
| 253.1 | 2.11 | 0.4 | 254.1 | 1.23 | 0.4 | 255.1 | 1.38 | 0.4 |

| | | | | | | | | |
|---|---|---|---|---|---|---|---|---|
| 256.0 | 1.45 | 0.4 | 257.0 | 1.92 | 0.4 | 258.0 | 2.10 | 0.4 |
| 259.0 | 3.18 | 0.4 | 260.0 | 3.18 | 0.4 | 261.0 | 4.48 | 0.4 |
| 262.0 | 6.08 | 0.4 | 263.0 | 8.27 | 0.4 | 264.1 | 9.06 | 0.4 |
| 265.1 | 9.40 | 0.4 | 266.1 | 9.15 | 0.4 | 267.2 | 8.13 | 0.4 |
| 268.2 | 6.85 | 0.4 | 269.3 | 5.26 | 0.4 | 270.3 | 4.69 | 0.4 |
| 271.4 | 3.52 | 0.4 | 272.5 | 2.59 | 0.4 | 273.6 | 3.03 | 0.4 |
| 274.6 | 2.85 | 0.4 | 275.7 | 2.35 | 0.4 | 276.8 | 2.95 | 0.4 |
| 277.9 | 2.74 | 0.4 | 279.0 | 2.49 | 0.4 | 280.2 | 3.13 | 0.4 |
| 281.3 | 3.58 | 0.4 | 282.4 | 3.70 | 0.4 | 283.6 | 4.50 | 0.4 |
| 284.7 | 4.59 | 0.4 | 285.9 | 4.29 | 0.4 | 287.0 | 5.34 | 0.4 |
| 288.2 | 6.17 | 0.4 | 289.4 | 6.17 | 0.4 | 290.5 | 6.83 | 0.4 |
| 291.7 | 7.67 | 0.4 | 292.9 | 7.74 | 0.4 | 294.1 | 8.47 | 0.4 |
| 295.3 | 9.44 | 0.4 | 296.6 | 8.68 | 0.4 | 297.8 | 9.62 | 0.4 |
| 299.0 | 9.64 | 0.4 | 300.3 | 9.74 | 0.4 | 301.5 | 9.14 | 0.4 |
| 302.8 | 9.46 | 0.4 | 304.0 | 8.85 | 0.4 | 305.3 | 8.72 | 0.4 |
| 306.6 | 8.46 | 0.4 | 307.9 | 8.00 | 0.4 | 309.2 | 7.63 | 0.4 |
| 310.5 | 7.38 | 0.4 | 311.8 | 6.97 | 0.4 | 313.1 | 7.15 | 0.4 |
| 314.4 | 6.19 | 0.3 | 315.8 | 5.68 | 0.3 | 317.1 | 6.07 | 0.3 |
| 318.5 | 6.01 | 0.3 | 319.8 | 4.76 | 0.3 | 321.2 | 5.78 | 0.3 |
| 322.6 | 4.92 | 0.3 | 324.0 | 4.46 | 0.3 | 325.4 | 4.63 | 0.3 |
| 326.8 | 3.98 | 0.3 | 328.2 | 4.53 | 0.3 | 329.6 | 3.69 | 0.3 |
| 331.1 | 3.47 | 0.3 | 332.5 | 3.26 | 0.3 | 334.0 | 3.37 | 0.3 |
| 335.4 | 4.38 | 0.3 | 336.9 | 3.55 | 0.3 | 338.4 | 2.97 | 0.3 |
| 339.9 | 3.00 | 0.3 | 341.4 | 2.58 | 0.3 | 342.9 | 3.05 | 0.3 |
| 344.4 | 3.08 | 0.3 | 346.0 | 2.30 | 0.3 | 347.5 | 3.29 | 0.3 |
| 349.1 | 2.53 | 0.3 | 350.6 | 1.79 | 0.3 | 352.2 | 2.41 | 0.3 |
| 353.8 | 2.29 | 0.3 | 355.4 | 1.78 | 0.3 | 357.0 | 2.22 | 0.3 |
| 358.6 | 2.03 | 0.3 | 360.3 | 1.88 | 0.3 | 361.9 | 1.43 | 0.3 |
| 363.6 | 2.08 | 0.3 | 365.2 | 1.66 | 0.3 | 366.9 | 1.67 | 0.3 |
| 368.6 | 1.59 | 0.3 | 370.3 | 1.46 | 0.3 | 372.0 | 1.33 | 0.3 |
| 373.7 | 1.50 | 0.3 | 375.4 | 1.44 | 0.3 | 377.2 | 0.95 | 0.3 |
| 378.9 | 1.09 | 0.3 | 380.7 | 1.32 | 0.3 | 382.5 | 1.16 | 0.3 |
| 384.3 | 0.86 | 0.3 | 386.1 | 1.17 | 0.3 | 387.9 | 1.02 | 0.3 |
| 389.8 | 1.04 | 0.3 | 391.6 | 0.61 | 0.3 | 393.5 | 1.23 | 0.3 |
| 395.3 | 0.67 | 0.2 | 397.2 | 0.50 | 0.2 | 399.1 | 0.62 | 0.2 |
| 401.1 | 0.68 | 0.2 | 403.0 | 0.34 | 0.2 | 404.9 | 0.85 | 0.2 |
| 406.9 | 0.46 | 0.2 | 408.9 | 0.82 | 0.2 | 410.8 | 0.81 | 0.2 |
| 412.8 | 1.18 | 0.3 | 414.9 | 1.23 | 0.3 | 416.9 | 1.49 | 0.3 |
| 418.9 | 2.72 | 0.3 | 421.0 | 4.91 | 0.3 | 423.1 | 5.73 | 0.4 |
| 425.2 | 5.08 | 0.4 | 427.3 | 2.96 | 0.4 | 429.4 | 1.79 | 0.4 |
| 431.5 | 0.97 | 0.4 | 433.7 | 1.43 | 0.3 | 435.8 | 1.12 | 0.3 |
| 438.0 | 1.59 | 0.3 | 440.2 | 1.05 | 0.3 | 442.4 | 0.83 | 0.3 |
| 444.7 | 1.11 | 0.3 | 446.9 | 0.98 | 0.3 | 449.2 | 0.69 | 0.3 |
| 451.5 | 1.11 | 0.3 | 453.8 | 1.16 | 0.3 | 456.1 | 1.42 | 0.3 |
| 458.4 | 1.28 | 0.3 | 460.8 | 1.96 | 0.3 | 463.2 | 1.91 | 0.3 |
| 465.6 | 2.01 | 0.3 | 468.0 | 1.76 | 0.2 | 470.4 | 1.71 | 0.2 |
| 472.9 | 1.85 | 0.2 | 475.3 | 1.79 | 0.2 | 477.8 | 2.21 | 0.2 |
| 480.3 | 2.31 | 0.2 | 482.9 | 2.80 | 0.2 | 485.4 | 2.50 | 0.2 |
| 488.0 | 2.59 | 0.2 | 490.6 | 2.92 | 0.2 | 493.2 | 3.05 | 0.2 |
| 495.8 | 3.51 | 0.2 | 498.5 | 3.42 | 0.2 | 501.1 | 3.58 | 0.2 |
| 503.8 | 3.84 | 0.2 | 506.6 | 3.88 | 0.2 | 509.3 | 4.22 | 0.2 |
| 512.1 | 4.32 | 0.2 | 514.9 | 4.40 | 0.2 | 517.7 | 4.65 | 0.2 |
| 520.5 | 4.89 | 0.2 | 523.3 | 4.85 | 0.2 | 526.2 | 4.88 | 0.2 |
| 529.1 | 5.05 | 0.2 | 532.0 | 5.53 | 0.2 | 535.0 | 5.66 | 0.2 |
| 538.0 | 6.14 | 0.2 | 541.0 | 7.07 | 0.2 | 544.0 | 8.93 | 0.2 |
| 547.0 | 9.28 | 0.2 | 550.1 | 7.67 | 0.2 | 553.2 | 6.61 | 0.2 |

| | | | | | | | | |
|---|---|---|---|---|---|---|---|---|
| 556.4 | 5.82 | 0.2 | 559.5 | 5.65 | 0.2 | 562.7 | 5.38 | 0.2 |
| 565.9 | 5.27 | 0.2 | 569.1 | 5.48 | 0.2 | 572.4 | 5.04 | 0.2 |
| 575.7 | 5.33 | 0.2 | 579.0 | 5.37 | 0.2 | 582.4 | 5.07 | 0.2 |
| 585.7 | 5.34 | 0.2 | 589.1 | 4.95 | 0.2 | 592.6 | 4.99 | 0.2 |
| 596.1 | 4.83 | 0.2 | 599.6 | 4.71 | 0.2 | 603.1 | 4.83 | 0.2 |
| 606.6 | 4.98 | 0.2 | 610.2 | 4.91 | 0.3 | 613.9 | 5.04 | 0.3 |
| 617.5 | 5.03 | 0.3 | 621.2 | 5.18 | 0.3 | 624.9 | 5.62 | 0.3 |
| 628.7 | 5.44 | 0.3 | 632.5 | 5.67 | 0.3 | 636.3 | 5.82 | 0.3 |
| 640.2 | 5.82 | 0.3 | 644.1 | 5.99 | 0.3 | 648.0 | 7.04 | 0.3 |
| 652.0 | 7.09 | 0.3 | 656.0 | 7.59 | 0.3 | 660.0 | 8.83 | 0.3 |
| 664.1 | 9.94 | 0.3 | 668.2 | 10.89 | 0.3 | 672.4 | 11.58 | 0.3 |
| 676.5 | 11.83 | 0.3 | 680.8 | 11.63 | 0.3 | 685.1 | 10.87 | 0.3 |
| 689.4 | 9.82 | 0.3 | 693.7 | 8.71 | 0.3 | 698.1 | 7.57 | 0.3 |
| 702.6 | 7.88 | 0.3 | 707.0 | 6.60 | 0.3 | 711.6 | 6.27 | 0.3 |
| 716.1 | 5.03 | 0.3 | 720.7 | 5.63 | 0.3 | 725.4 | 4.68 | 0.3 |
| 730.1 | 4.81 | 0.3 | 734.8 | 4.52 | 0.3 | 739.6 | 5.15 | 0.3 |
| 744.5 | 4.48 | 0.3 | 749.4 | 4.19 | 0.3 | 754.3 | 3.82 | 0.4 |
| 759.3 | 4.01 | 0.4 | 764.3 | 3.64 | 0.4 | 769.4 | 3.44 | 0.4 |
| 774.5 | 3.48 | 0.4 | 779.7 | 3.07 | 0.4 | 785.0 | 2.06 | 0.5 |
| 790.3 | 1.79 | 0.6 | 795.6 | 0.97 | 0.8 | 801.0 | 0.35 | 1.1 |

## APPENDIX 2

### CAPTURE CROSS SECTIONS

Neutron Separation energies:

| | | | |
|---|---|---|---|
| $^{20}Ne + n$ | = | 6.76 | MeV |
| $^{21}Ne + n$ | = | 10.37 | MeV |
| $^{22}Ne + n$ | = | 5.20 | MeV |
| $^{197}Au + n$ | = | 6.51 | MeV |

---

### $^{20}Ne$

| $E_n$ keV | σ mb | Δσ mb | $E_n$ | σ | Δσ | $E_n$ | σ | Δσ |
|---|---|---|---|---|---|---|---|---|
| 4.1 | 22.3 | 28.8 | 4.5 | 90.4 | 29.3 | 4.9 | -17.8 | 26.6 |
| 5.3 | 63.7 | 25.3 | 5.7 | 44.6 | 27.8 | 6.1 | 19.4 | 23.5 |
| 6.5 | -23.0 | 19.0 | 6.9 | 9.1 | 16.4 | 7.4 | 19.7 | 14.9 |
| 7.8 | -1.8 | 14.0 | 8.2 | 44.6 | 13.3 | 8.6 | 39.6 | 12.6 |
| 9.0 | 21.2 | 12.5 | 9.4 | 13.3 | 12.5 | 9.8 | 9.5 | 11.8 |
| 10.2 | 5.2 | 11.5 | 10.7 | -57.4 | 10.9 | 11.1 | -15.4 | 10.9 |
| 11.5 | -12.6 | 10.3 | 12.0 | 33.6 | 10.2 | 12.4 | 11.0 | 9.4 |
| 12.8 | 16.8 | 9.2 | 13.3 | 26.4 | 8.7 | 13.7 | 17.5 | 8.1 |
| 14.1 | 11.6 | 8.0 | 14.5 | 14.2 | 7.4 | 15.0 | 30.2 | 6.9 |
| 15.4 | 10.2 | 6.2 | 15.9 | 5.0 | 5.8 | 16.4 | -1.1 | 5.9 |
| 16.8 | 9.1 | 5.4 | 17.2 | 14.1 | 5.1 | 17.7 | -6.5 | 4.8 |
| 18.2 | -3.2 | 4.5 | 18.6 | 17.1 | 4.7 | 19.0 | -14.7 | 4.5 |
| 19.5 | -4.9 | 4.2 | 19.9 | 16.0 | 4.1 | 15.4 | -3.1 | 3.8 |
| 20.8 | -12.1 | 3.6 | 21.3 | -2.6 | 3.5 | 21.9 | 4.0 | 3.2 |
| 22.4 | -3.9 | 3.2 | 22.9 | 10.7 | 3.6 | 23.3 | 0.0 | 3.5 |
| 23.7 | 13.7 | 3.3 | 24.2 | 5.8 | 3.0 | 24.6 | 4.5 | 2.9 |
| 25.1 | -5.3 | 2.7 | 25.6 | -5.7 | 2.6 | 26.1 | 1.5 | 2.6 |
| 26.6 | -0.6 | 2.7 | 27.1 | -2.7 | 2.7 | 27.7 | -1.8 | 2.6 |
| 28.2 | 9.5 | 2.6 | 28.8 | 7.6 | 2.4 | 29.3 | 18.8 | 2.8 |
| 29.7 | 14.9 | 2.6 | 30.1 | -0.3 | 2.6 | 30.6 | -0.2 | 2.4 |
| 31.0 | 1.6 | 2.3 | 31.4 | 4.2 | 2.4 | 31.9 | 3.2 | 2.3 |
| 32.3 | -1.3 | 2.3 | 32.8 | 2.4 | 2.3 | 33.3 | -6.6 | 2.3 |
| 33.8 | 9.5 | 2.3 | 34.3 | 1.1 | 2.3 | 34.8 | 8.9 | 2.3 |
| 35.3 | 5.2 | 2.2 | 35.9 | 9.2 | 2.0 | 36.4 | -0.8 | 1.9 |
| 37.0 | -0.8 | 1.9 | 37.6 | -10.2 | 1.9 | 38.2 | 3.1 | 1.9 |
| 38.8 | 5.8 | 1.8 | 39.4 | 0.5 | 1.8 | 40.0 | 10.5 | 1.7 |
| 40.7 | 1.3 | 1.6 | 41.4 | 2.9 | 1.5 | 42.0 | -5.0 | 1.4 |
| 42.7 | 3.2 | 1.4 | 43.5 | 0.6 | 1.4 | 44.2 | 6.3 | 1.4 |
| 45.0 | -3.9 | 1.4 | 45.7 | -1.8 | 1.4 | 46.5 | -1.5 | 1.4 |
| 47.1 | 1.1 | 2.1 | 47.6 | -1.5 | 2.1 | 48.0 | 6.3 | 2.0 |
| 48.4 | -2.1 | 1.9 | 48.8 | 1.5 | 1.9 | 49.3 | -0.8 | 1.9 |
| 49.7 | -7.1 | 1.9 | 50.2 | 1.1 | 1.8 | 50.6 | -0.5 | 1.9 |
| 51.1 | -1.8 | 1.9 | 51.5 | 1.6 | 2.0 | 52.0 | -6.0 | 1.9 |
| 52.5 | -1.0 | 2.0 | 53.0 | -4.9 | 2.0 | 53.5 | 3.4 | 2.0 |
| 54.0 | 6.1 | 2.0 | 54.5 | 9.4 | 1.8 | 55.0 | 0.6 | 1.7 |
| 55.5 | 1.6 | 1.7 | 56.0 | 1.3 | 1.6 | 56.6 | 0.8 | 1.6 |
| 57.1 | 1.5 | 1.5 | 57.7 | -8.4 | 1.6 | 58.2 | -2.3 | 1.7 |
| 58.8 | -3.6 | 1.7 | 59.4 | -4.2 | 1.7 | 60.0 | 0.8 | 1.6 |
| 60.6 | 7.8 | 1.6 | 61.2 | 1.0 | 1.6 | 61.8 | -1.0 | 1.6 |
| 62.4 | 7.4 | 1.5 | 63.0 | 0.0 | 1.5 | 63.7 | -0.6 | 1.5 |
| 64.3 | 4.0 | 1.4 | 65.0 | -2.3 | 1.4 | 65.7 | 3.4 | 1.4 |
| 66.3 | -1.0 | 1.3 | 67.0 | 3.1 | 1.2 | 67.7 | 1.0 | 1.2 |
| 68.4 | -0.6 | 1.2 | 69.2 | -0.3 | 1.1 | 69.9 | 0.2 | 1.1 |

| | | | | | | | | |
|---|---|---|---|---|---|---|---|---|
| 70.7 | -0.3 | 1.1 | 71.4 | -0.5 | 1.2 | 72.2 | -3.2 | 1.2 |
| 73.0 | 1.9 | 1.2 | 73.8 | 4.2 | 1.2 | 74.6 | -1.1 | 1.2 |
| 75.4 | 4.7 | 1.2 | 76.2 | 3.2 | 1.1 | 77.1 | 5.2 | 1.1 |
| 78.0 | -0.6 | 1.1 | 78.8 | -3.1 | 1.2 | 79.7 | -0.6 | 1.2 |
| 80.7 | 1.0 | 1.2 | 81.6 | -6.0 | 1.3 | 82.5 | 2.6 | 1.3 |
| 83.5 | 5.0 | 1.2 | 84.5 | 6.6 | 1.1 | 85.5 | 1.8 | 1.1 |
| 86.5 | 3.7 | 1.1 | 87.5 | 0.2 | 1.1 | 88.6 | -0.6 | 1.1 |
| 89.6 | -3.6 | 1.1 | 90.7 | -3.6 | 1.1 | 91.8 | 3.6 | 1.1 |
| 92.9 | -2.4 | 1.2 | 94.1 | 3.2 | 1.3 | 95.3 | 5.3 | 1.3 |
| 96.5 | -1.1 | 1.3 | 97.7 | 2.3 | 1.3 | 98.9 | -4.7 | 1.3 |
| 100.2 | 8.6 | 1.2 | 101.5 | 5.8 | 1.2 | 102.8 | -0.6 | 1.2 |
| 104.1 | -1.9 | 1.3 | 105.5 | -1.6 | 1.3 | 106.9 | 2.9 | 1.3 |
| 108.3 | 2.6 | 1.3 | 109.7 | 0.6 | 1.4 | 111.2 | 2.7 | 1.4 |
| 112.7 | -5.2 | 1.4 | 114.2 | -2.9 | 1.4 | 115.8 | 1.6 | 1.4 |
| 117.4 | 6.1 | 1.3 | 119.0 | 3.1 | 1.3 | 120.7 | 3.1 | 1.2 |
| 122.4 | 2.1 | 1.3 | 124.1 | 3.1 | 1.3 | 125.9 | 4.0 | 1.2 |
| 127.7 | -1.9 | 1.3 | 129.6 | 3.1 | 1.2 | 131.5 | 2.4 | 1.1 |
| 133.4 | -0.8 | 1.1 | 135.4 | 3.1 | 1.0 | 137.4 | -1.0 | 1.0 |
| 139.5 | -3.2 | 1.1 | 141.6 | 0.8 | 1.1 | 143.8 | 3.6 | 1.1 |
| 146.0 | 11.0 | 1.0 | 148.3 | 11.6 | 0.9 | 150.6 | 11.0 | 0.9 |
| 153.0 | 6.0 | 0.9 | 155.4 | 0.5 | 0.8 | 157.9 | 1.1 | 0.9 |
| 160.4 | 3.1 | 0.9 | 163.0 | 1.5 | 1.0 | 165.7 | -1.6 | 1.1 |
| 168.5 | 2.3 | 1.1 | 171.3 | -3.2 | 1.1 | 174.2 | 0.5 | 1.1 |
| 177.1 | -1.3 | 1.1 | 180.1 | 0.6 | 1.0 | 183.3 | 0.3 | 1.0 |
| 186.4 | -1.5 | 1.0 | 189.7 | 1.6 | 1.0 | 193.1 | 1.6 | 0.9 |
| 196.5 | 1.8 | 1.0 | 200.1 | 0.0 | 1.2 | 203.7 | 0.0 | 1.7 |
| 207.5 | 0.2 | 2.6 | 211.3 | -0.3 | 4.1 | 215.3 | 11.5 | 3.7 |

$^{21}$NE

| | | | | | | | | |
|---|---|---|---|---|---|---|---|---|
| 4.1 | 16.5 | 35.3 | 4.5 | 13.4 | 35.8 | 4.9 | -23.7 | 32.6 |
| 5.3 | 0.8 | 30.9 | 5.7 | 18.7 | 34.1 | 6.1 | 31.2 | 29.0 |
| 6.5 | -13.8 | 23.4 | 6.9 | 2.6 | 20.1 | 7.4 | 28.5 | 18.4 |
| 7.8 | -0.7 | 17.1 | 8.2 | -18.1 | 16.2 | 8.6 | 26.0 | 15.5 |
| 9.0 | 8.8 | 15.3 | 9.4 | 27.4 | 15.4 | 9.8 | -7.8 | 14.4 |
| 10.2 | -7.4 | 14.0 | 10.7 | 4.1 | 13.4 | 11.1 | 6.7 | 13.4 |
| 11.5 | -6.9 | 12.6 | 12.0 | -3.3 | 12.5 | 12.4 | 3.8 | 11.4 |
| 12.8 | 19.8 | 11.4 | 13.3 | 18.6 | 10.7 | 13.7 | 2.7 | 9.9 |
| 14.1 | 0.5 | 9.8 | 14.5 | 3.9 | 9.0 | 15.0 | 4.3 | 8.3 |
| 15.4 | 6.2 | 7.6 | 15.9 | -2.7 | 7.1 | 16.4 | -0.3 | 7.2 |
| 16.8 | 3.1 | 6.7 | 17.2 | -4.6 | 6.2 | 17.7 | -5.5 | 5.9 |
| 18.2 | 2.3 | 5.5 | 18.6 | 7.3 | 5.8 | 19.0 | -0.2 | 5.5 |
| 19.5 | -6.5 | 5.2 | 19.9 | 5.6 | 5.0 | 20.4 | -2.6 | 4.7 |
| 20.8 | -0.9 | 4.5 | 21.3 | -0.2 | 4.3 | 21.9 | -0.4 | 4.1 |
| 22.4 | -4.1 | 3.9 | 22.9 | 3.1 | 4.4 | 23.3 | 3.3 | 4.2 |
| 23.7 | 4.9 | 4.1 | 24.2 | -1.6 | 3.7 | 24.6 | 0.1 | 3.5 |
| 25.1 | 3.2 | 3.4 | 25.6 | 0.8 | 3.3 | 26.1 | -1.8 | 3.3 |
| 26.6 | -2.5 | 3.3 | 27.1 | -0.3 | 3.3 | 27.7 | -2.8 | 3.2 |
| 28.2 | 4.5 | 3.2 | 28.8 | 2.0 | 3.0 | 29.3 | 6.1 | 3.4 |
| 29.7 | 4.8 | 3.2 | 30.1 | -0.7 | 3.1 | 30.6 | 2.7 | 3.0 |
| 31.0 | 2.2 | 3.0 | 31.4 | -0.7 | 2.9 | 31.9 | -1.1 | 2.8 |
| 32.3 | 0.5 | 2.8 | 32.8 | -0.4 | 2.8 | 33.3 | -2.2 | 2.8 |
| 33.8 | 2.4 | 2.9 | 34.3 | -0.3 | 2.8 | 34.8 | 1.2 | 2.8 |
| 35.3 | 1.7 | 2.7 | 35.9 | 0.3 | 2.4 | 36.4 | 1.4 | 2.4 |
| 37.0 | -2.6 | 2.3 | 37.6 | -0.4 | 2.4 | 38.2 | 0.7 | 2.3 |

| | | | | | | | | |
|---|---|---|---|---|---|---|---|---|
| 38.8 | -0.6 | 2.2 | 39.4 | 0.2 | 2.2 | 40.0 | 2.0 | 2.0 |
| 40.7 | 0.7 | 1.9 | 41.4 | 1.0 | 1.8 | 42.0 | -1.4 | 1.8 |
| 42.7 | -0.3 | 1.7 | 43.5 | -0.8 | 1.7 | 44.2 | 3.1 | 1.7 |
| 45.0 | -2.0 | 1.7 | 45.7 | -2.2 | 1.7 | 46.5 | -0.6 | 1.8 |
| 47.1 | 1.4 | 2.6 | 47.6 | 0.8 | 2.6 | 48.0 | 4.2 | 2.5 |
| 48.4 | -0.5 | 2.4 | 48.8 | -0.8 | 2.3 | 49.3 | 1.0 | 2.4 |
| 49.7 | -1.8 | 2.3 | 50.2 | 0.8 | 2.2 | 50.6 | -0.9 | 2.3 |
| 51.1 | 8.3 | 2.4 | 51.5 | 11.5 | 2.5 | 52.0 | 13.2 | 2.5 |
| 52.5 | 10.1 | 2.6 | 53.0 | 5.7 | 2.5 | 53.5 | 6.3 | 2.5 |
| 54.0 | -0.0 | 2.4 | 54.5 | 3.0 | 2.2 | 55.0 | -1.5 | 2.1 |
| 55.5 | 1.9 | 2.1 | 56.0 | 1.7 | 1.9 | 56.6 | -1.9 | 1.9 |
| 57.1 | 1.3 | 1.9 | 57.7 | -2.2 | 2.0 | 58.2 | 1.3 | 2.0 |
| 58.8 | -0.5 | 2.0 | 59.4 | -2.3 | 2.0 | 60.0 | 1.3 | 2.0 |
| 60.6 | 2.8 | 1.9 | 61.2 | -1.3 | 1.9 | 61.8 | -1.6 | 1.9 |
| 62.4 | 1.2 | 1.8 | 63.0 | 0.9 | 1.9 | 63.7 | -1.2 | 1.8 |
| 64.3 | 3.3 | 1.8 | 65.0 | -0.5 | 1.8 | 65.7 | 0.9 | 1.7 |
| 66.3 | 1.3 | 1.7 | 67.0 | 0.1 | 1.5 | 67.7 | -0.7 | 1.5 |
| 68.4 | -1.0 | 1.5 | 69.2 | 0.5 | 1.4 | 69.9 | 0.8 | 1.4 |
| 70.7 | -0.1 | 1.4 | 71.4 | -0.2 | 1.5 | 72.2 | -2.0 | 1.5 |
| 73.0 | -0.8 | 1.5 | 73.8 | 3.0 | 1.5 | 74.6 | -1.5 | 1.5 |
| 75.4 | 2.3 | 1.5 | 76.2 | 1.6 | 1.4 | 77.1 | 1.0 | 1.3 |
| 78.0 | -0.1 | 1.4 | 78.8 | -1.1 | 1.5 | 79.7 | 0.9 | 1.5 |
| 80.7 | 0.4 | 1.5 | 81.6 | -1.4 | 1.6 | 82.5 | 0.3 | 1.5 |
| 83.5 | 0.7 | 1.5 | 84.5 | 1.7 | 1.5 | 85.5 | 1.2 | 1.3 |
| 86.5 | 2.2 | 1.3 | 87.5 | -0.7 | 1.3 | 88.6 | -0.8 | 1.3 |
| 89.6 | 0.5 | 1.3 | 90.7 | 1.4 | 1.4 | 91.8 | 3.2 | 1.4 |
| 92.9 | 1.1 | 1.5 | 94.1 | 2.9 | 1.6 | 95.3 | 4.6 | 1.6 |
| 96.5 | 6.2 | 1.6 | 97.7 | 7.3 | 1.6 | 98.9 | 7.3 | 1.7 |
| 100.2 | 5.2 | 1.5 | 101.5 | 1.8 | 1.5 | 102.8 | 0.9 | 1.5 |
| 104.1 | -0.4 | 1.5 | 105.5 | -0.9 | 1.5 | 106.9 | -0.6 | 1.6 |
| 108.3 | -0.3 | 1.6 | 109.7 | 1.9 | 1.7 | 111.2 | -0.6 | 1.7 |
| 112.7 | 0.5 | 1.8 | 114.2 | -1.3 | 1.7 | 115.8 | 0.7 | 1.7 |
| 117.4 | 2.6 | 1.6 | 119.0 | 0.8 | 1.5 | 120.7 | 1.5 | 1.5 |
| 122.4 | 0.3 | 1.6 | 124.1 | 2.4 | 1.6 | 125.9 | 1.1 | 1.5 |
| 127.7 | -1.5 | 1.6 | 129.6 | 1.8 | 1.5 | 131.5 | 0.6 | 1.4 |
| 133.4 | 1.5 | 1.3 | 135.4 | 5.6 | 1.2 | 137.4 | 5.3 | 1.3 |
| 139.5 | 4.5 | 1.3 | 141.6 | 4.4 | 1.3 | 143.8 | 2.6 | 1.3 |
| 146.0 | 1.2 | 1.2 | 148.3 | 0.3 | 1.1 | 150.6 | 0.8 | 1.1 |
| 153.0 | 0.2 | 1.1 | 155.4 | 0.5 | 1.1 | 157.9 | 1.7 | 1.1 |
| 160.4 | 0.5 | 1.1 | 163.0 | -0.8 | 1.2 | 165.7 | -1.1 | 1.3 |
| 168.5 | 2.3 | 1.3 | 171.3 | -1.3 | 1.3 | 174.2 | 0.3 | 1.3 |
| 177.1 | 0.1 | 1.3 | 180.1 | 0.1 | 1.2 | 183.3 | 1.0 | 1.2 |
| 186.4 | 0.5 | 1.2 | 189.7 | 0.0 | 1.2 | 193.1 | 1.0 | 1.1 |
| 196.5 | 0.2 | 1.2 | 200.1 | -0.5 | 1.5 | 203.7 | 2.3 | 2.0 |
| 207.5 | 1.0 | 3.2 | 211.3 | 4.2 | 5.1 | 215.3 | 2.7 | 4.5 |

$^{22}$NE

| | | | | | | | | |
|---|---|---|---|---|---|---|---|---|
| 4.1 | 56.6 | 37.6 | 4.5 | 12.5 | 38.1 | 4.9 | -42.5 | 34.6 |
| 5.3 | 2.9 | 32.8 | 5.7 | 26.2 | 36.2 | 6.1 | 8.0 | 30.7 |
| 6.5 | 21.0 | 24.9 | 6.9 | -11.1 | 21.3 | 7.4 | 28.4 | 19.6 |
| 7.8 | 18.5 | 18.3 | 8.2 | 3.9 | 17.2 | 8.6 | 23.6 | 16.5 |
| 9.0 | 7.3 | 16.3 | 9.4 | -2.8 | 16.3 | 9.8 | 29.3 | 15.5 |
| 10.2 | -3.7 | 14.9 | 10.7 | -17.9 | 14.3 | 11.1 | -9.3 | 14.3 |
| 11.5 | 1.3 | 13.5 | 12.0 | 7.2 | 13.3 | 12.4 | 9.9 | 12.2 |

| | | | | | | | | |
|---|---|---|---|---|---|---|---|---|
| 12.8 | 12.7 | 12.1 | 13.3 | -10.1 | 11.3 | 13.7 | -2.7 | 10.5 |
| 14.1 | 10.0 | 10.5 | 14.5 | 6.7 | 9.6 | 15.0 | 6.7 | 8.9 |
| 15.4 | 6.1 | 8.2 | 15.9 | 2.7 | 7.5 | 16.4 | 0.9 | 7.7 |
| 16.8 | 11.1 | 7.2 | 17.2 | 4.1 | 6.7 | 17.7 | -2.5 | 6.3 |
| 18.2 | -5.6 | 6.0 | 18.6 | 5.1 | 6.1 | 19.0 | -0.3 | 5.8 |
| 19.5 | -5.6 | 5.5 | 19.9 | 1.1 | 5.2 | 20.4 | -1.5 | 5.0 |
| 20.8 | 2.5 | 4.9 | 21.3 | 3.3 | 4.5 | 21.9 | -1.1 | 4.2 |
| 22.4 | -0.1 | 4.1 | 22.9 | 0.0 | 4.7 | 23.3 | -2.0 | 4.5 |
| 23.7 | 15.6 | 4.4 | 24.2 | 14.1 | 3.9 | 24.6 | 4.7 | 3.8 |
| 25.1 | 0.7 | 3.6 | 25.6 | -3.5 | 3.4 | 26.1 | 5.6 | 3.4 |
| 26.6 | -1.2 | 3.4 | 27.1 | -2.5 | 3.4 | 27.7 | -2.7 | 3.4 |
| 28.2 | -0.1 | 3.3 | 28.8 | 9.7 | 3.1 | 29.3 | 12.9 | 3.6 |
| 29.7 | 10.0 | 3.4 | 30.1 | 3.9 | 3.3 | 30.6 | 3.5 | 3.3 |
| 31.0 | 2.3 | 3.1 | 31.4 | 0.7 | 3.1 | 31.9 | -1.7 | 3.0 |
| 32.3 | 1.6 | 3.0 | 32.8 | -1.9 | 3.0 | 33.3 | -10.5 | 3.0 |
| 33.8 | -3.2 | 3.0 | 34.3 | -3.1 | 3.0 | 34.8 | -3.1 | 3.0 |
| 35.3 | 2.4 | 2.8 | 35.9 | 2.1 | 2.7 | 36.4 | 3.1 | 2.5 |
| 37.0 | 0.4 | 2.5 | 37.6 | -9.6 | 2.5 | 38.2 | 2.5 | 2.5 |
| 38.8 | -0.7 | 2.4 | 39.4 | -0.1 | 2.4 | 40.0 | 9.3 | 2.2 |
| 40.7 | 5.2 | 2.0 | 41.4 | 3.3 | 2.0 | 42.0 | -2.1 | 1.9 |
| 42.7 | 0.9 | 1.9 | 43.5 | 0.0 | 1.9 | 44.2 | 3.3 | 1.7 |
| 45.0 | -6.7 | 1.9 | 45.7 | -2.0 | 1.9 | 46.5 | -4.9 | 1.9 |
| 47.1 | -2.9 | 2.7 | 47.6 | -5.5 | 2.8 | 48.0 | 7.6 | 2.7 |
| 48.4 | 3.9 | 2.7 | 48.8 | -0.3 | 2.5 | 49.3 | -1.5 | 2.5 |
| 49.7 | -2.9 | 2.5 | 50.2 | 2.3 | 2.4 | 50.6 | -2.3 | 2.5 |
| 51.1 | -5.5 | 2.4 | 51.5 | -4.4 | 2.5 | 52.0 | -3.2 | 2.5 |
| 52.5 | -9.2 | 2.5 | 53.0 | -6.0 | 2.7 | 53.5 | 0.1 | 2.7 |
| 54.0 | 0.1 | 2.5 | 54.5 | 0.9 | 2.5 | 55.0 | 5.9 | 2.4 |
| 55.5 | 2.1 | 2.2 | 56.0 | 5.5 | 2.0 | 56.6 | 2.8 | 2.0 |
| 57.1 | 0.8 | 2.0 | 57.7 | -6.9 | 2.0 | 58.2 | -0.7 | 2.2 |
| 58.8 | -2.0 | 2.2 | 59.4 | -3.5 | 2.2 | 60.0 | -0.9 | 2.0 |
| 60.6 | 3.1 | 2.0 | 61.2 | 1.3 | 2.0 | 61.8 | 1.1 | 2.0 |
| 62.4 | 3.5 | 2.0 | 63.0 | 0.7 | 1.9 | 63.7 | -3.3 | 1.9 |
| 64.3 | 1.2 | 1.9 | 65.0 | 0.4 | 1.9 | 65.7 | 1.3 | 1.9 |
| 66.3 | 3.2 | 1.7 | 67.0 | 3.9 | 1.6 | 67.7 | -0.4 | 1.6 |
| 68.4 | 0.0 | 1.6 | 69.2 | -0.7 | 1.6 | 69.9 | 1.1 | 1.6 |
| 70.7 | 0.1 | 1.6 | 71.4 | -3.1 | 1.6 | 72.2 | -5.1 | 1.6 |
| 73.0 | -2.0 | 1.6 | 73.8 | 0.1 | 1.6 | 74.6 | -1.2 | 1.6 |
| 75.4 | -0.3 | 1.6 | 76.2 | 3.9 | 1.6 | 77.1 | 4.3 | 1.4 |
| 78.0 | -0.7 | 1.4 | 78.8 | -3.1 | 1.6 | 79.7 | -4.3 | 1.6 |
| 80.7 | 1.1 | 1.6 | 81.6 | -6.9 | 1.6 | 82.5 | -0.8 | 1.6 |
| 83.5 | 1.7 | 1.6 | 84.5 | 2.0 | 1.6 | 85.5 | 5.9 | 1.4 |
| 86.5 | 3.1 | 1.4 | 87.5 | 1.9 | 1.4 | 88.6 | 0.8 | 1.4 |
| 89.6 | -2.1 | 1.4 | 90.7 | -3.9 | 1.4 | 91.8 | -0.1 | 1.4 |
| 92.9 | -4.5 | 1.6 | 94.1 | 0.3 | 1.6 | 95.3 | -0.4 | 1.6 |
| 96.5 | -0.7 | 1.7 | 97.7 | 2.0 | 1.7 | 98.9 | 0.0 | 1.7 |
| 100.2 | 3.6 | 1.6 | 101.5 | 5.9 | 1.6 | 102.8 | -1.5 | 1.6 |
| 104.1 | -4.7 | 1.6 | 105.5 | -0.3 | 1.7 | 106.9 | 2.5 | 1.7 |
| 108.3 | 2.3 | 1.7 | 109.7 | -0.3 | 1.7 | 111.2 | 1.9 | 1.9 |
| 112.7 | -0.9 | 1.9 | 114.2 | -3.5 | 1.7 | 115.8 | 2.1 | 1.7 |
| 117.4 | 5.3 | 1.7 | 119.0 | -1.5 | 1.6 | 120.7 | -2.0 | 1.6 |
| 122.4 | -3.2 | 1.6 | 124.1 | -0.8 | 1.7 | 125.9 | 0.0 | 1.6 |
| 127.7 | -2.3 | 1.7 | 129.6 | 3.7 | 1.6 | 131.5 | 2.5 | 1.4 |
| 133.4 | 1.2 | 1.4 | 135.4 | 2.5 | 1.3 | 137.4 | -2.8 | 1.3 |
| 139.5 | -3.7 | 1.4 | 141.6 | 1.1 | 1.4 | 143.8 | 0.1 | 1.4 |
| 146.0 | 2.7 | 1.3 | 148.3 | 2.8 | 1.3 | 150.6 | 1.7 | 1.1 |

| | | | | | | | | |
|---|---|---|---|---|---|---|---|---|
| 153.0 | 0.4 | 1.1 | 155.4 | 0.8 | 1.1 | 157.9 | 1.1 | 1.3 |
| 160.4 | 0.7 | 1.1 | 163.0 | -0.7 | 1.3 | 165.7 | -2.3 | 1.3 |
| 168.5 | 2.3 | 1.4 | 171.3 | -1.2 | 1.4 | 174.2 | 0.5 | 1.4 |
| 177.1 | -0.8 | 1.4 | 180.1 | 1.2 | 1.3 | 183.3 | 0.0 | 1.3 |
| 186.4 | -1.2 | 1.3 | 189.7 | 0.5 | 1.3 | 193.1 | 0.3 | 1.3 |
| 196.5 | 1.7 | 1.3 | 200.1 | -0.1 | 1.6 | 203.7 | 0.7 | 2.2 |
| 207.5 | 2.7 | 3.3 | 211.3 | 4.0 | 5.3 | 215.3 | 5.5 | 4.9 |

REFERENCES


1 E. Burbidge, G. Burbidge, W. Fowler, F. Hoyle, Rev. Mod. Phys. 29(1957)547

2 B. Allen, J. Gibbons, R. Macklin, Adv. in Nucl. Phys. 4(1971)205

3 I. Iben, Ap. J. 196(1075)525

4 I. Iben, Ap. J. 208(1976)165

5 A. Unsöld, The New Cosmos, Springer Verlag, New York 1980

6 A. Cameron, Essays in Astrophysics, ed. D. D. Clayton, Cambridge Univ. Press 1981

7 J. Truran, I. Iben, Ap. J. 216(1977)979

8 F. Vaughn, et al., Phys. Rev. 118(1960)683

9 H. Cohen, J. Fowler, Phys. Rev. 114(1960)194

10 R. Chrien, Proc. Conf. on Nucl. Cross Sections, BNL 425(1975)139

11 R. Macklin, J. Gibbons, Phys. Rev 159(1967)1007

12 F. Hensley, KfK Report 2918(1980)

13 α,β,γ Spectroscopy, ed. K. Siegbahn, North Holland Publ. Co., Amsterdam 1965

14 B. Leugers, KfK Report 2895(1979)

15 J. Almeida, D. Erbe, G. Rupp, F. Käppeler, KfK 3068(1980)14

16 Fast Neutron Physics, ed. J. Marion, J. Fowler, Intersc. Publ. Inc. New York 1960

17 D. Garber, R. Kinsey, BNL 325(1976)

18 G. Reffo, private communication

19 D. Smith, G. Polk, T. Miller, Nucl. Instr. and Meth. 64(1968)157

20 F. Fröhner, Gulf General Atomic GA-8380(1968)

21 G. Walter, K. Wisshak, to be published

22 D. D. Clayton, Principles of Stellar Evolution and Nucleosynthesis, Mc Graw Hill, New York 1968

23 C. Barnes, Adv. Nucl. Phys. 4(1971)133

24 J. Lynn, Theory of Resonance Neutron Reactions, Clarendon Press, Oxford 1968

25 H. Lutz, et al., Nucl. Phys. A95(1967)591

26 A. Howard, et al., Nucl. Phys. A512(1970)317

27 I. Iben, Ap. J. 196(1975)549

28 V. Trimble, Rev. Mod. Phys. 47(1975)877

29 D. D. Clayton, Stellar Nucleosynthesis, ed. W. Arnett, Gordon and Breach, New York 1968

30 P. Seeger, et al., Ap. J. Suppl. Ser. 11(1965)121

31 D. D. Clayton, R. Ward, Ap. J. 193(1974)397

32 F. Käppeler, et al., KfK Report 3210(1981)

33 R. Ulrich, Explosive Nucleosynthesis p.139, eds. D. Schramm, W. Arnett, Austin, Univ. of Texas Press 1978

34 R. Ward, M. Newman, Ap. J. 219(1978)195

35 I. Iben, Ap. J. 217(1977)788

36 S. Woosley, W. Fowler, J. Holmes, At. and Nucl. Data Tables 22(1978)371

37 H. Weigmann, R. Macklin, J. Harvey, Phys. Rev. C 14(1976)1328

38 R. Macklin, Nucl. Sci. and Engineering 78(1981)110

39 W. Fowler, G. Caughlan, B. Zimmermann, Ann. Rev. Astr. and Astrophys. 13(1975)69

40 K. Lang, Astrophysical Formulae p.378, Springer Verlag, New York 1980

41 J. Cosner, I. Iben, J. Truran, Ap. J. Lett. 238(1980)L91